UNIVERSITY OF SOUTHAMPTON

ABSTRACT

FACULTY OF SCIENCE

CHEMISTRY

Doctor of Philosophy

THE VAPOUR PHASE PHOTOPHYSICS OF SOME SUBSTITUTED AROMATIC MOLECULES

by

Geoffrey Denis Abbott, B.Sc., M.Sc.

The first observations of vapour phase fluorescent exciplexes, formed between photo-excited substituted aromatic molecules and one of a variety of ground state species, are reported.

From fluorescence decay and steady-state quenching results, the rate constants for the various formation and decay processes of one such exciplex, that formed between 1,4 Dicyanonaphthalene (1,4 DCN) and 2,5 Dimethyl 2,4 Hexadiene (DMHD) were extracted. The thermodynamic properties of this exciplex were also obtained from the temperature dependence of these rate constants. The values of these thermodynamic properties were compared with those found by other workers for similar systems in the solution phase.

A CNDO/S-CI molecular orbital method was used to predict the electronic structures of some substituted benzene molecules. Using such a method the energies of the excited singlet and triplet energies for such species were calculated. These values were then used in conjunction with a group theoretical analysis to suggest assignments for some of the electronic bands in various vapour phase triplet-triplet absorption experiments.

A novel sampling technique for the detection of atmospheric pollutants has also been described.

THE VAPOUR PHASE PHOTOPHYSICS OF SOME SUBSTITUTED AROMATIC MOLECULES

A thesis submitted to the
University of Southampton
in partial fulfilment of
the requirements for the
degree of

DOCTOR OF PHILOSOPHY

BY

GEOFFREY DENIS ABBOTT, B.Sc., M.Sc.

DEPARTMENT OF CHEMISTRY

SEPTEMBER 1980

'True piety is acting what one knows'

MATTHEW ARNOLD, Notebooks (1868).

ACKNOWLEDGEMENTS

Firstly I thank Professor David Phillips for being an excellent supervisor both on the personal side and also for his encouragement, ideas and his willingness to allow me to pursue my interests.

I also wish to express, most warmly, my gratitude to Dr. Desmond O'Connor, without whose help the most important part of this thesis would not have been accomplished.

I thank Professor Ian Beattie for providing financial support for most of the duration of this work.

Dr. John Dyke, I thank for providing the computer program necessary for the molecular orbital calculations undertaken in this work. I also thank Dr. Anthony Rest for allowing me to use his equipment for the work recorded in Chapter 6 of this thesis.

I thank all members, both past and present, of the Photochemistry group who have always provided a stimulating environment to work in. Two people - Dr. Jack Hargreaves whose friendship and wit kept me going at the worst of times and Dr. Satoshi Hirayama, for first suggesting the vapour phase exciplex work, I would like to thank in name.

My other good friends, Bob Wyatt, Irene Levandovsky, Tim McAlindon, John 'Smokey' Naylor, John 'Pants' Overstall, Rog Brentnall, John 'Bear' Liddy, Ian 'Tricky' Trickle I thank for their personal advice, witty repartee, their fags and the pints of Marston's bitter they procured for me from that most holy of institutions - The 'Vine' Inn.

I am very grateful to Sandy White for her excellent typing and for proof-reading the Acknowledgements section of this thesis.

Lastly, and the most deserving of thanks, I thank my family, especially my brothers Chris and Mike, for their personal support and down-to-earth advice and as a small token of my gratitude I dedicate this thesis to them.

To Rita, Denis, Michael, Christopher, Eileen,

Helen and Roger.

CONTENTS

		Page
CHAPTER 1.	GENERAL INTRODUCTION	1
CHAPTER 2.	EXPERIMENTAL	19
2.1.	Steady State Fluorescence Spectra	19
2.2.	Measurement of Fluorescence Lifetimes	21
2.2.1.	Time-Correlated Single Photon Counting	21
2.2.2.	Pulsed Lasers	26
2.3.	Data Analysis	35
2.4.	Preparation of Sample Cells	39
2.5.	High Temperature Furnaces	43
2.6.	Chemicals	48
CHAPTER 3.	THE 9-CYANOANTHRACENE/AMINE VAPOUR PHASE EXCIPLEXES	51
3.1.	Introduction	51
3.2.	Results and Discussion	52
3.3.	Conclusions	63
CHAPTER 4.	THE 1,4 DICYANONAPHTHALENE/2,5 DIMETHYL 2,4 HEXADIENE VAPOUR PHASE EXCIPLEX	65
4.1.	Introduction	65
4.2.	Exciplex Kinetics	68
4.3.	Results and Discussion	73
4.3.1.	Steady State Measurements	73
4.3.2.	Kinetic Measurements	94
4.3.3.	Evaluation and discussion of the rate constants and thermodynamic properties for the formation and decay processes of the 1,4 DCN/DMHD vapour phase exciplex	101
4.4.	Conclusions	119

CHAPTER 5. SEMI-EMPIRICAL MOLECULAR ORBITAL CALCULATIONS 122

5.1. Introduction 122

5.2. Molecular Quantum Mechanics 122

5.3. Total Energy of a many electron closed shell molecular system 126

5.4. The Self-Consistent Field (SCF) Equation and the LCAO Approximation 130

5.5. The CNDO Approximations 133

5.6. Configuration Interaction 141

5.7. Validity of the CNDO/S-CI Method 143

5.8. Predictions of CNDO/S-CI Method 147

CHAPTER 6. THE DETECTION LIMITS OF SULPHUR DIOXIDE USING THE MATRIX ISOLATION SAMPLING TECHNIQUE 192

6.1. Introduction 192

6.2. Experimental 193

6.3. Results 194

6.4. Conclusions 199

UNIVERSITY OF SOUTHAMPTON

ABSTRACT

FACULTY OF SCIENCE

CHEMISTRY

Doctor of Philosophy

THE VAPOUR PHASE PHOTOPHYSICS OF SOME SUBSTITUTED AROMATIC MOLECULES

by

Geoffrey Denis Abbott, B.Sc., M.Sc.

The first observations of vapour phase fluorescent exciplexes, formed between photo-excited substituted aromatic molecules and one of a variety of ground state species, are reported.

From fluorescence decay and steady-state quenching results, the rate constants for the various formation and decay processes of one such exciplex, that formed between 1,4 Dicyanonaphthalene (1,4 DCN) and 2,5 Dimethyl 2,4 Hexadiene (DMHD) were extracted. The thermodynamic properties of this exciplex were also obtained from the temperature dependence of these rate constants. The values of these thermodynamic properties were compared with those found by other workers for similar systems in the solution phase.

A CNDO/S-CI molecular orbital method was used to predict the electronic structures of some substituted benzene molecules. Using such a method the energies of the excited singlet and triplet energies for such species were calculated. These values were then used in conjunction with a group theoretical analysis to suggest assignments for some of the electronic bands in various vapour phase triplet-triplet absorption experiments.

A novel sampling technique for the detection of atmospheric pollutants has also been described.

CHAPTER ONE

GENERAL INTRODUCTION

CHAPTER ONE

GENERAL INTRODUCTION

In 1963 Leonhardt and Weller[1] reported the appearance of a new, broad, structureless band in the fluorescence spectra of mixed solutions of perylene and N,N dimethylaniline which was red-shifted from the perylene fluorescence. Since there was no corresponding feature in the absorption spectrum they interpreted the new emitting species as being a charge-transfer type of excited state complex, now called an exciplex.

An exciplex is defined as a stoichiometric complex that is associated in an excited electronic state and dissociative in its ground state.[2] An excimer is a 1:1 exciplex formed between identical atoms or molecules.[3] Excimer fluorescence was first detected by Förster and Kasper[4] who observed emission from a complex formed between excited singlet state and ground state pyrene molecules. Both singlet and triplet[5] exciplexes have been invoked as molecular complexes formed in the interactions of electronically excited aromatic molecules with a wide variety of quenchers. Exciplexes of 1:2 stoichiometry[6-11] are known to exist (the term exterplex[7] has been proposed for these termolecular complexes). Extensive studies of intramolecular complexes have also been made where exciplex interaction between two moieties of the same molecule occurs.[12-18]

The salient features of the energetics of exciplex formation and decay are often interpreted in terms of a potential energy diagram, shown in figure 1.1, which was first proposed by Stevens and Ban.[19] The geometric coordinate is the interplanar distance, R_{A-Q}, between the two species forming the complex. Such a diagram illustrates the red shift of the exciplex emission, $h\nu_E^{max}$, from the monomer 0-0 fluorescence band, $h\nu_M^{0-0}$. It can also be seen from figure 1.1 that following radiative decay of the exciplex, a repulsive ground state surface is populated and hence dissociation of the

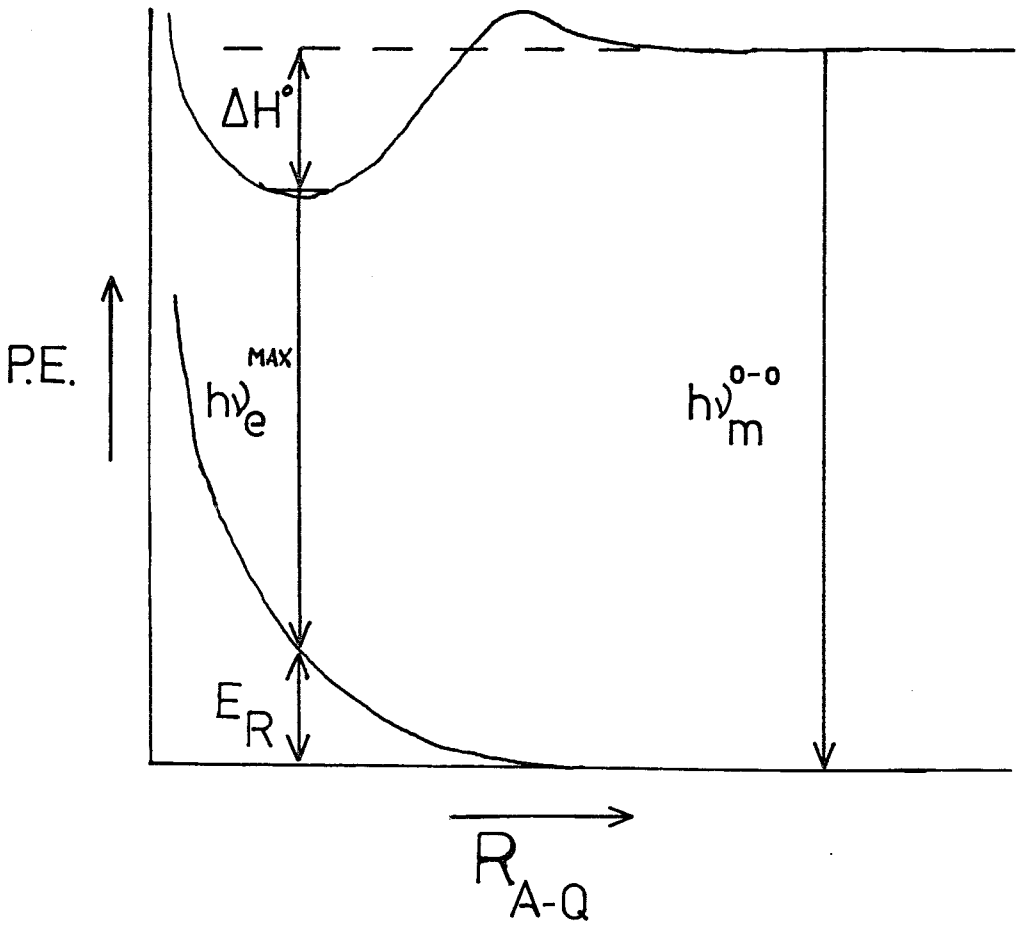

ΔH^{o} : Exciplex binding energy

E_R : Ground state repulsion energy

$h\nu_m^{0-0}$: Energy of A* 0-0 monomer fluorescence energy

$h\nu_e^{MAX}$: Energy of exciplex fluorescence maximum

FIGURE 1.1

complex will occur within a period of the intermolecular vibrations in the composite system, thus rationalizing the absence of any fine structure in the exciplex emission spectrum. The depth of the potential well, ΔH^{o}, in the excited surface is equal to the exciplex binding energy. As is clear in figure 1.1, the following relation holds for the energy of the monomer 0-0 fluorescence band,

$$h\nu_{M}^{0-0} = \Delta H^{o} + h\nu_{E}^{MAX} + E_{R} \qquad (1.1)$$

Weller et al.[1,20] at first believed that the exciplex was stabilised by electron transfer from the donor, D, to the acceptor, A, where either A^{1} or D^{21} can be the primarily excited species. Thus the exciplex was interpreted as a singlet charge-transfer complex $^{1}(A^{-} D^{+})$ which was unstable in the ground state $^{1}(AD)$. Consequently the emission process was considered to be a charge-transfer transition,[22]

$$^{1}(A^{-}D^{+}) \rightarrow {}^{1}(AD) + h\nu_{E} \qquad (1.2)$$

Indirect evidence in favour of the charge-transfer nature of exciplexes came from flash photolysis experiments[1,20,23] which indicated that the radical anion of the acceptor and the radical cation of the donor are formed direct from the exciplex singlet state. Exciplexes have also been generated electrochemically through reaction of the radical ions.[24-26] If the exciplex is considered as a "pure" charge-transfer state then its energy above the separated ground-state species in the gas phase is given by

$$E^{1}(A^{-}D^{+}) - E(AD) = h\nu_{E}^{MAX} = IP_{D} - EA_{A} - C \qquad (1.3)$$

where IP_{D} is the ionization potential of the donor, EA_{A} is the electron affinity of the acceptor and C is a constant for the particular combination

of A and D and represents mainly the Coulombic attraction energy. When the exciplex is dissolved in solvent further stability will be conferred by the solvation process[27] and thus eq.(1.3) becomes,

$$h\nu_{E}^{MAX} = IP_D - EA_A - C - \Delta H_e^{SOL} \qquad (1.4)$$

where ΔH_e^{SOL} is the enthalpy of solvation. From equation (1.4) the energy of the exciplex emission should be linearly correlated with IP_D and EA_A. Such correlations have been found experimentally.[28,29] Since IP_D and EA_A are related to the polarographic oxidation potential of the donor, E_D^{OX}, and to the polarographic reduction potential of the acceptor, E_A^{RED}, respectively then $h\nu_E^{MAX}$ should also be linearly correlated with E_D^{OX} and E_A^{RED}.[22] Again such correlations have been observed.[30-32] It has also been found that in cases where relatively strong acceptors are combined with relatively strong donors (so that virtually pure charge-transfer complexes are produced in the excited state), the energies of the exciplex emission bands in n-hexane are directly related to the differences of the polarographic oxidation and reduction potentials measured in polar solvents such as acetonitrile or dimethylformamide:[31,32]

$$h\nu_{E}^{MAX}(\text{hexane}) = E_D^{OX} - E_A^{RED} - \Delta \qquad (1.5)$$

with $\Delta = 0.10 \pm 0.08$ eV.

Therefore the charge-transfer character of exciplexes has been clearly established.

However, some workers[28,32,33] have found that the emission energies of a large number of exciplexes are lower than one would expect if only charge-transfer interactions were present. Dipole moments for these complexes have also been measured to have values between 10 and 14 Debye.[32-36]

Kuzmin[36] calculated that the dipole moment of an exciplex in which complete charge-transfer occurs has a value of 16.8 Debye; hence the view that the exciplex is a "pure" charge-transfer state[1] implied relatively large dipole moments which were not found by experiment. In excimers, which have very low or even zero dipole moments,[32,33] the most important contribution to their stability has been ascribed to the effect of exciton resonance.[37] Exciton resonance interactions result from the delocalisation of the excitation energy amongst both components, represented as,

$$A^*A \leftrightarrow AA^* \qquad (1.6)$$

The charge-transfer state of an exciplex often has an energy close to that of the lowest excited singlet states of both the components and hence, as Weller et al[27,33] pointed out, a more precise description of the exciplex electronic structure should include the effects of exciton resonance. An interaction between the charge-transfer state $^1(A^-D^+)$ and the non-polar locally excited complex states, $^1(A^*D)$ and $^1(AD^*)$, would lead to further stabilization of the charge-transfer state and a lower value, relative to the value expected for a "pure" charge-transfer complex, of the dipole moment.[22] This view therefore rationalised the experimental observations discussed above. Thus it is now generally accepted that a general resonance formulation of the exciplex applies, represented as

$$A^-D^+ \leftrightarrow A^+D^- \leftrightarrow A^*D \leftrightarrow AD^* \qquad (1.7)$$

and the electronic structure of the exciplex is best described by a wave function Ψ_{EXCIPLEX},

$$\Psi_{EXCIPLEX} = C_1 \Psi_1(A^-D^+) + C_2 \Psi_2(A^+D^-)$$

$$+ C_3 \Psi_3(A^*D) + C_4 \Psi_4(AD^*) \qquad (1.8)$$

Eq.(1.8) is analogous to Mulliken's[38] description of the electronic structure for ground state complexes. When the acceptor, A, is the primarily excited species molecular orbital calculations[39] have shown that $C_1 > C_2$ and $C_3 > C_4$ but that both the locally excited (A*D) and the charge-transfer (A^-D^+) configurations contribute to the exciplex state. The wave functions $\Psi(A^-D^+)$ and $\Psi(DA^*)$ correspond to the configurations shown in figure 1.2(a)[39] where d represents the highest occupied molecular orbital of D, a* the lowest unoccupied molecular orbital of A. $\Psi_{EXCIPLEX}$ reflects the interaction of these configurations and, as shown in figure 1.2(b), this interaction depends on the overlap of d and a, the highest occupied molecular orbitals of the donor and acceptor respectively.

Another approach which has led to insights into the structure of exciplexes has been made by examining the kinetics of exciplex formation and decay.[40] Birks et al[41] suggested and confirmed that in non-polar solvents the kinetics of excimer formation follow a simple mechanism. Weller et al[1] and Mataga et al[42] proposed the same type of mechanism to account for their observations on exciplex systems, which may be written as,[40]

$$A \xrightarrow{h\nu} A^* \qquad (1.9)$$

$$A^* + Q \underset{k_4}{\overset{k_3}{\rightleftharpoons}} (AQ)^* \xrightarrow{k_6} \text{PRODUCTS}$$

$$A^* \xrightarrow{k_1} A + h\nu_M \qquad A^* \xrightarrow{k_2} A \qquad (AQ)^* \xrightarrow{k_5} A + Q + h\nu_E$$

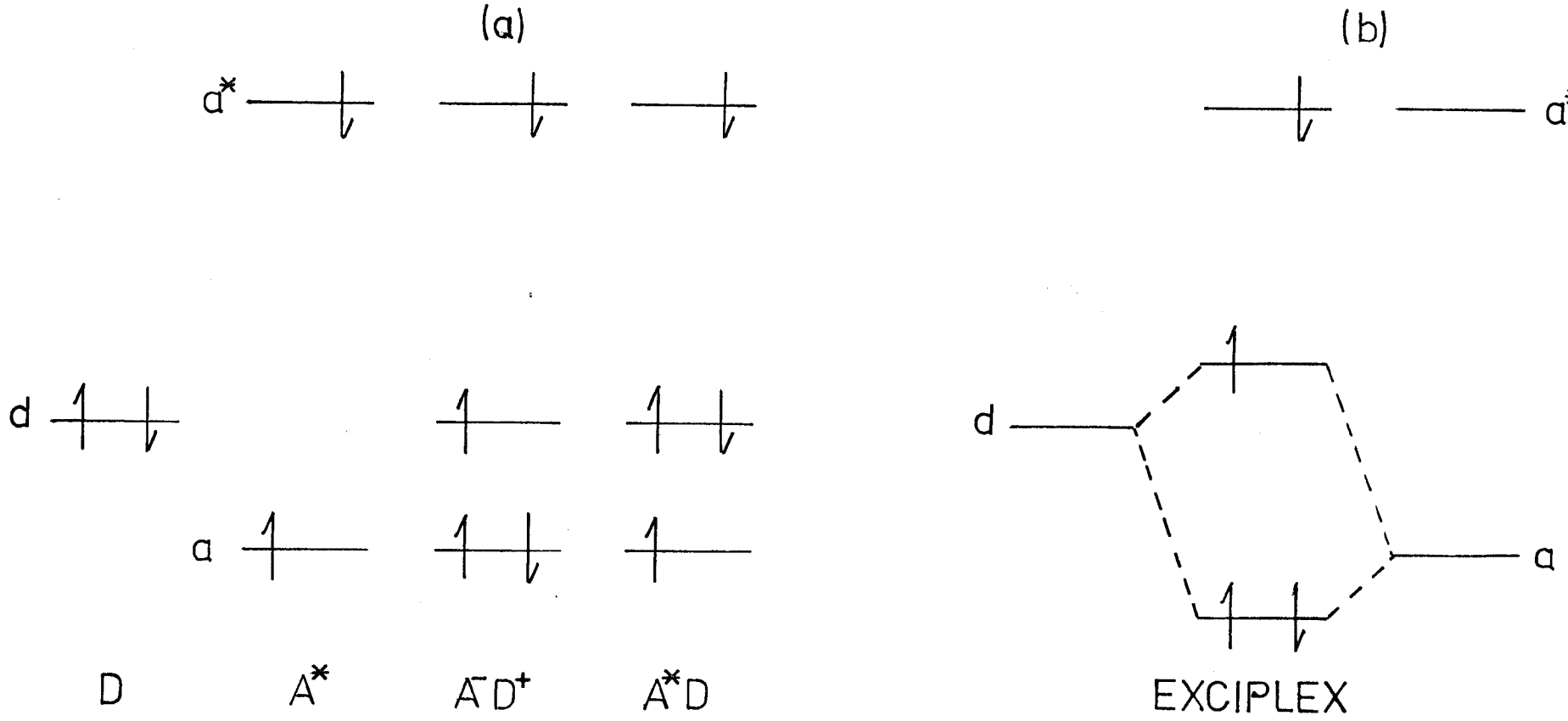

FIGURE 1.2. Schematic representation of energy levels corresponding to M.O.'s of D and A. d represents the highest occupied MO of the donor, a and a* the highest occupied and lowest unoccupied MO's of the acceptor. (a) Charge-transfer (A^-D^+) and locally excited (A*D) configurations. (b) Molecular orbital representation of the interaction between (A^-D^+) and A*D.

As shown in (1.9) the kinetic scheme is based on the establishment of an equilibrium between the complex and its precursors, the excited monomer (A*) and the quencher (Q). (In this work Q will be used instead of D unless charge-transfer states are specifically referred to). A more detailed outline of this mechanism will be given in the introduction to Chapter 4. It has been shown that the above mechanism stands up very well to detailed kinetic tests on a variety of exciplex systems in non-polar[43-47] and slightly polar solvents.[48] In a study on the kinetics of the formation and disappearance of the vapour phase excimer formed by 1-azabicyclo(2,2,2) octane at room temperature, it was confirmed that the mechanism given in (1.9) was also followed with the additional complicating feature introduced by quenching of the excimer by ground state amine.[49]

Equilibrium thermodynamic properties have been measured for a number of exciplex systems[29,31,33,50-53] by analysis of steady-state spectral data. Such calculations employ Stevens-Ban plots[19] from which binding energies can be obtained if certain assumptions about the relative magnitudes of the rates of the various formation and depletion processes of the exciplex are made. However, as McDonald and Selinger[54] have pointed out, there are dangers involved in the use of such plots. This aspect is discussed in more detail in Chapter 4. Thermodynamic properties have also been determined from the temperature dependence of the individual rate constants shown in (1.9).[44-48] The rate constants were extracted from the complete analyses of steady-state data and the decay curves of the emitting states formed on excitation by ultra-violet light pulses in the nanosecond time domain.[40] In non-polar solvents binding energies as large as 12 kcal.mole^{-1} have been found while the loss of entropy has been calculated for many systems to be 20 e.u. or more.

The effect of solvent on exciplex properties has been a very controversial area of research in recent years. In general, with increase in solvent polarity both the fluorescence quantum yield, ϕ_E, and the decay time, τ_E, have been observed to decrease.[55,56] Two interpretations have been proposed to account for these observations. (a) Knibbe et al[55] have suggested that a non-fluorescent solvated radical ion pair $A_S^- \cdots D_S^+$ is formed directly from the encounter of A* and D with a rate constant $k_I(\varepsilon)$ that increases with solvent polarity. This process competes with the exciplex (AD)* formation reaction which has a rate constant, k_3, that is independent of solvent polarity. In polar solvents $k_I(\varepsilon)$ will increase thus reducing the quantum yield of exciplex fluorescence by the solvent-dependent factor $k_3/\{k_3 + k_I(\varepsilon)\}$ without affecting the exciplex lifetime. However, $A_S^- \cdots D_S^+$ can also result from ionic dissociation within (AQ)*, a process which again is dependent on solvent polarity; this process is held responsible for the observed decrease in the lifetime in more polar solvents. (b) Mataga et al[56] proposed a solvent-induced change in the electronic structure of the exciplex. As discussed previously the exciplex is considered to be a resonance hybrid of the electron transfer configuration (A^-D^+) mixed with the locally excited configuration (A*D). Mataga et al argue that, on the one hand, mixing of these configurations leads to an increase of the binding energy, but on the other hand such an interaction decreases the dipole moment of the complex. In more polar solvents electrostatic stabilisation of the charge-transfer configuration will result in an increase in the weight of the charge-transfer contribution, a_1, to the total wave function, $\Psi_{EXCIPLEX}$ in eq.(1.8), and thus increasing the dipole moment of the complex. k_5, the radiative rate

constant for exciplex decay (see kinetic scheme in (1.9)) is related to the transition dipole moment $\bar{M}_E$ for the exciplex through the equation,[59]

$$\bar{M}_E = \left| \frac{3\, hc^3\, k_5}{64\pi^4 n\, \nu_E^3} \right|^{\frac{1}{2}} \qquad (1.10)$$

$\bar{M}_E$ in turn is given by:

$$\bar{M}_E = \langle \Psi_E | \bar{\mu}_{op} | \Psi_G \rangle \qquad (1.11)$$

in which $\bar{\mu}_{op}$ is the electric dipole moment operator. Ψ_E is given by eqn.(1.9) and Ψ_G, the wave function for the dissociative ground state, is given by,

$$\Psi_G = \Psi_o(AD) \qquad (1.12)$$

If the second and fourth terms are neglected in eqn.(1.8), as previously discussed, $\bar{M}_E$ is then given by,

$$\bar{M}_E = a_1 \langle \Psi_1(A^-D^+) | \bar{\mu}_{op} | \Psi_o(AD) \rangle + a_3 \langle \Psi_3(A^*D) | \bar{\mu}_{op} | \Psi_o(AD) \rangle \qquad (1.13)$$

The matrix element $\langle \Psi_3(A^-D^+) | \bar{\mu}_{op} | \Psi_o(AD) \rangle$ is approximately proportional to the overlap of the donor orbital in D and the acceptor orbital in A;[59] consequently it is rather small and decreases with increasing intermolecular distance. As the exciplex becomes more ionic a_3 decreases; thus, the dominating term in $\bar{M}_E$, $a_3 \langle \Psi_3(A^*D) | \bar{\mu}_{op} | \Psi_o(AD) \rangle$ decreases in more polar solvents. This therefore results in a decrease in k_5 with increasing solvent polarity. Mataga et al[56] also argue that ionic dissociation of the exciplex in polar solvents will cause an increase in the non-radiative rate, k_6. This is therefore another possible

mechanism which must be considered when attempting to rationalise the effect of solvent polarity on ϕ_E and τ_E.

Definitive experimental evidence for either one of these mechanisms is scarce.[48,57,58] In a detailed study on the Pyrene-N,N Dimethylaniline exciplex employing photoconductivity and laser flash photolysis techniques[57] it was shown that radical ions were formed very rapidly in the highly polar solvents acetonitrile (ε = 37.5) and acetone (ε = 20.7) and hence that mechanism (a) was in all likelihood followed. However, with decrease in solvent polarity the photocurrent was drastically reduced. In n-hexane (ε = 1.89) although no ion formation could be detected by photocurrent measurements, weak transient absorptions, similar to those of the pyrene anion, were detected. These were tentatively assigned to absorptions by the polar exciplex. Thus in this case it was more difficult to make a definite statement about the mechanism. In moderately polar solvents, ε = 5 - 12, small photocurrents were measured and mechanism (a) seemed to be more suitable than (b), although it was suggested that continuous structural change of the exciplex was probably playing a minor role in its decay processes. O'Connor and Ware[45,48] were able to extract values for individual rate constants and their temperature coefficients for the formation and decay processes of the α-Cyanonaphthalene/1,2 Dimethylcyclopentene system in three solvents, n-hexane (ε = 1.89), diethylether (ε = 4.3) and ethyl acetate (ε = 6.0). The radiative rate constant was shown to decrease with increasing solvent polarity, an effect caused by mechanism (b). However, k_6 exhibited a slight decrease which is more difficult to rationalise using current theories of solvation effects. Meeus et al,[58] again from a detailed kinetic study, measured an increase in the non-radiative rate constant, k_6, for the 2-Methylnaphthalene/

N-methyl-piperidine system in going from a non-polar solvent to a moderately polar solvent. Such an increase is expected but they also measured an increase in k_5 which, again, is difficult to explain. Owing to the nature of the experiments performed by O'Connor and Ware[45,48] and Meeus et al,[58] the formation of radical ions would be difficult to detect. To summarise, in highly polar solvents, such as acetonitrile, Taniguchi et al have confirmed that the mechanism (a), first proposed by Knibbe et al,[55] is being followed. No definite statements, however, can yet be made from the studies in non-polar and moderately polar solvents. Thermodynamic properties have also been measured as a function of solvent polarity; however the reported trends fit no consistent pattern.[29,45,48,52,53,58,59] As is therefore evident the effect of solvent on exciplex properties is not yet very well understood. A comparison with the properties of a vapour phase exciplex, where such solvation effects are absent could shed more light on the above problems.

Until very recently the only observations of emission from exciplexes formed in the vapour phase were those involving either Mercury (^3P_o)[60-62] or Cadmium (^3P_o)[63] atoms as excited state partners. In 1978 Phillips et al[64-66] reported the growth of a broad, structureless emission band red-shifted from the fluorescence of photo-excited 9-cyanoanthracene (9CNA) on the addition of any one of the following easily ionisable amines, N,N dimethyl-aniline (DMA), triethylamine (TEA) or tri-n-butylamine (TBA). The experiments were performed at elevated temperatures such that all the components of each mixture were in the vapour phase. This work forms part of this thesis and, as will be discussed in Chapter 3, these were the first observations of fluorescent exciplexes formed between complex polyatomic molecules in the vapour phase. Subsequent to this discovery there have

been studies by Lim et al[67,68] on vapour phase exciplexes formed in mixtures of electronically excited tetracyanobenzene (TCNB) and a variety of methylated benzenes. From the analysis of steady-state spectroscopic and quenching data these workers suggested that the feedback process, k_4 in (1.9), was relatively unimportant in such systems. However, they were unable to measure individual rate constants due to the lack of sensitivity and time resolution in their conventional lifetime apparatus. Hirayama[69] has also characterised exciplex formation in vapour phase mixtures of any one of the following 9-cyanoanthracene derivatives, 9-cyano-10-ethylanthracene, 9-cyano-10-phenylanthracene or 9,10 dicyanoanthracene, in the presence of N,N-dimethylaniline. Exciplex emission has also been observed in vapour phase mixtures of 9,10 dicyanoanthracene and one of a variety of non-amine additives.[70]

There have been no detailed studies involving the measurement of the individual rate constants and their temperature coefficients for the various formation and depletion processes for a vapour phase exciplex. It is the purpose of the work described in Chapter 4 to fill this gap.

In Chapter 5 the electronic structures of some substituted aromatic hydrocarbons are predicted. The CNDO/S (with configuration interaction) semi-empirical molecular orbital method was used to calculate the energies of the singlet and triplet excited electronic levels and the oscillator strengths for ground state to singlet excited state electronic transitions. The results were used in conjunction with a group theoretical analysis, to assign electronic bands in various vapour phase singlet-singlet and triplet-triplet absorption experiments.[71,72] Since these calculations do not include the effect of solvent the method used would probably be of

value in predicting the properties of excited state dimers and complexes in the vapour phase. The present calculations are a first step towards achieving this goal.

In Chapter 6, the detection limits of sulphur dioxide are determined using a novel sampling technique.

REFERENCES

1. H. Leonhardt and A. Weller, Ber.Bunsenges.Phys.Chem., 67, 791 (1963).

2. J. B. Birks in "The Exciplex", M. Gordon and W. R. Ware, Eds. Academic Press, New York, 1975.

3. E. C. Lim (Ed.),"Molecular Luminescence", p.907, W. A. Benjamin Inc., New York, 1969.

4. Th. Förster and K. Kasper, Z.Phys.Chem., N.F. 1, 275 (1954).

5. H. Beens and A. Weller in "Molecular Luminescence", E. C. Lim, Ed., Academic Press, New York, 1975.

6. H. Beens and A. Weller, Chem.Phys.Lett., 2, 82 (1968).

7. D. Creed and R. A. Caldwell, J.Am.Chem.Soc., 96, 7369 (1974).

8. R. A. Caldwell, D. Creed and H. Ohta, J.Am.Chem.Soc., 97, 3246 (1975).

9. K. H. Grellman and U. Suckow, Chem.Phys.Lett., 32, 250 (1975).

10. J. Saltiel, D. E. Townsend, B. D. Watson and P. Shannon, J.Am.Chem.Soc., 97, 5688 (1975).

11. A. Nakajima, Journal of Luminescence, 16, 279 (1978).

12. E. A. Chandross and H. T. Thomas, Chem.Phys.Lett., 9, 393 (1971).

13. T. Okada, T. Fujita, M. Kubota, S. Masaki, N. Mataga, R. Ide, Y. Sakata and S. Misumi, Chem.Phys.Lett., 14, 563 (1972).

14. G. S. Beddard, R. Davidson and A. Lewis, J.Photochem., 1, 491 (1973).

15. M. Itoh, T. Mimura, H. Usui and T. Okamoto, J.Am.Chem.Soc., 95, 4388 (1973).

16. N. Nakashima, M. Murakawa and N. Mataga, Bull.Chem.Soc.Japan, 49, 854 (1976).

17. S. Masaki, T. Okada, N. Mataga, Y. Sakata and S. Misumi, Bull.Chem. Soc.Japan, 49, 1277 (1976).

18. P. J. Wagner and D. A. Ersfeld, J.Am.Chem.Soc., 98, 4515 (1976).

19. B. Stevens and M. I. Ban, Trans.Faraday Soc., 60, 1515 (1964).

20. A. Weller, Pure Appl.Chem., 16, 115 (1968).

21. H. Knibbe and A. Weller, Z.Phys.Chem., N.F. 56, 99 (1967).

22. H. Beens and A. Weller, in "Organic Molecular Photophysics", Vol.2, J. B. Birks, Ed., Wiley-Interscience, London, 1975.

23. H. Yamashiti, H. Kokubun and M. Koizumi, Bull.Chem.Soc.Japan, 41, 2312, (1968).

24. A. J. Bard and S. M. Park, in "The Exciplex", M. Gordon and W. R. Ware, Eds., Academic Press, New York, 1975.

25. A. Weller and K. A. Zachariasse, Chem.Phys.Lett., 10, 590 (1971).

26. H. Tachikawa and L. R. Faulkner, J.Am.Chem.Soc., 98, 5569 (1976).

27. A. Weller in "The Exciplex", M. Gordon and W. R. Ware, Eds., Academic Press, New York, 1975.

28. N. Mataga and K. Ezumi, Bull.Chem.Soc.Japan, 40, 1355 (1967).

29. H. Knibbe, Ph.D. Thesis, Free University, Amsterdam (1969).

30. H. Knibbe, D. Rehm and A. Weller, Z.Phys.Chem., N.F. 56, 96 (1967).

31. H. Knibbe, D. Rehm and A. Weller, Ber.Bunsenges.Phys.Chem., 73, 839 (1969).

32. D. Rehm and A. Weller, Z.Phys.Chem., N.F. 69, 183 (1970).

33. H. Beens and A. Weller, Acta Phys.Polon., 34, 593 (1968).

34. N. Mataga, T. Okada and N. Yamamoto, Bull.Chem.Soc.Japan, 39, 2562 (1966).

35. H. Beens, H. Knibbe and A. Weller, J.Chem.Phys., 47, 1183 (1967).

36. M. G. Kuzmin and L. N. Guseva, Chem.Phys.Lett., 3, 71 (1969).

37. Th.Förster and K. Kasper, Z.Elektrochem., 59, 976 (1955).

38. R. S. Mulliken, J.Am.Chem.Soc., 74, 811 (1952).

39. E.J.J. Groenen and P. N.Th. Van Velzen, J.Mol.Phys., 35, 19 (1978).

40. W. R. Ware, Pure Appl.Chem., 41, 635 (1975).

41. J. B. Birks, D. J. Dyson and I. H. Munro, Proc.Roy.Soc.London, Ser.A, 275, 575 (1963).

42. N. Mataga, T. Okada and K. Ezumi, J.Mol.Phys., 10, 201 (1966).

43. W. R. Ware and H. P. Richter, J.Chem.Phys., 48, 1595 (1968).

44. W. R. Ware, D. Watt and J. D. Holmes, J.Am.Chem.Soc., 96, 7853 (1974).

45. D. V. O'Connor and W. R. Ware, J.Am.Chem.Soc., 98, 4076 (1976).

46. D. Creed, P. H. Wine, R. A. Caldwell and L. A. Melton, J.Am.Chem.Soc., 98, 621 (1976).

47. M. H. Hui and W. R. Ware, 98, 4718 (1976).

48. D. V. O'Connor and W. R. Ware, J.Am.Chem.Soc., 101, 121 (1979).

49. A. M. Halpern, J.Am.Chem.Soc., 96, 4392 (1974).

50. D. Rehm and A. Weller, Israel J.Chem., 8, 259 (1970).

51. N. Nakashima, N.Mataga, F. Ushio and C. Yamanaka, Z.Phys.Chem., N.F., 79, 150 (1972).

52. T. Okada, N. Matsui, H. Oohari, N. Matsumoto and N. Mataga, J.Chem.Phys., 49, 4717 (1968).

53. S. Murata, H. Kokubun and M. Koizumi, Z.Phys.Chem., N.F., 70, 47 (1970).

54. R. J. McDonald and B. K. Selinger, Mol.Photochem., 3, 99 (1974).

55. H. Knibbe, K. Röllig, F. P. Schäfer and A. Weller, J.Chem.Phys., 47, 1184 (1967).

56. N. Mataga, T. Okada and N. Yamamoto, Chem.Phys.Lett., 1, 119 (1967).

57. Y. Taniguchi, Y. Nishina and N. Mataga, Bull.Chem.Soc.Japan, 45, 764 (1972).

58. F. Meeus, M. Van der Auweraer and F. C. De Schryver, J. Am.Chem.Soc., 102, 4017 (1980).

59. N. Mataga and T. Kubota in "Molecular Interactions and Electronic Spectra", Marcel Dekker, New York, 1970.

60. C. G. Freeman, M. J. McEwan, R.F.C. Claridge and L. F. Phillips, Chem.Phys.Lett., 9 571 (1971).

61. K. Luther, H. R. Wendt and H. E. Hunziker, Chem.Phys.Lett., 33, 146 (1975).

62. A. B. Callear and C. G. Freeman, Chem.Phys.Lett., 45, 204 (1977).

63. P. D. Morten, C. G. Freeman, M. J. McEwan, R.F.C. Claridge and L. F. Phillips, Chem.Phys.Lett., 16, 148 (1972).

64. S. Hirayama, G. D. Abbott and D. Phillips, Chem.Phys.Lett., 56, 497 (1978).

65. S. Hirayama and D. Phillips, J.Chem.Soc., Faraday Trans.II, 74, 2035 (1978).

66. G. D. Abbott, C. G. Cureton, K. Hara, S. Hirayama and D. Phillips, J.Photochem., 9, 260 (1978).

67. J. Prochorow, S. Okajima and E. C. Lim, Chem.Phys.Lett., 66, 590 (1978).

68. S. Okajima and E.C. Lim, Chem.Phys.Lett., 70, 283 (1980).

69. S. Hirayama, Chem.Phys.Lett., 63, 596 (1979).

70. S. Hirayama and D. Phillips, J.Phys.Chem in press.

71. M.E. Sime, Ph.D. Thesis, University of Southampton, 1978.

72. R.D.S. Stevens, R. Bonneau, J. Joussot-Dubien, J.Chem.Phys. 57, 5340 (1972).

CHAPTER TWO

EXPERIMENTAL

CHAPTER TWO

EXPERIMENTAL

2.1. STEADY STATE FLUORESCENCE SPECTRA

The steady-state fluorescence emission and excitation spectra were recorded on a home-built spectrofluorimeter, a block diagram of which is shown in figure 2.1. This instrument was designed to obtain spectra of higher sensitivity and superior resolution than the commercially available fluorimeters which was very important in this work due to the low quantum yield of emission of vapour phase exciplex systems. The light from a Xenon 450W lamp (L) (Wotan Type XBO 450 W/2), powered by a voltage and current stabilised power supply (PS), was focussed onto the entrance slits of a Bausch and Lomb High Intensity monochromator, M1 (model 33-86-76, reciprocal dispersion = 3.2 nm/mm). The wavelength-resolved excitation light was then collected and focussed by a second lens into the sample chamber (S) which was designed to accommodate a high temperature furnace, see Section 2.5.The furnace heated a suprasil quartz cuvette (1 x 1 cm) in which the sample was contained. The total transmitted intensity of the excitation beam passing through the cell was monitored by an RCA photodiode (P) and displayed on a microammeter (MA). Sample fluorescence emerging at 90^{o} to the excitation beam was wavelength resolved by an emission monochromator (M2), a Hilger-Watts D330 grating monochromator (reciprocal dispersion = 2.8 nm/mm) and detected by an RCA 1P28 photomultiplier tube (PT) which was powered by an Isotope Development Ltd. power supply (HT) operated at 1 kV. The P.M.T. signal was measured by a Victoreen picoammeter (PA) and recorded on a Servoscribe RE 542 Chart Recorder (CR). The monochromators were calibrated using the emission lines of a low pressure mercury lamp.

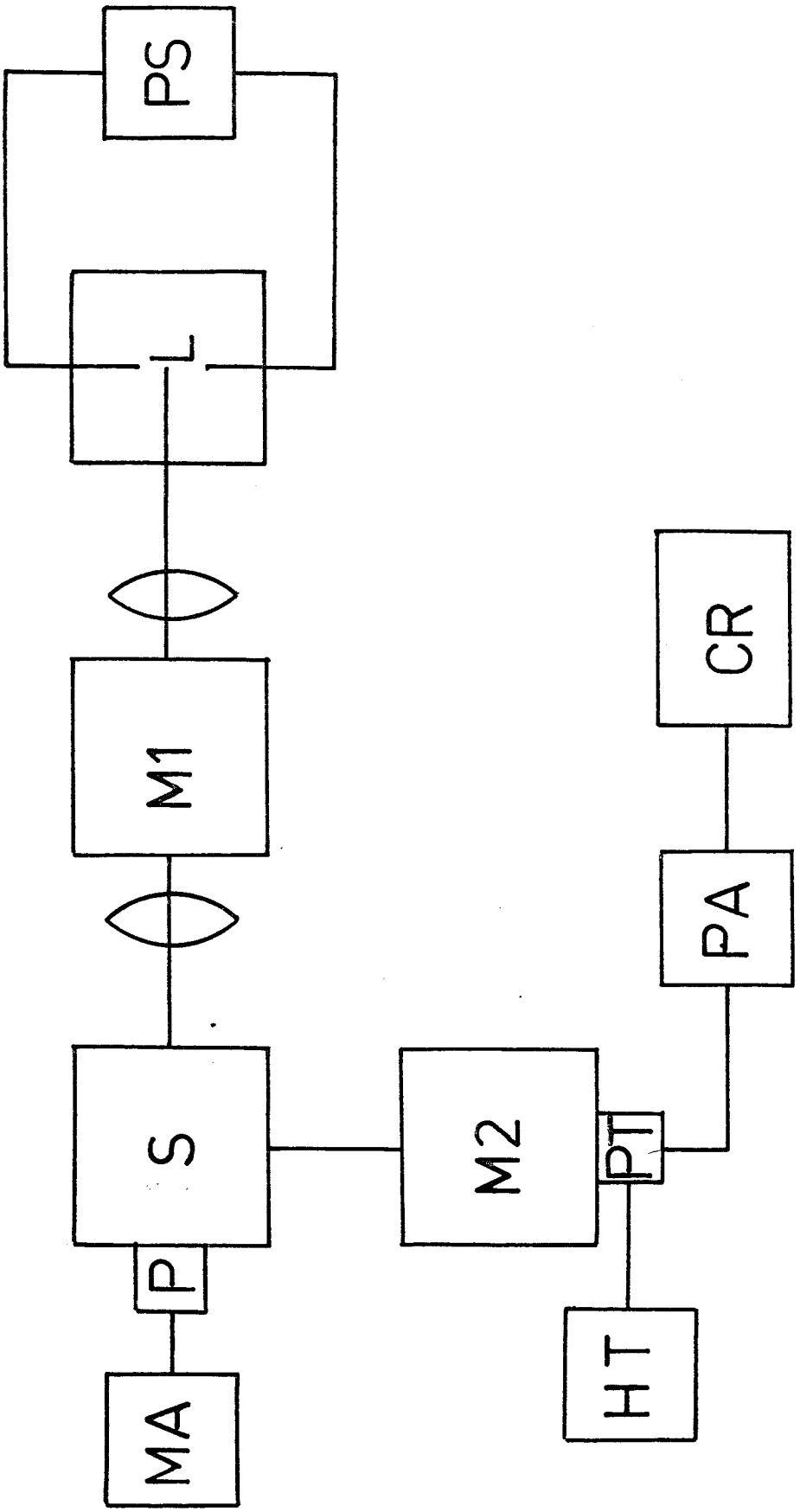

FIGURE 2.1. HOME-BUILT SPECTROFLUORIMETER

2.2. MEASUREMENT OF FLUORESCENCE LIFETIMES

2.2.1. Time-Correlated Single Photon Counting.

Fluorescence decay curves were collected using time-correlated single photon counting which is now widely used in the investigation of the behaviour of excited states.[1-4] In this technique, see figure 2.2, a sample is repetitively excited with short pulses of light, the duration of the excitation pulse depending on the excitation source being used. When an excitation pulse is emitted an electrical signal is generated through a wire pick-up in the lamp body and this is timed by a constant fraction timing discriminator (CFTD) which sends a square-wave logic pulse to the START input of a time-to-amplitude converter TAC. At this time a voltage ramp is initiated, which increases linearly with time in the TAC. On absorption of the excitation pulse the sample fluoresces and when a single fluorescent photon impinges on the photocathode of a high-gain fast photomultiplier (PT) an anode pulse is sent to another CFTD which provides a logic pulse for the STOP instruction of the TAC - this terminates the voltage ramp. The amplitude reached by the voltage ramp is proportional to the time difference between START and STOP and is sent to a multichannel pulse height analyser (MCPHA) in the form of a voltage pulse where one count is added in the analyser memory to the channel that corresponds to the amplitude of the pulse. The time width per channel can be varied by selecting a time range for the full scale of the TAC ramp which corresponds to the total width of the MCPHA memory. When a sufficient number of counts have been collected in the analyser the number of counts in each channel is proportional to the probability of fluorescence emission in the time interval Δt at time $n \Delta t$, where n is the channel number and Δt the channel width in nano-

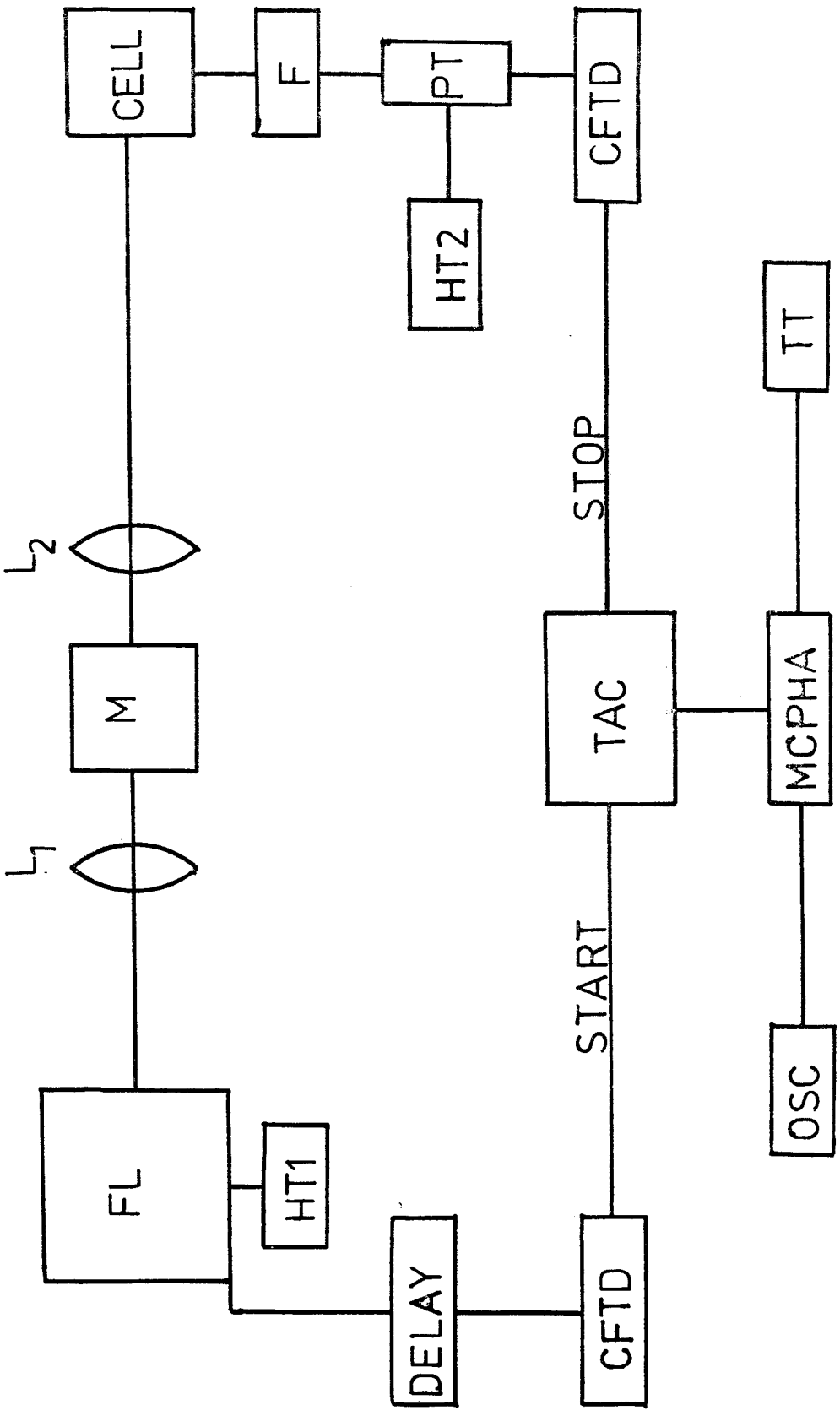

FIGURE 2.2. TIME-CORRELATED SINGLE PHOTON COUNTING APPARATUS

seconds. Thus the resultant histogram of the number of photons counted with time is directly proportional to the decay profile of the sample fluorescence. The contents of the MCPHA memory can be viewed at any time on an oscilloscope (OSC) and at the end of the experiment are then read out on a Data Dynamics ASR 33 teletype (TT) and stored on paper tape. Computer analysis was achieved on an ICL 2970 with Calcomp graphical plotting facilities.

a) Conventional Free-Running Spark Discharge Lamp.

For some of this work a conventional spark discharge lamp[5] (FL) was used as the excitation source in the above described experiment. The lamp was filled with hydrogen[5,6] to a pressure of 400 torr from a vacuum line and was discharged between two tungsten electrodes which were positioned about 1-2 nams. apart. A Brandenburg 807R stabilised power supply (HT1) was used to power the lamp at voltages between 5 and 7 kV. The repetition rate of the lamp, the frequency of the discharge, was found to increase when either the operating voltage was increased or the spark gap decreased but this was accompanied by a concomitant decrease in pulse intensity. Normally the lamp was operated at a repetition rate of 100 kHz which gave a pulse of full width half maximum (FWHM) of 6 nsecs.

b) Electronics and Optics.

As illustrated in figure 2.2 the light from the flash lamp (FL) was focussed by a lens (L_1) onto the entrance slits of a Hilger and Watts D330 monochromator (M) (linear dispersion - 2.6 nms/mm). The excitation light was then focussed onto the sample cell by another lens (L_2). Fluorescence was then monitored at 90° to the axis of the excitation light by a Mullard 56 DUVP PT operated at 2.5 kV. In some experiments a glass

filter (F) had to be placed in front of the PMT to exclude scattered light from the fluorescence. Corning (0-53) and (0-54) filters were found to be the most useful. The photomultiplier tube was chosen on the following criteria: (1) A fast transit time (the time taken for the photoejected electron to reach the anode). (2) A small transit time jitter (the difference in transit time of successive electrons). (3) A large signal-to-noise ratio (most noise arises from thermionic emission which results in a 'dark' count). The CFTD's were both Ortec 463 types. A pulse is rejected by a CFTD when its voltage amplitude is below a set threshold level.

It was necessary to ensure that the ratio of STOP/START counts was less than 1:100 to prevent pulse pile-up occurring.[4,7] Pulse pile-up is the situation when the number of STOP counts has reached such a high level that the TAC is biased towards early arriving photons. An RCS 250 MHz Counter/Timer was used to monitor the lamp START and PT STOP count rates. A Northern Scientific NS 600 MCPHA, operated in the pulse height analysis mode, was used to store the data. The calibration of the channel width of the MCPHA was made by using an arrangement[8] given in figure 2.3.

c) Calibration of the TAC/MCPHA combination.

A Spectra-Physics cavity dumper C/D (Model 366), see later (PULSED LASERS section (b)) for a more detailed description of this component, was used to provide stable R.F. pulses. The same pulse from the C/D triggered the START input of the TAC as was used, after a suitable set delay, to STOP the voltage ramp. This was repeated until a sufficient number of counts had been collected in the memory channel of the MCPHA which corresponded to that delay time. Thus by increasing the delay in

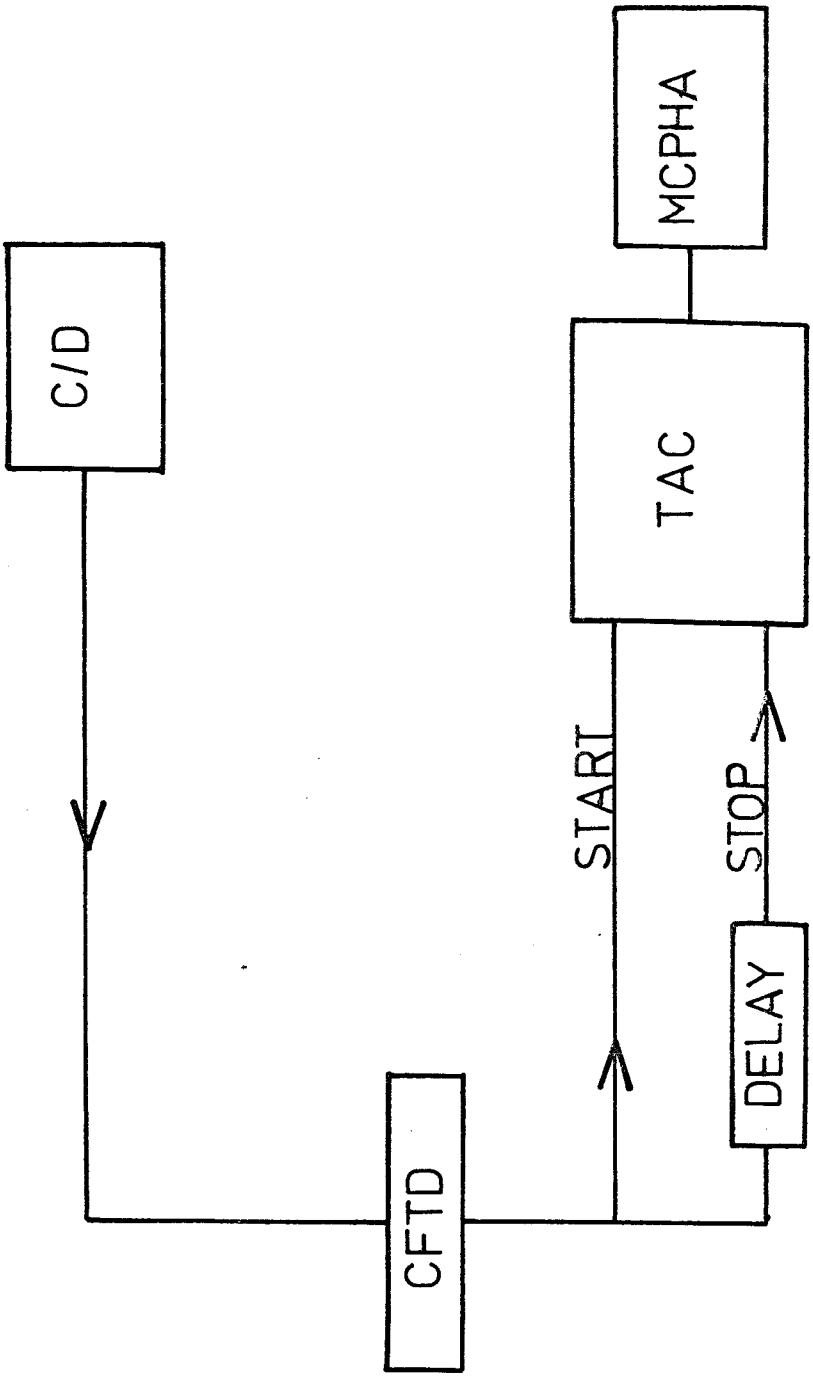

FIGURE 2.3. CALIBRATION OF THE TAC/MCPHA COMBINATION

suitable increments the delay time was plotted as a function of channel number. This plot results in a straight line, the gradient of which gives the channel width (nanoseconds/channel) of the MCPHA. This was carried out after each experiment had been completed.

2.2.2. Pulsed lasers

Pulsed lasers are an ideal excitation source for time-correlated single photon counting[9,10,11] since they provide a convenient source of stable, short, high-intensity pulses at high repetition rates. The high pulse intensity and repetition rate allow short data collection times, and, owing to the high stability of the pulse profiles, deconvolution procedures may be used with confidence. The light issuing from the laser is also very intense, well collimated, polarised and monochromatic, therefore no excitation monochromator is required. In the present work most of the fluorescence lifetimes were measured on a dye laser set-up shown in figure 2.4.[9] The lifetimes of the vapour phase exciplexes, which had low quantum yields of fluorescence, were measured using a more intense excitation source, the synchronously pumped dye laser system which is illustrated in figure 2.6. Dye lasers have been reviewed by Schaefer.[12]

a) The Dye Laser.

A Spectra-Physics model 166 Argon ion laser, operated CW all lines, with an output power of 3 - 3.5 watts was used to drive a jet-stream dye laser, Coherent Radiation model 590. The Ar^+ laser beam was focussed onto a flat sheet of dye passing from the dye jet (DJ) by the mirror A, where the dye solution (Rhodamine 6G in ethylene glycol) was pumped through the laser at a pressure of 40 p.s.i. Thus stimulated emission was induced in the dye and hence lasing occurred, where the dye laser cavity lies between

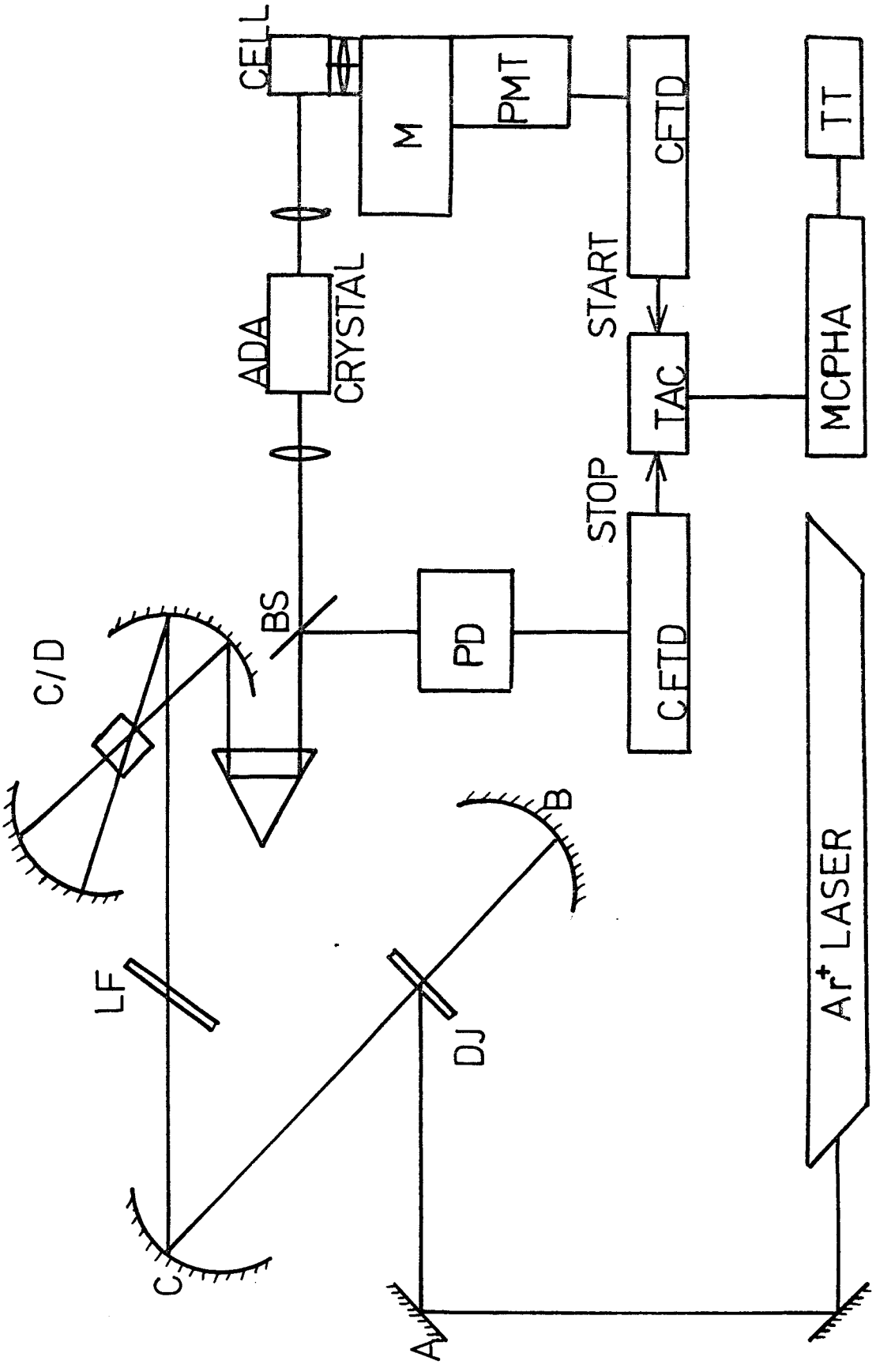

FIGURE 2.4. DYE LASER

mirror B and the cavity dumper C/D. Wavelength selection in the range 575-640 nms was achieved by using a 2-plate birefringent filter (LF) which was placed in the dye laser cavity. The cavity dumper (C/D), Spectra-Physics model 366, positioned at the output end of the laser replaced the normal output coupler. The mirrors in the C/D gave maximum reflectance to light at a wavelength of 600 nms.

b) The Cavity Dumper.[13]

Pulses of R.F. power were transmitted at a set frequency to the transducer (T), shown in figure 2.5, which was located on the non-optical face of a Bragg cell (BC) thus an acoustic wave train of the same frequency was set up across the cell. As an acoustic wave travels across the cell local variations in the refractive index will be induced such that the C.W. output from the dye laser, which is normally reflected off a mirror at point A through the Bragg cell and onto point D, is diffracted to point C and then reflected back to point B and emerges from the laser cavity via a prism as a pulse of laser light. The cavity dumper was operated at a frequency of 5 MHz which gave pulses with an average power of 100 mW and a peak power of 20W. The pulses were 'dumped out' at a period of 200 nanoseconds and had a F.W.H.M. equal to 10 nanoseconds.

c) Second Harmonic Generation.[14,15]

Most molecular systems of interest absorb light in the ultra-violet region and thus the tunable 575-640 nm. dye laser radiation must be frequency doubled. This was achieved by passing the laser output through a 90° pulse-matched angle and temperature tuned ADA crystal (JK Lasers) which resulted in second harmonic generation giving UV pulses tunable in the region 290-305 nms. On frequency doubling the pulse width was reduced

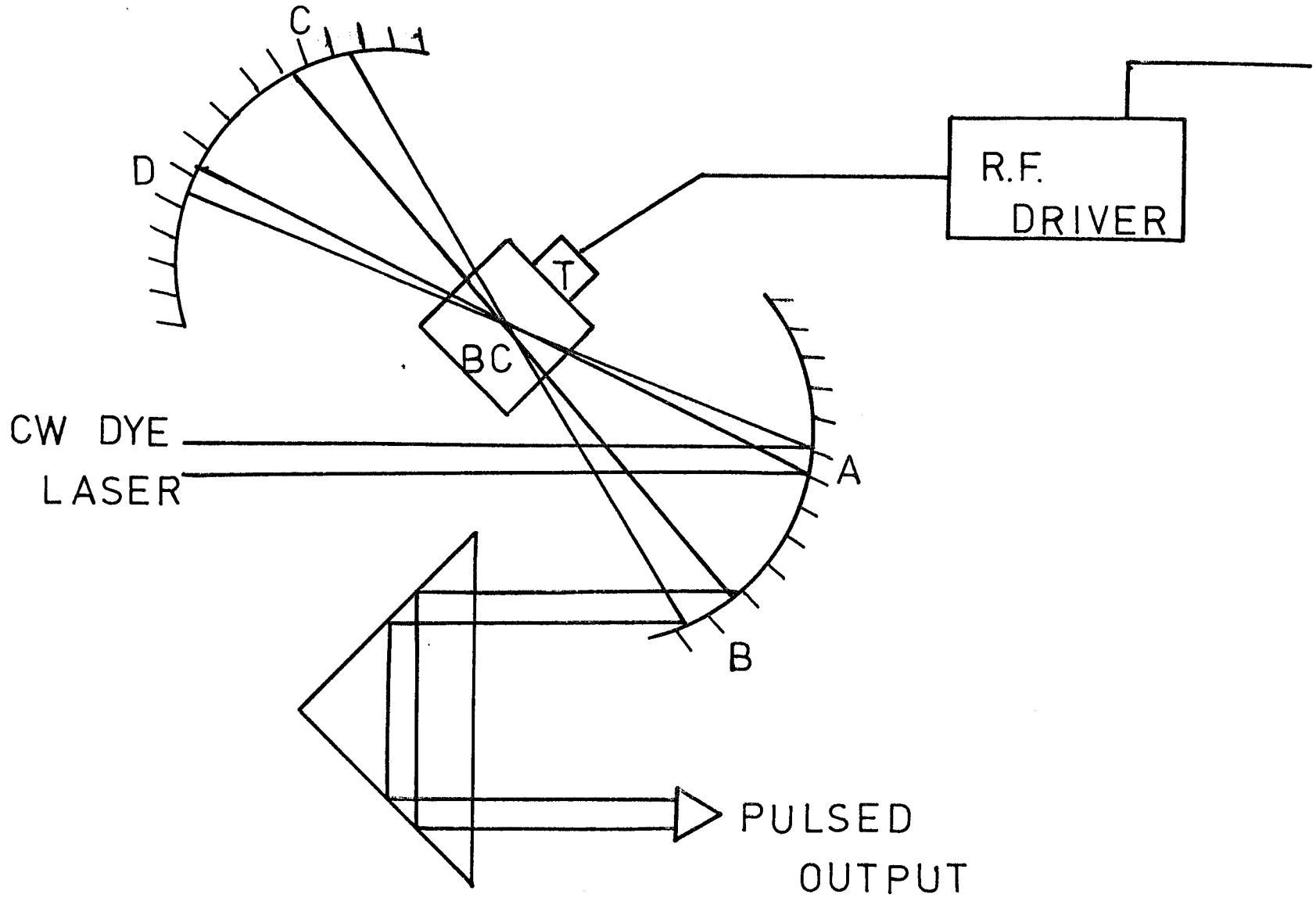

FIGURE 2.5. CAVITY DUMPER

by a factor equal to $(2)^{\frac{1}{2}}$ so that the F.W.H.M. of the doubled pulse was shortened to 7 nanoseconds. This is because the conversion efficiency is proportional to the square of the intensity of the fundamental.

d) Fluorescence Detection and Measurement of Fluorescence Lifetime.

Upon excitation the sample fluoresces and the fluorescence was wavelength resolved using a Monospek 1000 1 m. grating monochromator, M, (dispersion - 0.8 $nms.mm^{-1}$) and detected using a high-gain fast photo-multiplier (Mullard 56 DUVP), PMT. The method used for lifetime measurements was time-correlated single photon counting as described in section 2.2.1. However, an important difference in the use of a laser as an excitation source was that the TAC was used 'backwards',[9] i.e. the PMT pulses resulting from emitted photons were used to start the TAC voltage ramp and the excitation pulses immediately following the emitted pulses activated the STOP input. This inverted arrangement is employed because the TAC will not operate with a START pulse rate greater than about 200 kHz so that since the repetition rate of the laser excitation pulses is 5 MHz the normal arrangement, as described in section 2.2.1, becomes redundant. The count rate of the fluorescence intensity is always or can easily be attenuated to less than 200 kHz.

There are two possible methods for generating a STOP pulse, either:

a) As shown in figure 2.4 a beam splitter (BS) can be used to reflect a portion of the excitation pulse onto a fast photodiode, PD, which emits a signal via a CFTD to the STOP input of the TAC or

b) A logic pulse from the cavity dumper driver, which is synchronised with the excitation pulse, can be used as the STOP instruction. Tests have shown that there are no differences in the timing of single photons between these two methods.

The constant fraction discriminators (CFTD) and the TAC were Ortec models 463 and 473A respectively. The multichannel analyser was a Northern Scientific Model NS-600 (MCPHA).

e) Synchronously Pumped Mode Locked Dye Laser System.

The vapour phase exciplex has a very low absolute quantum yield of fluorescence and hence in order to measure the exciplex lifetime accurately using the time-correlated single photon counting method it was necessary to use an excitation source which was capable of generating high intensity and short width pulses. These requirements are satisfied by synchronously pumping a C.W. dye laser with a mode-locked argon ion laser, where tunable picosecond pulses with peak powers of 1 to 2 kW have been produced.[10,11,16-20]

In this work the experimental system, schematically illustrated in figure 2.6, incorporated a Spectra-Physics model 342 Mode Locker, ML, which was inserted in the cavity of a Spectra-Physics model 171 Argon Ion laser. The mode-locker, an opto-acoustic device, consisted of a piezo-electric transducer which was positioned on a non-optical face of the wavelength selection prism placed at one end of the laser cavity. A modulated R.F. signal from the mode-locker driver (Spectra-Physics model 452) is converted by the transducer into an acoustic standing wave in the quartz prism - this creates regions of compression and rarefraction across the prism and thus there is a spatially and temporally periodic change in the index of refraction. This causes a periodic loss in the laser cavity and if the modulating frequency, f_m, is set equal to the frequency difference between the longitudinal cavity modes of the laser, i.e. $f_m = c/2L$ where L is the cavity length and c is the speed of light, then the cavity modes of the laser are forced to maintain a fixed phase

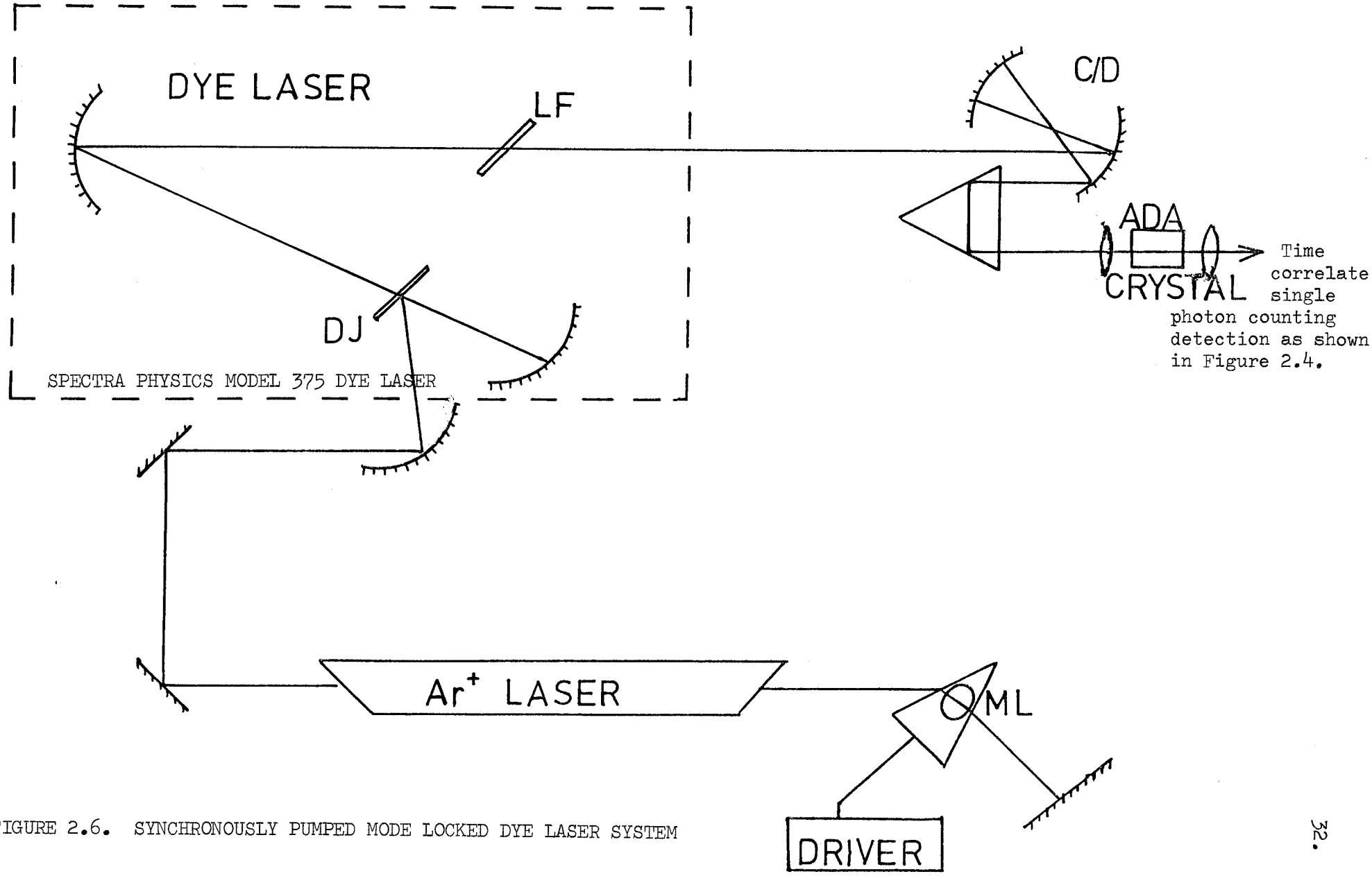

FIGURE 2.6. SYNCHRONOUSLY PUMPED MODE LOCKED DYE LASER SYSTEM

relationship with each other yielding a travelling pulse of light with a round-trip transit time of 2L/c. Thus the mode-locker acts as a shutter that opens and closes once during each round trip transit time of the laser light such that the pocket of light is at the shutter when the shutter is open and no light exists elsewhere in the cavity. If a normal output coupler is placed at one end of the cavity, then a train of short pulses, separated in time by 2L/c, will be emitted. This type of mode-locking is termed active, amplitude modulation mode-locking and has been reviewed.[21] In the experimental system used in this work the 514.5 nm argon ion emission line was mode-locked to give pulses of about 150 picoseconds F.W.H.M. with an average power of 800 mW. The pulses had a frequency period equal to the round trip time typically, where f_m equalled 80-100 MHz, giving a pulse separation of 10-12 nanoseconds. The pulse train from the pumping laser was then focussed onto the dye jet, DJ, of the tunable dye laser (Spectra-Physics model 375) producing mode-locked pulses in the dye laser cavity. In order that the coupling efficiency was maximised the cavity of the dye laser was extended so that the dye laser intermode spacing was an integral multiple of the argon ion laser mode locker frequency - this condition was fulfilled by matching the lengths of the dye laser cavity to the ion laser cavity to within $\pm$ 2×10^{-6} m. Thus, after the circulating dye laser pulse was generated inside the extended cavity, the dye jet was pumped synchronously by a pulse from the argon ion laser and a coincident dye laser pulse. This resulted in a continuous train of pulses with F.W.H.M. less than 10 picoseconds which were spaced by the cavity round-trip time of about 12 nanoseconds. Since this time interval was too short for the systems of interest a cavity dumper was

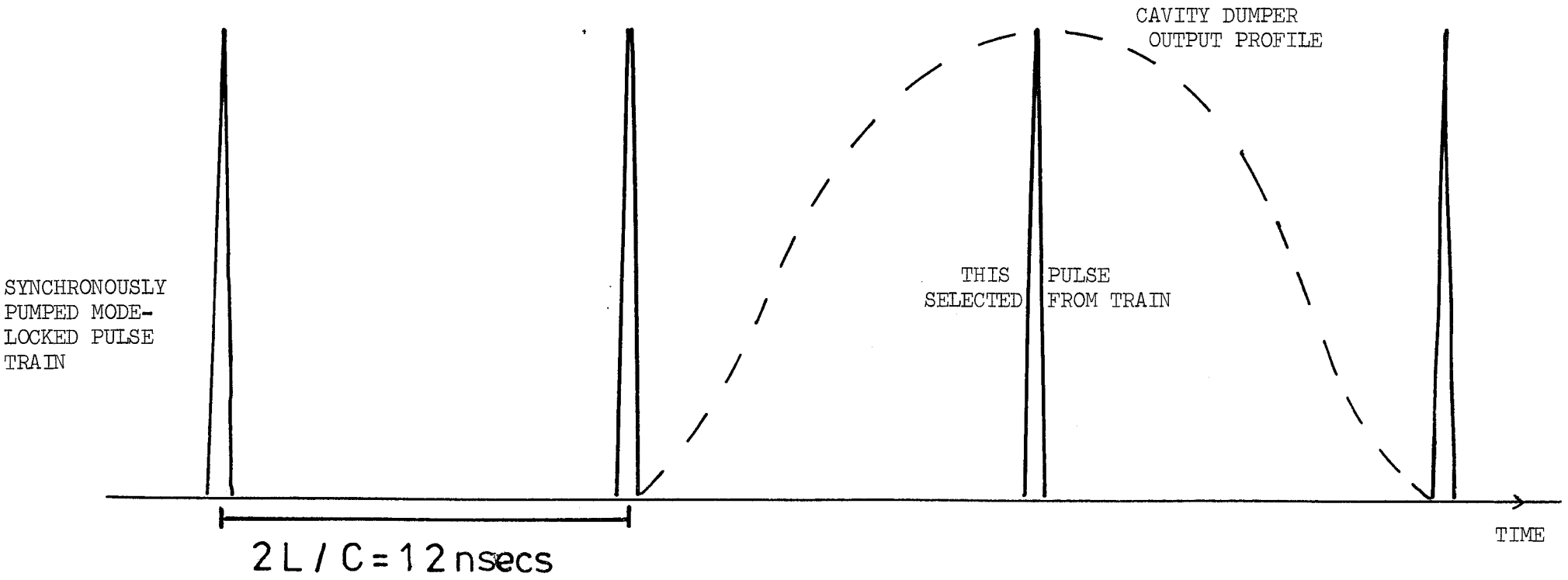
CAVITY DUMPER
OUTPUT PROFILE
SYNCHRONOUSLY
PUMPED MODE-
LOCKED PULSE
TRAIN
THIS PULSE
SELECTED FROM TRAIN
TIME
2L / C = 12 nsecs

FIGURE 2.7

used as a pulse selection device, as illustrated in figure 2.7, and since this was operated at a frequency equal to 5 MHz ,(see section 2.2.2(b)) , a train of short pulses with a separation of about 200 nanoseconds was obtained. This output excited the sample and the same method and experimental system, as described in section 2.2.2(d), detected and measured the excited state lifetimes. In this system a Mullard XP2020Q photomultiplier was used.

2.3. DATA ANALYSIS

Subsequent to excitation into its first excited singlet state a molecule can fluoresce or undergo various competing non-radiative processes. If the system is pulsed with an optical δ-function and there are no distortions introduced by the detector used to measure the fluorescence then the fluorescence will obey an exponential law:

$$G(t) = A \exp(-(\Sigma_i k_i)t) \qquad (2.1)$$

A is a pre-exponential factor determined by the amount of incident light absorbed and the fluorescence efficiency of the emitter. G(t) is the fluorescence intensity as a function of time and $\Sigma_i k_i$ is the sum of the rate constants of the various processes depleting the excited state. The fluorescence lifetime, τ , is defined as the time taken for the emission to decrease from any given value to 1/e times that value,

$$\text{i.e.} \quad \tau = 1/\Sigma_i k_i \qquad (2.2)$$

Significant deviations from the simple single exponential decay law often occur, e.g. if the fluorescence decay of two independently formed emitting excited states is observed then the intensity function will follow a

double exponential decay law, i.e. the decay will be a sum of two exponential decays.

$$G(t) = A_1 \exp\left(\frac{-t}{\tau_1}\right) + A_2 \exp\left(\frac{-t}{\tau_2}\right) \qquad (2.3)$$

where τ_1 and τ_2 are the lifetimes of the two states. Two component decays are also expected in the fluorescence of the excited state partner in an exciplex system. In practice, however, the true decay function cannot be measured directly. Firstly the excitation pulse is not a δ-function but has a finite width; thus measurements, such as those in this work, must often be made of fluorescent responses occurring in times comparable to the decay time of the excitation function itself. The measuring instrument also has an inherent limiting resolution time originating in distortions introduced by the photo-multiplier tube and the detection electronics. The effects of the excitation function and the instrument resolution are combined in an instrumental response function I(t). Thus the observed decay curve, F(t), is a convolution of the true decay of the sampler G(t) and the instrumental response function I(t). F(t) is thus expressed by a convolution integral:

$$F(t) = \int^{t} I(t').\, G(t-t').\, dt' \qquad (2.4)$$

To obtain I(t) experimentally the exciting pulse is scattered into the PMT and its profile is measured under the same conditions as are used to obtain the fluorescence decay curve. Following experimental measurement of both F(t) and I(t) the true decay law is extracted from the convolution integral by using a deconvolution procedure. A variety of techniques have been used to deconvolute fluorescence decay curves

and these have been reviewed in two recent articles.[22,23] The method used in this work was an iterative least squares convolution technique. Such a technique is recommended[22,23] especially for decay laws more complicated than a single exponential function or for measurements in which distortions of the decay data are present. A detailed description of the mathematics of this procedure has been given by Bevington[24] and its application to the analysis of fluorescence decay curves will be outlined in the following discussion. Fortran computer programs were available to analyse either single exponential or double exponential decays.

Firstly the most likely decay law for the sample fluorescence was predicted. For a single exponential trial values for the parameters A and τ (A_1, τ_1, A_2, τ_2 in the case of a trial double exponential function) were then chosen and submitted to the program. This trial function was then convoluted with the measured instrumental response function and the calculated convolution was compared with the experimental decay curve. The quality of the fit between the calculated result and the observed decay curve was judged by the value of the weighted sum of the squares of the residuals, χ^2 . χ^2 is given by

$$\chi^2 = \Sigma_i \; w_i \; (d_i)^2 = \text{CHI-SQUARED VALUE} \qquad (2.5)$$

where $d_i = Y(i) - Y(x_i)$ which is the residual for the ith channel, Y(i) being the observed data point and $Y(x_i)$ is the calculated value.

$$w_i \text{ (the weighting factor)} = \frac{1}{\sigma_i^2} \qquad (2.6)$$

where σ_i^2 is the variance, a measure of uncertainty, of each data point. In photon counting a Poisson distribution is sampled so that σ_i^2 is

derived from Poisson statistics and is simply the number of counts in the i'th channel.[25]

The values of the fitting parameters A and τ (or A_1, τ_1, A_2 and τ_2) are incremented or decremented iteratively until the χ^2 value reaches a minimum. At this stage the values of the fitting parameters obtained yield a decay law which, when convoluted with the measured instrument response function I(t), gives the most satisfactory fit to the observed decay curve F(t). On completion of the iterative procedure, in order to test the acceptability of the chosen fitting function, the 'goodness-of-fit' was judged by the value of the reduced chi-squared (χ^2_ν) function which is given by

$$\chi_\nu 2 = \frac{\chi 2}{\nu} \qquad (2.7)$$

ν is the number of degrees of freedom for the fitting procedure and equals the number of data points minus the number of fitting parameters. A good fit was indicated by a χ^2_ν value close to unity; if this requirement was not met it was likely that the wrong form for the trial decay function had been assumed. Calcomp graphical plots comparing the calculated with the experimental data points and a plot of the weighted residuals were used as a further guide in judging the quality of fit. Weighted residuals were calculated from the expression:

$$\text{Res}(i) = \frac{1}{\sigma i} \left(Y(i) - Y(x_i)\right) \qquad (2.8)$$

For a satisfactory fit the weighted residuals plot should show a random distribution about zero. As is the case with all curve-fitting procedures the simplest model that gives a satisfactory fit is taken as the most appropriate one. Thus if the decay data are well fitted by a

single exponential decay law then this is taken as the correct model for the decay curve. Only where a single exponential clearly failed to fit satisfactorily was recourse made to a double exponential function.

2.4. PREPARATION OF SAMPLE CELLS

As the technique for preparing samples for vapour phase work was novel a detailed description of the method will be given.

(a) A quartz cuvette, 1 cm. square, was attached to a length of glass tubing by a quartz-to-glass seal. Then using the appropriate glass blowing technique a Young's female connector (model PCJ5) was 'blown on' the end of the tubing and a constriction introduced 11 cms. from the bottom of the cuvette to give a cell of total length 18 cms. as shown in figure 2.8.(a)

(b) A very small weight, = 2×10^{-5} gms. of solid cyano-substituted naphthalene or anthracene (the excited species in the exciplex system) had to be added to each cell; this small weight was necessary since on sublimation at elevated temperatures this weight could give a pressure in the gas phase of about $\frac{1}{2}$ torr which is low enough to preclude any self-quenching effects such as excimer formation. In Stern-Volmer type quenching experiments this added weight must be the same for a range of samples. Obviously this could not be weighed out directly - the measurement would be too inaccurate. To overcome this problem a stock solution of the solid was made up in 100 mls. of n-pentane and then 0.5 mls. of this solution was pipetted into each cell. The solvent was then gently evaporated off by immersing the cell in warm water, thus leaving an accurately known weight of solid remaining in the cell.

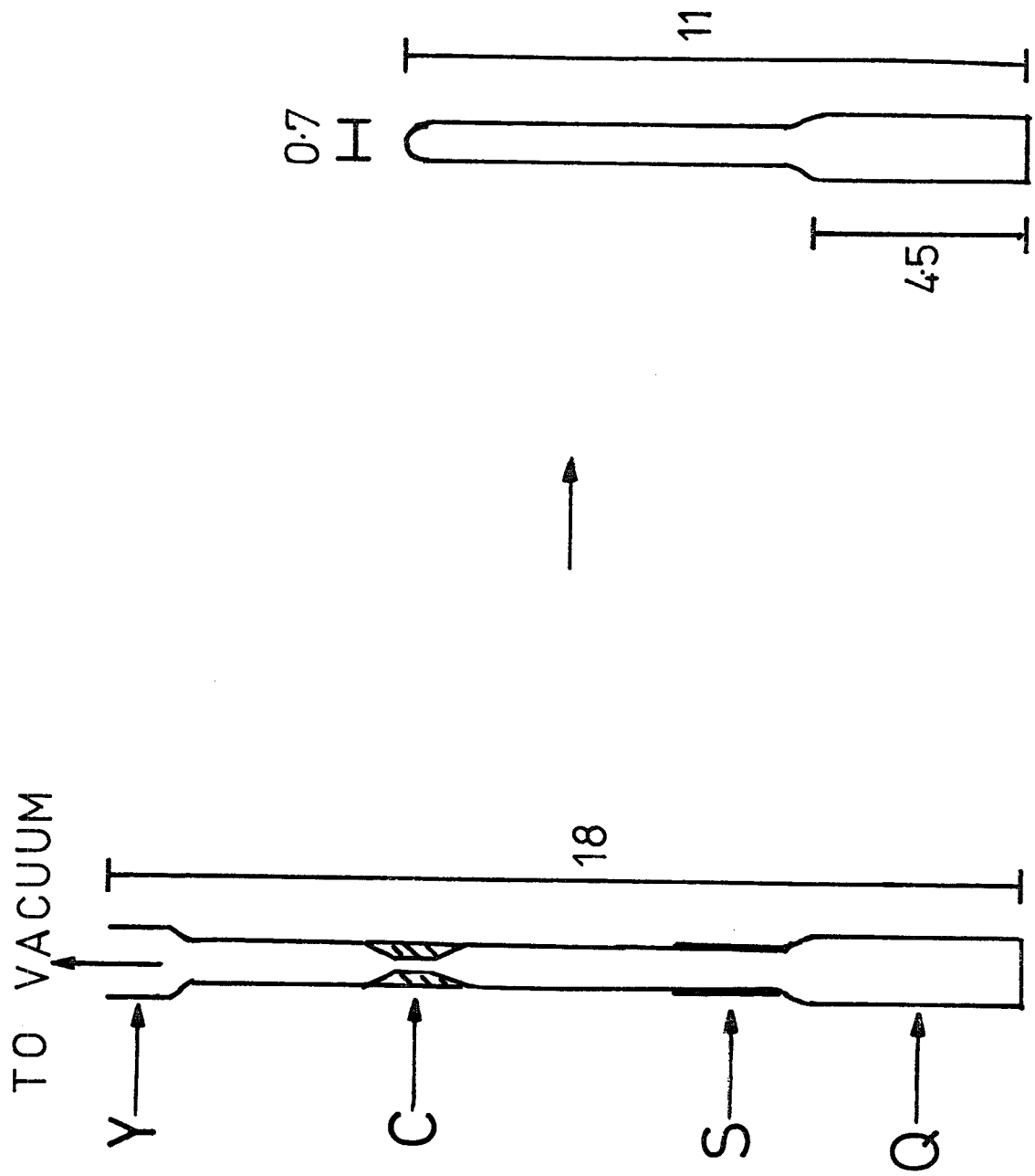

FIGURE 2.8 PREPARATION OF SAMPLE CELL FOR VAPOUR PHASE WORK

FIGURE 2.8

Diagram of Sample Cells for Vapour Phase Work

All measurements in centimetres.

(a) Before constriction is closed.

Y - Young's Female Connector (model PCJ5)

C - Constriction - this is heated until glass collapses to form an air-tight seal.

S - Graded Quartz-to-Glass seal.

Q - 1 cm square Quartz Cuvette.

(b) Sealed cell containing , at elevated temperatures, the vapour phase exciplex under study.

(c) The quenchers, either a diene or an amine and vibrational relaxer, n-pentane, were added to the cell with a calibrated Hamilton μl syringe or, when high pressures were required, by weighing out directly on a 5-figure balance. When vaporised at elevated temperatures the resulting pressures could then be calculated from the general gas equation, PV = nRT.

(d) Then the cell was attached by the Young's female connector, via a liquid nitrogen trap to prevent any sample contamination, to mercury-free, grease-free vacuum line maintained at a pressure of about 10^{-3} torr by the combination of an Edwards model ES50 rotary pump in series with an Edwards model E02 oil diffusion pump. Before opening up the cell to the vacuum the liquid quencher and relaxer were frozen down with liquid nitrogen. The air in the cell was then evacuated and then following 3 freeze-pump-thaw cycles the cell was sealed off by heating the constriction with an oxygen flame as shown in figure 2.8 (a) and pulled off resulting in a sample cell, shown in figure 2.8 (b), which could be accommodated in a high temperature furnace.

(e) After an experiment had been completed the volume of a cell could be measured. The procedure followed was to break off the glass tip of the cell and then, following thorough cleaning with the solvents appropriate to the mixture being studied, the cell and the tip were accurately weighed (W_A). Then the cell and tip were completely filled with water and re-weighed (W_R). Thus from the difference of the two weights the volume of the cell was calculated. The concentrations of the added quencher and relaxer could then be calculated accurately.

2.5. HIGH TEMPERATURE FURNACES

Two furnaces were used in this work - a 'home built' electrically heated furnace, illustrated in figure 2.9, and a commercial model made by Oxford Instruments, shown schematically in figure 2.10.

The 'home built' furnace consisted of a brass block, with four windows and a hollow cylindrical brass block which rested on top of the rectangular block. Heating elements (H_1, H_2, H_3, H_4) constructed of nichrome wire (65 percent Ni, 15 percent Cr and 20 percent Fe) wound around pyrex rods, were positioned in holes bored in the four corners of the lower block B_1, figure 2.9(a), into which the quartz cell fitted snugly.

The top of the sample cell was heated by the hollow cylindrical brass block (B_2) around which the nichrome wire, in series with the four heating elements, was wound. 'Fibrafrax' thermal insulation was packed around the whole arrangement. The heater current was regulated by a Zenith Variac voltage transformer which had a voltage output which could be varied from 0-270 volts. The temperature of the cell was determined by measuring the electromotive force generated by a chromel-alumel thermocouple, with the reference junction in crushed ice, using a Wheatstone bridge circuit. The temperature was then found found by referring to standard tables.[26]

Oxford Instruments Limited furnace. Model DN 704 HT.

The construction of the commercially made furnace, illustrated in figure 2.10, was principally of aluminium alloy, copper and stainless steel. The sample cell (S) snugly fitted into a sample holder (SH) which was top loaded through the sample entry port (E) into an inner sample compartment and electrically heated by a 39Ω heat exchange block positioned around the sample compartment. The heat exchange block (H) was powered by a temperature measurement and controller unit, Oxford Instruments

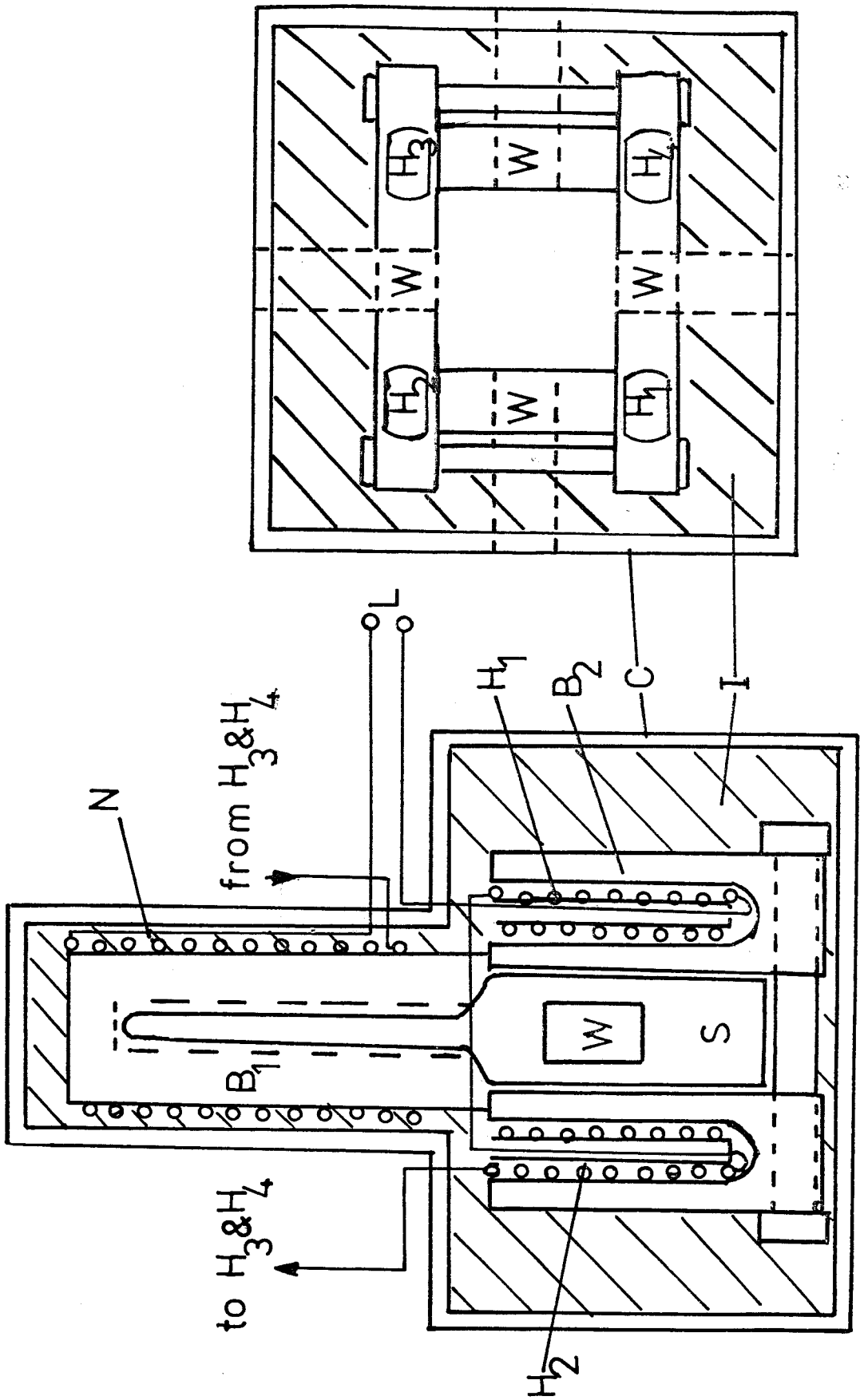

FIGURE 2.9. HOME-BUILT FURNACE

FIGURE 2.9. HOME BUILT FURNACE

(a) SIDE VIEW (b) TOP VIEW

L - Lead Wires to Voltage transformer

H - Heating Elements

B_1 - Upper hollow cylindrical brass block

B_2 - Lower brass heating block with four windows (W) to allow excitation and observation of emission.

I - 'Fibrefrax' Thermal Insulation

C - Outer walls made from brass plate painted matt black to reduce light scattering

S - Sample cell

N - Insulated nichrome wire wound around B, to heat the upper half of the cell.

model DTC-2, which provided up to 30 watts of output. Thus the temperature of the block was continuously variable from room temperature up to 550°K. A platinum resistance thermometer, fitted in the heat exchange block, was also connected to the DTC-2 unit where the temperature was indicated on a four-digit display. Electrical connections to the heater and temperature sensor were made via a 10 pin seal (SP) on the top plate of the furnace. To reduce the heat losses to a minimum the sample compartment was surrounded by a vacuum insulation jacket (VJ) which was evacuated to a pressure of 10^{-3} torr prior to use via the valve V. However, there was a temperature difference between the sample cell and the heat exchange block due to thermal losses by conduction, thus the temperature of the cell was also measured using a chromel-alumel thermocouple (T); in this way a temperature accuracy of about $\pm$ 1°K could be achieved. Synthetic sapphire windows (SW) were fitted to the inner sample compartment to deal with the temperature range required. The problem is not with the temperature characteristics of quartz in terms of transmittance but the method of mounting the windows. The quartz windows are fixed in holders using an adhesive which is at the limits of its working range at the high temperatures used in this work. However, sapphire can be brazed into the window mounts and thus is suitable for high temperature work. In the spectral region investigated in this work synthetic sapphire still has a % transmittance $\geq$80%. The windows on the outer vacuum jacket are not exposed to the high temperatures of the inner compartment and thus quartz, % transmittance = 100%, is still suitable window material, QW.

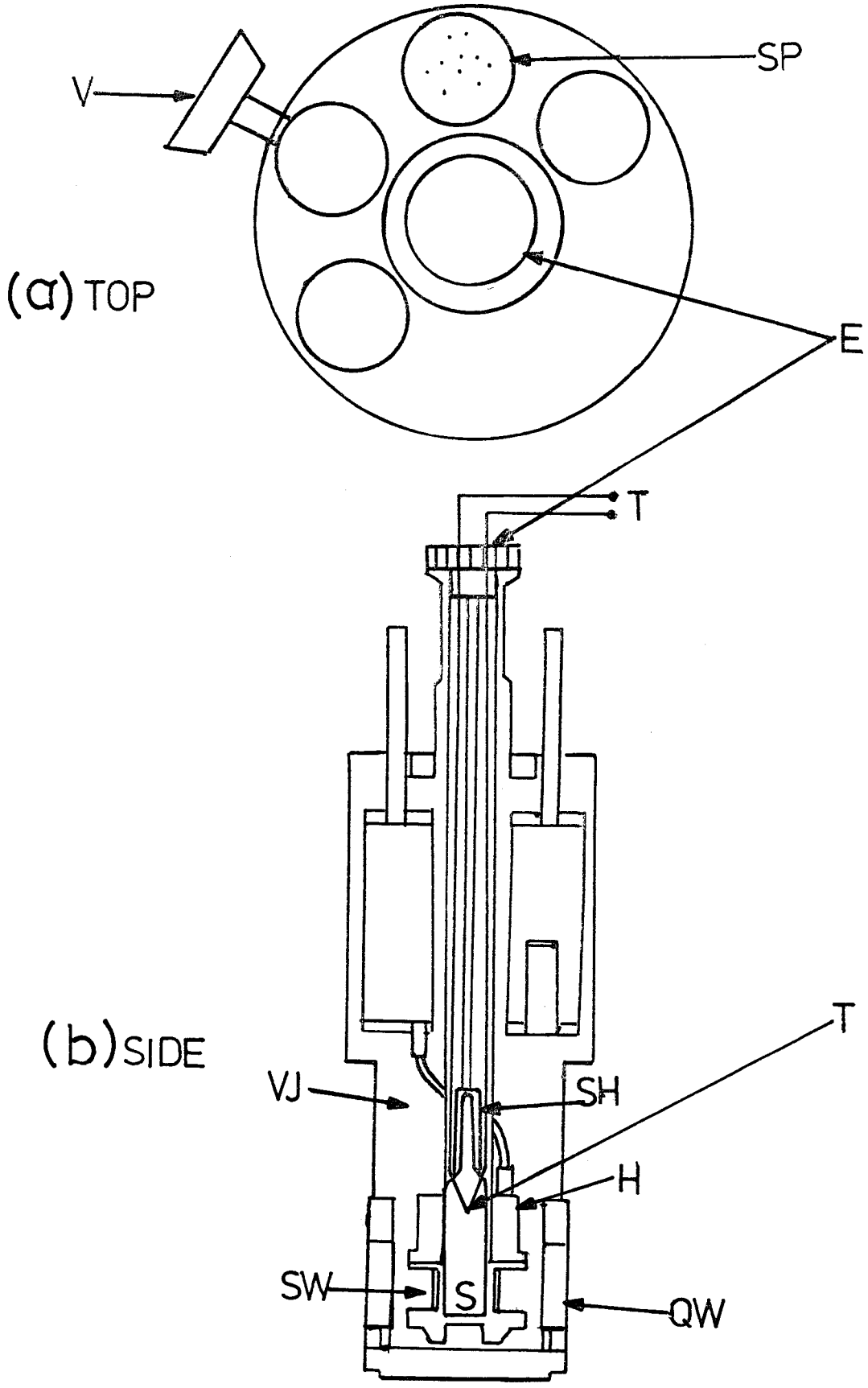

FIGURE 2.10 OXFORD INSTRUMENTS LIMITED FURNACE

2.6. CHEMICALS

The chemicals and purification methods used were as follows:

1,4 Dicyanonaphthalene (1,4 DCN). This was a gift from Dr. D. R. Arnold, University of Western Ontario, Canada. This was recrystallised and then sublimed three times in a vacuum. No fluorescing impurities were detected using 250 nm. excitation.

9 cyanoanthracene (9 CNA). Aldrich Chemicals. This was purified in the same way as 1,4 DCN.

2,5 Dimethyl 2,4 Hexadiene. (DM HD). Aldrich Chemicals. This was fractionally distilled and the middle fraction (bp = 134°C) retained which was stored below 0°C under nitrogen.

Triethylamine (TEA). B.D.H. The pale yellow impure liquid was firstly dried by refluxing over potassium hydroxide pellets for about two hours and then fractionally distilled under nitrogen in the presence of sodium wire. The middle fraction was retained (bp = 89°C) and stored under nitrogen.

N,N Dimethylaniline (DMA). B.D.H. Purified by fractional distillation under reduced pressure (bp = 90.5°, 29 torr) and stored under nitrogen.

Tri-n-propylamine (TNP). B.D.H. This was purified in the same way as TEA (bp = 154°C).

Tri-n-butylamine (TNB). B.D.H. The impure liquid was dried using the same method as for TEA and then fractionally distilled under reduced pressure (bp = 91°C, 9 torr).

N-pentane. B.D.H. This was distilled under nitrogen. (bp = 36°C). No fluorescent impurities were detected using broad-band excitation.

REFERENCES

1. W. R. Ware, in 'Creation and Detection of the Excited State'. Vol.1A, A.A. Lamola, Ed., Marcel Dekker, New York 1971.

2. J. B. Birks and I. H. Muncro, in 'Progress in Reaction Kinetics'. Vol.4, G. Porter, Ed., Pergamon, Oxford, 1967.

3. J. Yguerabide, in 'Methods in Enzymology'. Vol.26, C.H.W. Hirs and S. N. Timasheff, Eds., Academic Press, New York, 1972.

4. A.E.W. Knight and B. K. Selinger, Aust.J.Chem., 26, 1 (1973).

5. I. B. Berlman, D. J. Steingraber and M. J. Benson. Rev.Sci.Instrum., 39, 54 (1968).

6. C. Lewis, W. R. Ware, L. J. Doemeny and T. L. Nemzek, Rev.Sci.Instrum., 44, 107 (1973).

7. G. A. Morton. Appl.Optics, 7, 1 (1973).

8. M. G. Littmam. Rev.Sci.Instrum., 45, 1608 (1974).

9. K. P. Ghiggino, A. J. Roberts and D. Phillips, J.Phys.E., 1980, 13, (In Press).

10. K. G. Spears, L. E. Cramer and L. D. Hoffland. Rev.Sci.Instrum., 49, 255 (1978).

11. V. J. Koester and R. M. Dowben. Rev.Sci.Instrum., 49, 1186 (1978).

12. F. S. Schaefer, 'Dye Lasers', Topics in Applied Physics, 1, Springer-Verlag, Berlin (1973).

13. K. P. Ghiggino, D. Phillips, K. Salisbury and M. D. Swords, J.Photochem., 7, 141 (1977).

14. P. A.Franken, A. E. Hill, G. Peters and G. Weinreich. Phys.Rev.Letters, 7, 118 (1961).

15. B. G. Huth and Y. C. Kiang. J.Appl.Phys., 40, 4976 (1961).

16. C. K. Chan. Spectra-Physics Technical Bulletin No.8, June (1978).

17. C. K. Chan and S. O. Sari. Appl.Phys.Letters, 25, 403 (1974).

18. J. M. Harris, R. W. Crisman and F. E. Lyte. Appl.Phys.Letters, 26, 16 (1975).

19. C. V. Shank and E. P. Ippen. Appl.Phys.Letters, 24, 373 (1974).

20. J. De Vries, D. Bebelaar and J. Langelaar. Optics Comm., 18, 24 (1976).

21. A. E. Siegman and D. J. Kuizenga. Opto-Electronics, 6, 43 (1974).

22. A. E. McKinnon, A. G. Szabo and D. R. Miller, J.Phys.Chem., 81, 1565 (1977).

23. D. V. O'Connor, W. R. Ware and J. C. Andre. J.Phys.Chem., 83, 1333, (1979).

24. P. R. Bevington, in 'Data Reduction and Error Analysis for the Physical Sciences'. McGraw-Hill, New York, 1969.

25. D.J.S. Birch and R. E. Imhof, J.Phys.E., 10, 1044 (1977).

26. 'Handbook of Chemistry and Physics', Ed. R. C. Weast, C.R.C. Press (1975-1976).

CHAPTER THREE

THE 9-CYANOANTHRACENE/AMINE VAPOUR PHASE EXCIPLEXES

CHAPTER THREE

THE 9-CNA/AMINE VAPOUR PHASE EXCIPLEXES

3.1. INTRODUCTION

Exciplex formation is one of the most efficient mechanisms for the quenching of electronically excited states by ground state species. As has been discussed in CHAPTER ONE, numerous studies on the behaviour and nature of exciplexes in the solution phase have been made on which reviews have been written.[1-5]

Vapour phase exciplex formation between polyatomic molecules had not been reported previous to the work discussed in this chapter.[7,8,9] However, there is no evidence to suggest that exciplex formation between polyatomic molecules is not a widespread phenomenon in the vapour phase. The fact that they have not been observed is because relatively high temperatures (~ 470 K) are required to vaporise the usual exciplex-forming molecules. At these elevated temperatures it is expected that dissociation of such complexes will be enhanced resulting in low exciplex emission yields.[6]

In this chapter steady-state emission, excitation and ultra-violet absorption spectra for vapour phase mixtures of photo-excited 9-cyanoanthracene (9 CNA) and any one of the following amines, N, N Dimethylaniline (DMA), Triethylamine (TEA) or Tributylamine (TBA), will be shown. The results for the quenching of 9 CNA fluorescence by TBA will also be presented. Using these results the evidence for the formation of vapour phase exciplexes in the above systems will then be discussed. Some of the results and spectra have already been published by Abbott et al.[7,8]

Apart from being of interest in themselves, the discovery of exciplexes in the vapour phase is important for two other reasons, (a) the effect of solvent on the properties of solution phase complexes is not yet fully understood. The determination of the properties of similar systems in which such solvent effects are absent may be of some value in the elucidation of such a problem. (b) As shown in figure (1.1) exciplexes decay radiatively to a dissociative ground state surface, hence they could have a practical value as gas phase lasing systems.

3.2. RESULTS AND DISCUSSION

The UV-visible absorption and fluorescence spectra of 9 CNA in the vapour phase are shown in figure 3.1. The spectral shape was found to be insensitive to temperature.[9]

When TEAwas added to 9 CNA (pressure = 0.5 torr) at 458 K, quenching of the 9 CNA fluorescence was observed and this was accompanied by the appearance of a new, structureless, broad emission band red-shifted from the fluorescence spectrum of the photo-excited 9 CNA. Excitation was into the first allowed electronic absorption band of 9 CNA at 365 nm. The emission spectrum for a 9 CNA/TEA mixture, (concentration of TEA = 4.4×10^{-2} moles dm^{-3}, pressure (TEA) = 1260 TORR) is shown in figure 3.2, where the dashed line represents the spectral shape of the unquenched 9 CNA fluorescence. The intensity of the long-wavelength band was dependent on the concentration of amine added and the growth in this feature with increasing concentration of amine was accompanied by a further quenching of the 9 CNA monomer fluorescence. Similar behaviour

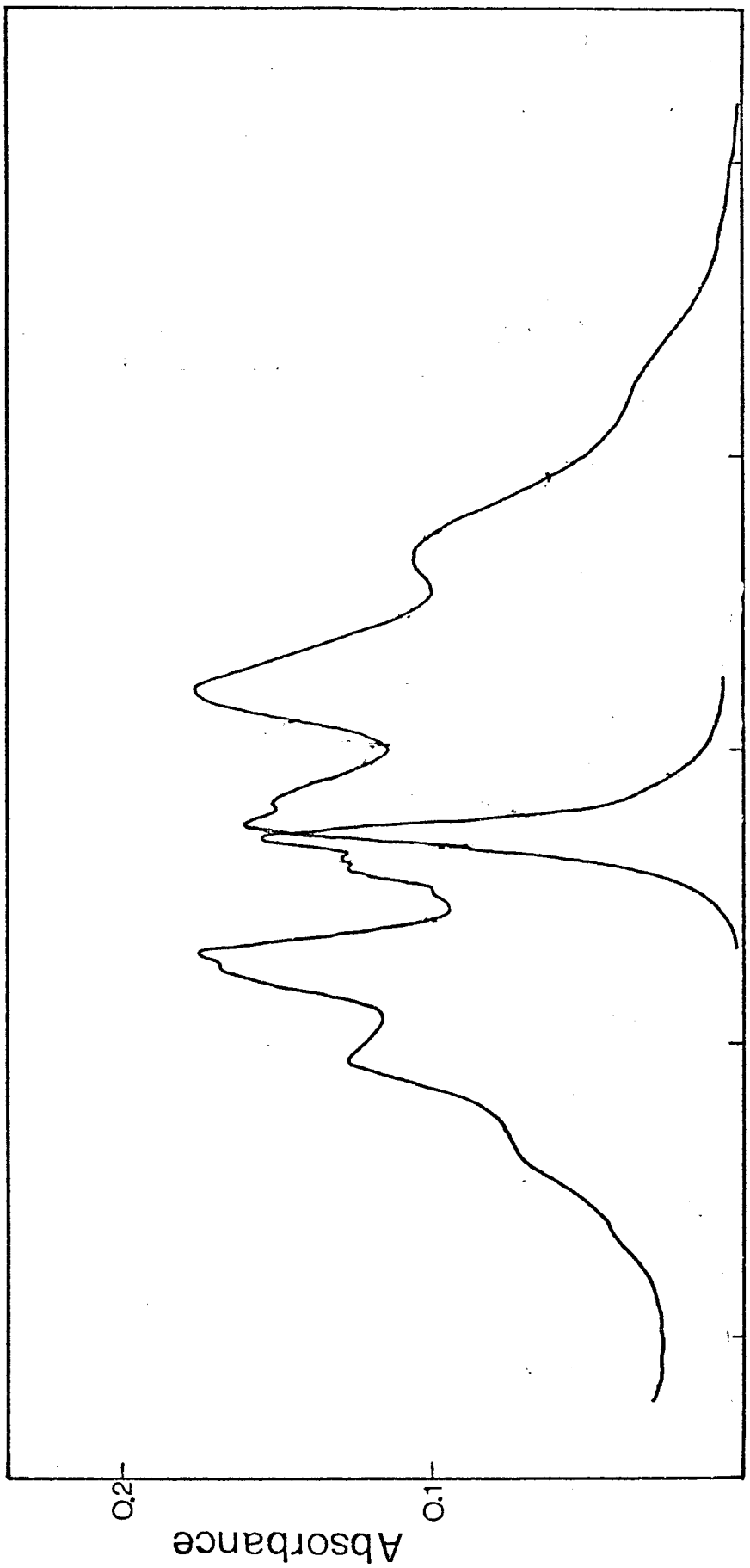

FIGURE 3.1 UV-Visible Absorption and Fluorescence spectra of 9 CNA in the Vapour Phase (Temperature = 444K). The Fluorescence spectra were observed for excitation at 365 nm.

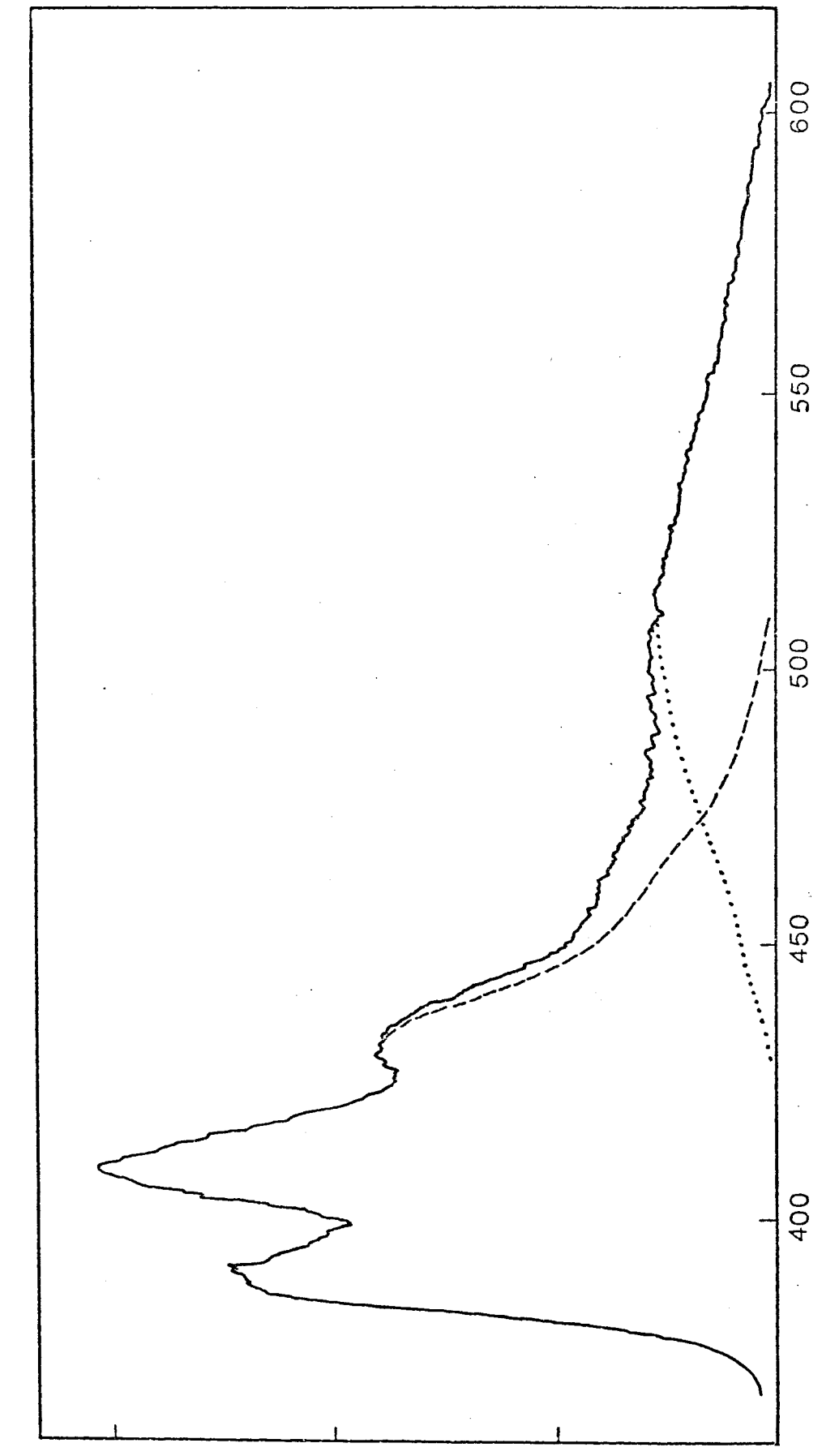

FIGURE 3.2 Fluorescence emission spectrum of 9 CNA/TEA system at 458°K ———— Emission of photo-excited 9 CNA in presence of (7.9×10^{-3}, 248 torr) of TEA; (- - - - - -) Monomeric Emission; (.....) New Emission.

was observed for vapour phase mixtures of 9 CNA/TBA and 9CNA/DMA whose emission spectra are compared with that of the 9 CNA/TEA system in figure 3.3. In all these cases the short-wavelength emission is typical of structured 9 CNA vapour phase fluorescence (see figure 3.1). When any one of 9 CNA, TEA, TBA, DMA was excited alone at 365 nm under exactly the same conditions of temperature, pressure and spectrometer sensitivity the broad long-wavelength band was absent in every case. Hence the new emitting species cannot be one of the following, (1) A fluorescent excimer formed by the photoassociation of 9 CNA,[10] (2) a luminescent product arising from the thermal degradation of 9 CNA or any one of the above amines, (3) an emitting impurity in one of the components in any of the above mixtures.

The other possibilities are, that the new emission is (4) the result of the radiative decay of a ground state 9 CNA/amine molecular complex which has been excited by absorbing light in the same spectral region as the 9 CNA monomer or (5) fluorescence from a product formed between 9 CNA and the amine which, again, is excited by competing with 9 CNA for incident light. Either a ground state complex or a product would be observed in the electronic absorption spectrum of the 9 CNA/amine mixture where one or more, generally broad and structureless, absorption bands would be found. These new bands usually overlap on the long wavelength edge of the lowest energy component, in this case the band due to absorption by 9 CNA. However, the spectra, shown in figure 3.4, of the 9 CNA/TEA (b) and 9 CNA/TBA (c) systems were identical with the spectrum of a sample containing only 9 CNA (a), following correction for the amine absorptions which occur at shorter wavelengths to that of the 9 CNA.

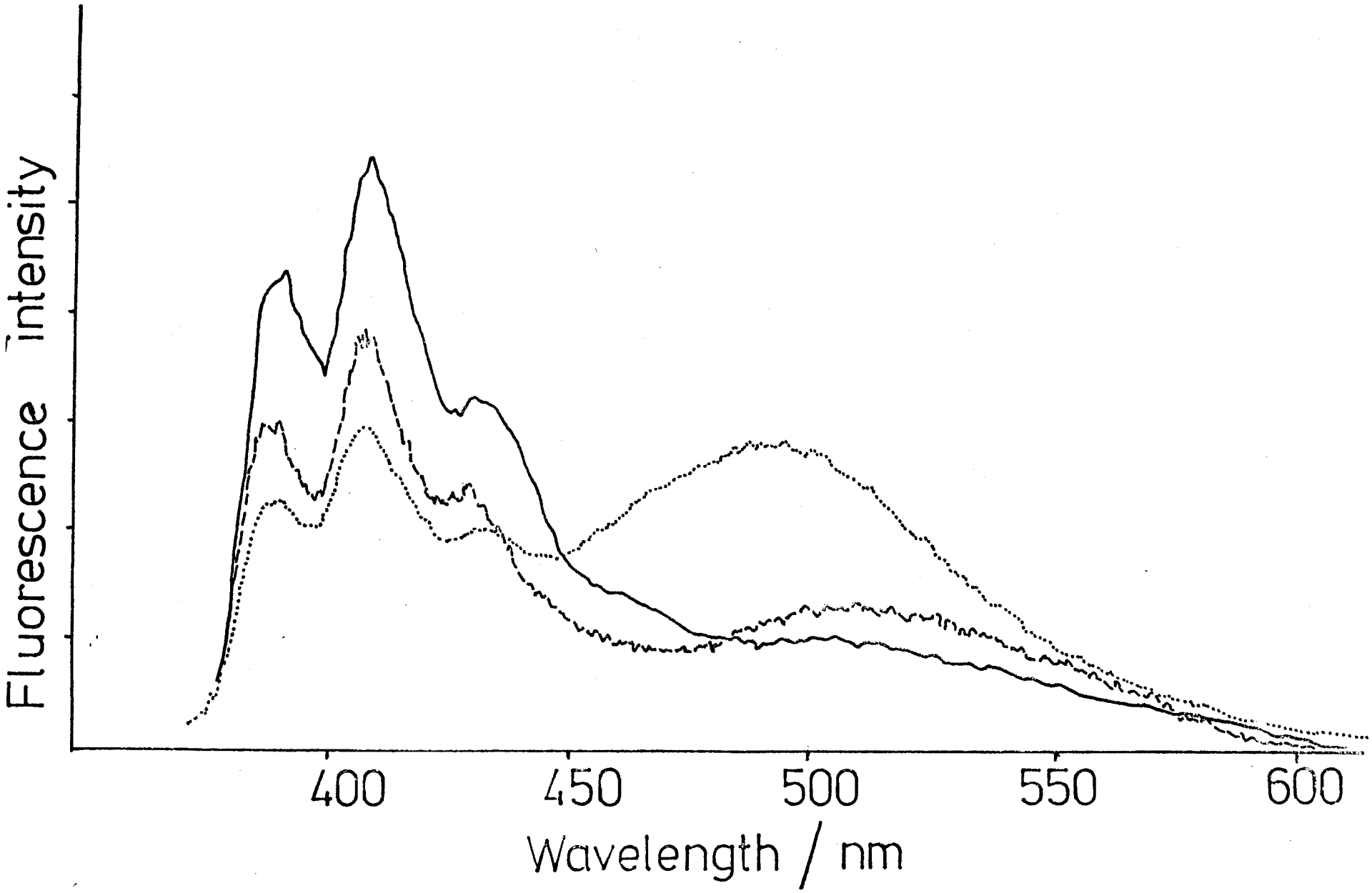

FIGURE 3.3 Fluorescence Emission Spectra of 9 CNA/AMINE Systems. .... 9 CNA/N,N DMA (504K), N,N DMA = 7.9×10^{-3}M; --- 9 CNA/TBA (504K), TBA = 1.8×10^{-2}; —— 9 CNA/TEA (458K) TEA = 4.4×10^{-2}M.

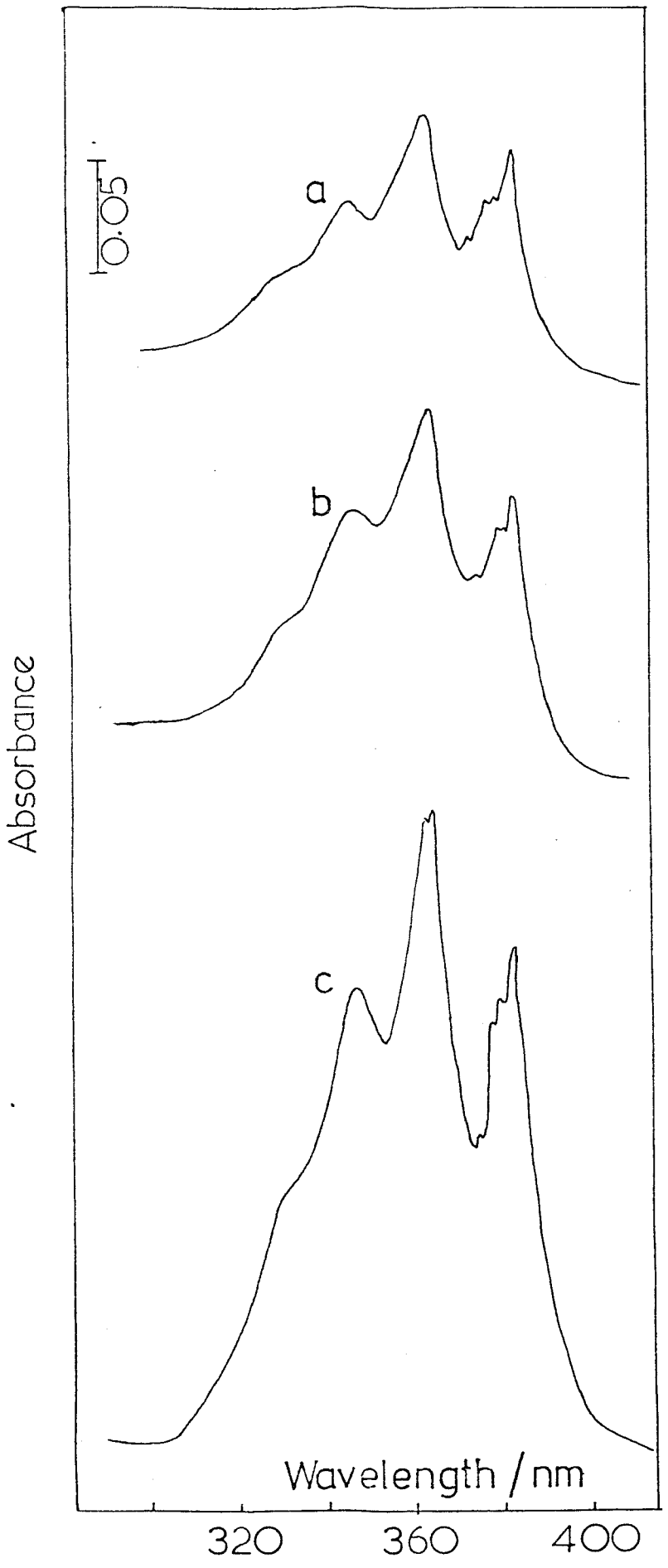

FIGURE 3.4 UV Absorption Spectra of 9 CNA and 9 CNA/AMINE mistures in the vapour phase.
(a) 9 CNA Alone (b) 9 CNA/TBA (c) 9 CNA/THA.

In the case of 9 CNA/DMA it was more difficult to correct for the amine as its absorption band began to become significant at wavelengths just below 350nm. The differing intensities of the bands going from (a) to (c) in figure 3.4 are simply due to the fact that at the time this work was done an efficient method for introducing equal weights, exactly, of 9 CNA into each sample cell had not been devised. Subsequently the method, as described in 2.4 (b) of the EXPERIMENTAL Chapter, was conceived from which cells containing equal concentrations of 9 CNA could be made up easily. Fluorescence excitation spectra make use of an emission measurement, which is capable of very great amplification, to record information which relates to an absorption process, and for totally vibrationally relaxed samples in the vapour phase the fluorescence excitation spectrum will be identical to the UV absorption spectrum for a fluorescent monomeric species. Again, if a ground state complex was formed in any of the 9 CNA/amine mixtures new bands would appear in their excitation spectra which would not have been present in the absorption spectrum of 9 CNA. As shown in figure 3.5 the excitation spectra, monitored at an emission wavelength about equal to the maximum of the new bands in figure 3.3 (515 nms), for 9 CNA/DMA (a), 9 CNA/TBA (b) and 9 CNA/TEA (c) were all found to be identical to the UV absorption spectrum of 9 CNA. Therefore the spectra in figures 3.4 and 3.5 prove the absence of any ground-state association in the 9 CNA/amine mixtures and there is also no spectral evidence for product formation.

From all these spectroscopic results, it therefore seemed reasonable to assign the new emission bands in figure 3.3 to the fluorescent decay of exciplexes. These were the first reported observations of vapour phase exciplexes formed between polyatomic molecules.

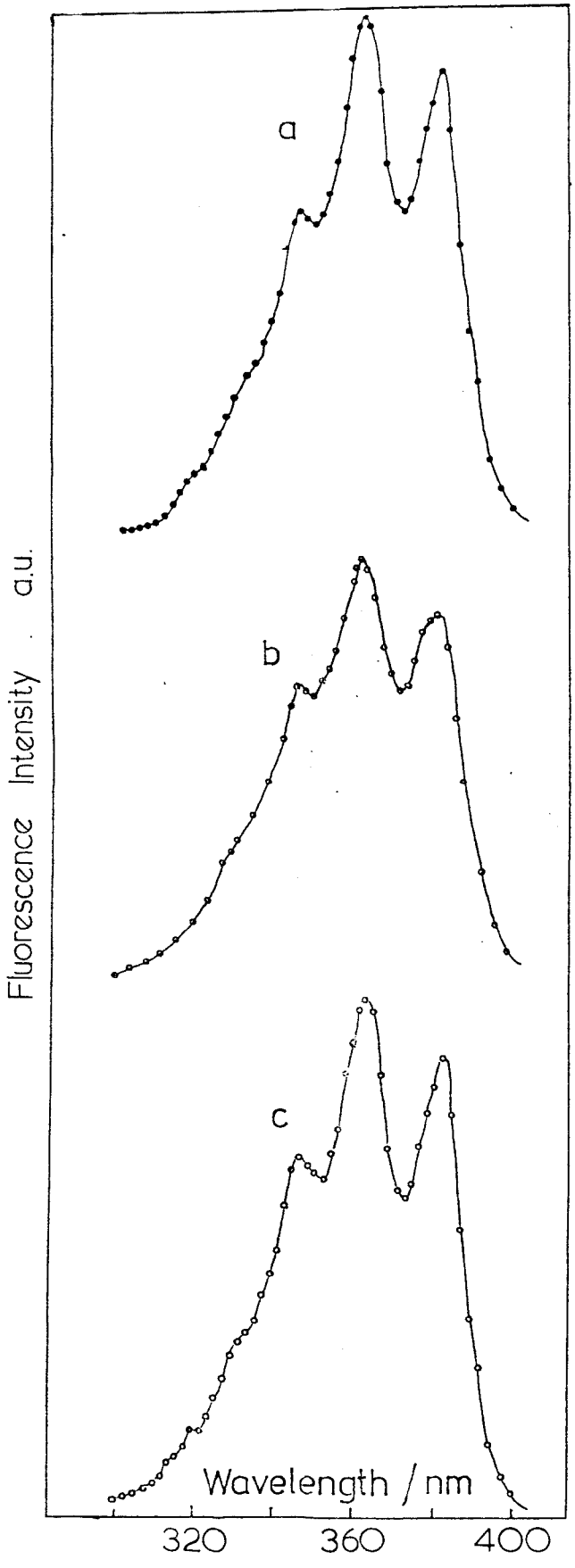

FIGURE 3.5 Fluorescence Excitation Spectra of 9 CNA/AMINE mixtures recoreded at an emission wavelength equal to λ_{MAX} of new emission bands shown in Figure 3.3.
(a) 9 CNA/N,N DMA (b) 9 CNA/TBA (c) 9 CNA/TEA.

For the 9 CNA/DMA system, characteristic exciplex emission was also observed in cyclohexane solution. The emission spectra for the vapour phase, (a), and solution phase systems, (b), are compared in figure 3.6. Since the intensity of the exciplex emission is less in the solution phase than in the vapour phase, even though a higher concentration of DMA was added in solution, it seems that the fluorescence quantum yield of the solution phase exciplex is less than that in the vapour phase. The dipole moment of the vapour phase exciplex can be calculated from the comparison of spectra in figure 3.6 using the solvent-shift technique.[3] This has been done in Chapter 4, see TABLES 4.1 and 4.2. The value of the dipole moment was found to be 13.8 Debyes, indicating a large contribution from the charge-transfer configuration to exciplex stability.[11] A more detailed discussion of this aspect is given in Chapter 4.

Hirayama[9] measured the fluorescence decay times for the 9 CNA/DMA exciplex in both phases. The decay of the total emission (from monomer and exciplex) was found to be double exponential. The long-lived component had lifetimes equal to 25.1 ns in the vapour phase (Temperature = 504 K) and 60.2 ns in the solution phase. The decay time of the short-lived component was too short for measurement using the conventional time-correlated single photon counting technique. Although a tentative mechanism was proposed to explain the different results in the two phases, this was based on the variation of individual rate constants which could not be measured due to the short lifetime of the unquenched 9 CNA fluorescence and the limiting resolution of the conventional lifetime apparatus. This aspect is discussed in much more detail in the introduction to Chapter 4.

FIGURE 3.6 (a) Vapour phase exciplex emission from 9 CNA/DMA System at 504K : (———) Total Emission in the presence of DMA (7.9 c 10^{-3}M, 248 torr); (-----) Monomer Emission
(b) Exciplex Emission from the 9 CNA/DMA system in cyclohexane: (———) Total emission in the presence of DMA (3.8 x 10^{-2}M); (-----) Monomer Emission.

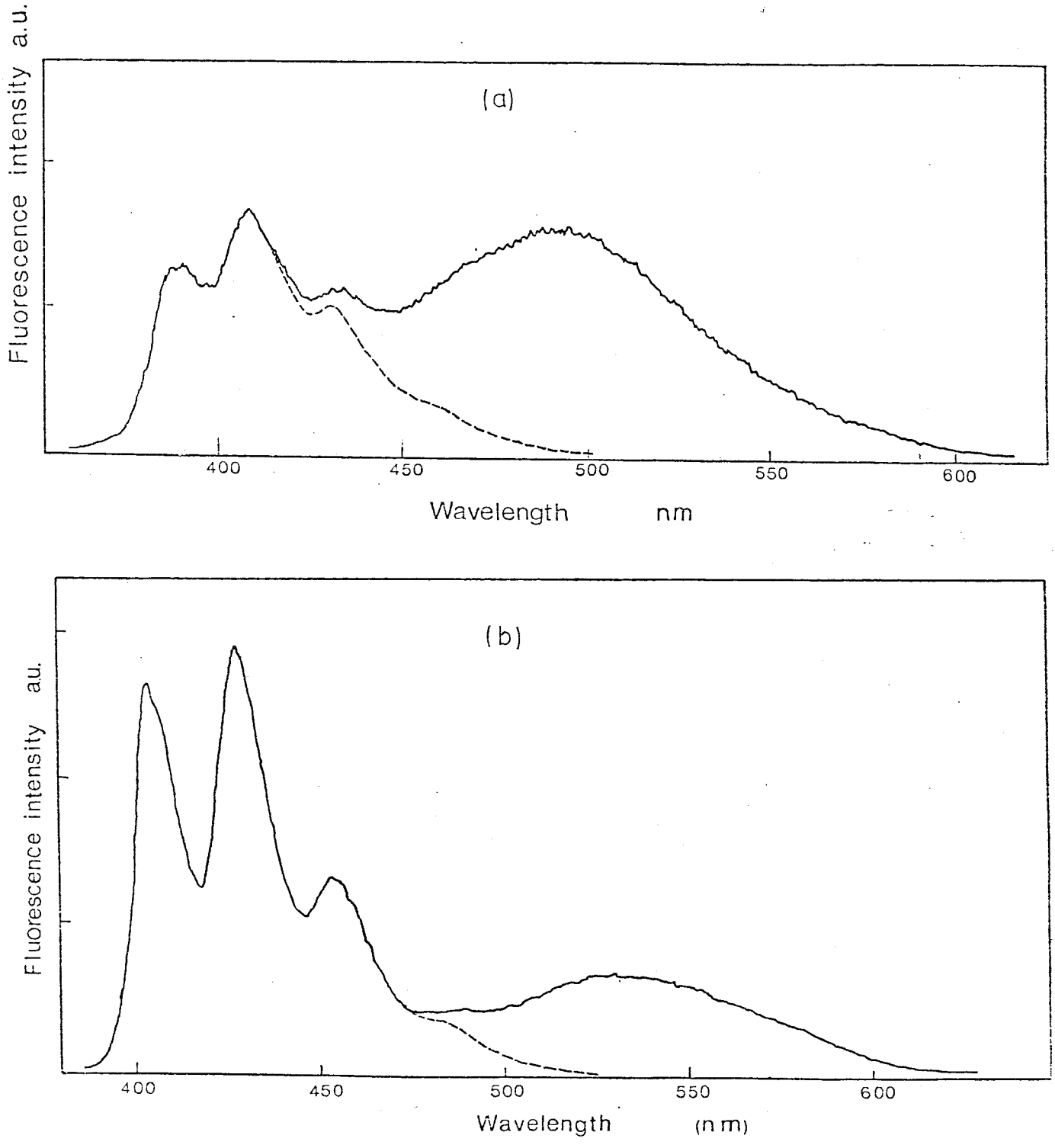

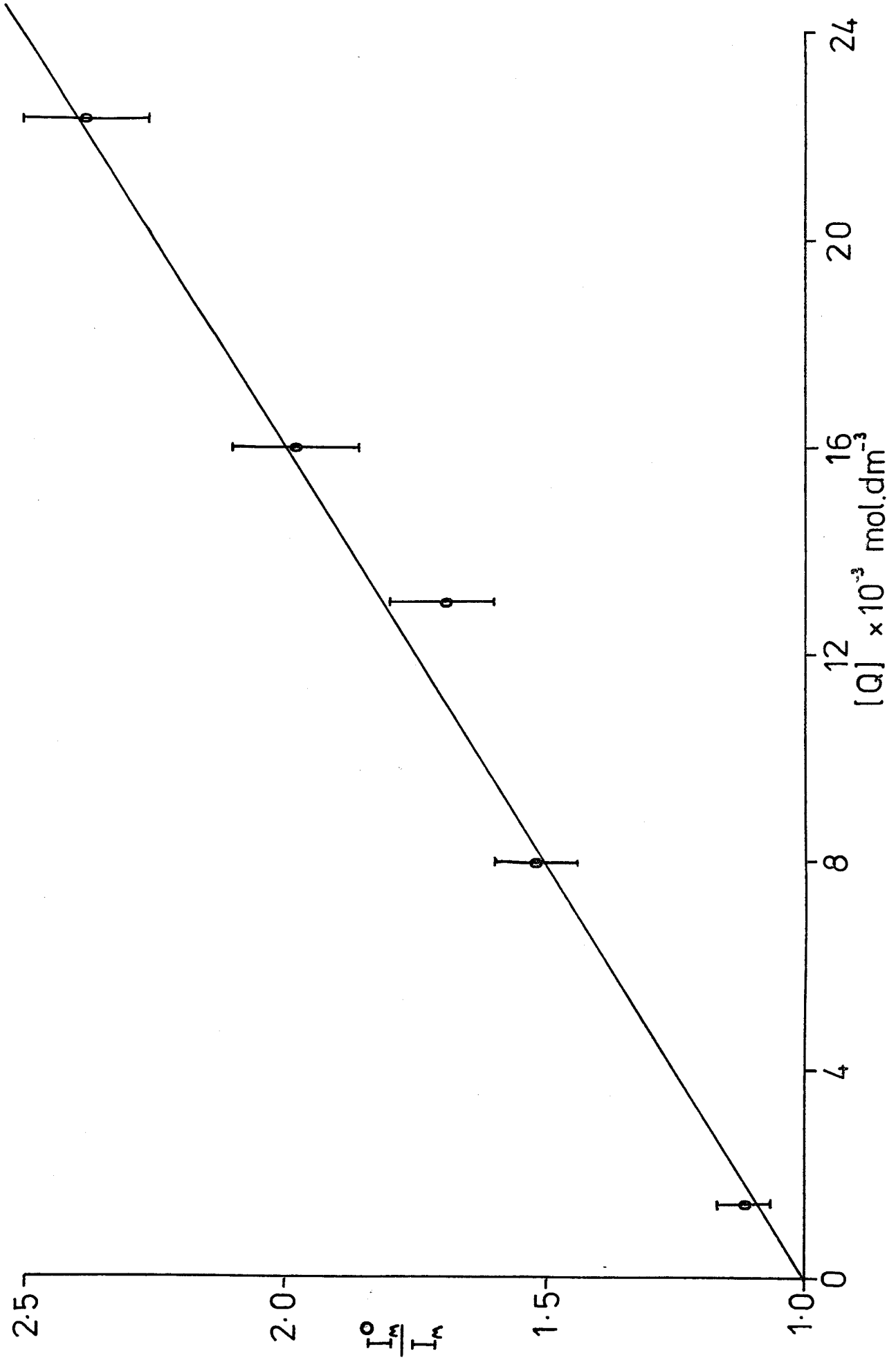

FIGURE 3.7 Stern-Volmer Plot for quenching of 9 CNA Fluorescence by TBA at 504K.

The quenching of the steady-state 9 CNA fluorescence by TBA was studied which followed a linear Stern-Volmer relationship, see figure 3.7, with a binolecular quenching rate constant equal to 0.17×10^{11} $dm^3\ mol^{-1}\ sec^{-1}$ at 504 K.

This is about an order of magnitude less than the hard-sphere gas-kinetic collision rate (which has a value of 7.7×10^{11} $dm^3\ mol^{-1}\ sec^{-1}$ at 504 K, see equation 4.39). The fact that the slope of the Stern-Volmer plot is linear is further evidence that a ground-state complex is not formed for this system.[4] Again as a detailed study of the kinetics of the transients could not be undertaken no definite statements about the reasons for the value of this quenching rate constant can be made.

3.3. CONCLUSIONS

Vapour phase exciplexes formed between polyatomic molecules have been characterised spectroscopically. The results of this preliminary study have supported the contention that the phenomenon would be general, and led directly to the work described in the following chapter, in which a detailed kinetic study of vapour phase exciplex formation in a related pair of polyatomic molecules was carried out.

REFERENCES

1. "The Exciplex", M. Gordon and W.R. Ware, Eds., Academic Press, New York, 1975.

2. A. Weller, Pure Appl. Chem., 16, 115 (1968).

3. H. Beens and A. Weller, in "Organic Molecular Photophysics", Vol. 2, J.B. Birks, Ed., Wiley-Interscience, London, 1975.

4. W.R. Ware, Pure Appl. Chem., 41, 635 (1975).

5. M. Ottolenghi, Acc. Chem. Res., 6, 153 (1973).

6. B. Stevens and P.J. McCartin, Mol. Phys., 8, 597 (1964).

7. G.D. Abbott, S. Hirayama and D. Phillips, Chem. Phys. Lett., 56, 497 (1978).

8. G.D. Abbott, C.G. Cureton, K. Hara, S. Hirayama and D. Phillips, J. Photochem., 9, 260 (1978).

9. S. Hirayama and D. Phillips, J. Chem. Soc., Faraday Trans. II, 74, 2035 (1978).

10. E.Z.M. Ebeid, S.E. Morsi, M.A. El-Bayroumi and J.O. Williams, J. Chem. Soc., Faraday Trans. I, 74, 1457 (1978).

11. M. G. Kuzmin and L.N. Guseva, Chem. Phys. Lett., 3, 71 (1969).

CHAPTER FOUR

THE 1,4 DICYANONAPHTHALENE/2,5 DIMETHYL 2,4 HEXADIENE VAPOUR PHASE EXCIPLEX

CHAPTER 4

THE 1,4 DCN/DMHD VAPOUR PHASE EXCIPLEX

4.1 INTRODUCTION

One of the objects of this work was to measure individual rate constants for the various formation and decay processes of a vapour phase exciplex. This required a detailed experimental study of the transient kinetics of such a complex. An estimate of the thermodynamic properties could then be obtained by studying the temperature dependence of these rate constants.

Such a study could not be undertaken for the 9CNA/amine systems discussed in the previous chapter for the following reasons. The lifetime of the vibrationally relaxed first excited singlet state of unquenched 9CNA was measured to be 3.8 ns in the vapour phase at a temperature of about 453 K. Thus on adding varying concentrations of amine, in an attempt to study the photokinetics of 9CNA/amine exciplex formation, the monomer lifetime was quenched to a value which could not be resolved by the conventional time-correlated single photon counting instrument. The dye laser system (see figure 2.4) could not be employed to measure these very short lifetimes since its tunable excitation wavelength range, 290 to 305 nm, was displaced from the spectral region required to excite into the first allowed electronic absorption band of 9CNA (see figure 3.1).

However, the first allowed absorption band of the substituted naphthalenes[1] does overlap the dye laser excitation spectral range; hence the emission spectra of vapour phase mixtures of photo-excited cyano-substituted naphthalenes and a variety of electron donating partners, with suitable ionisation potentials, were systematically investigated for the appearance of characteristic exciplex fluorescence peaks. It was

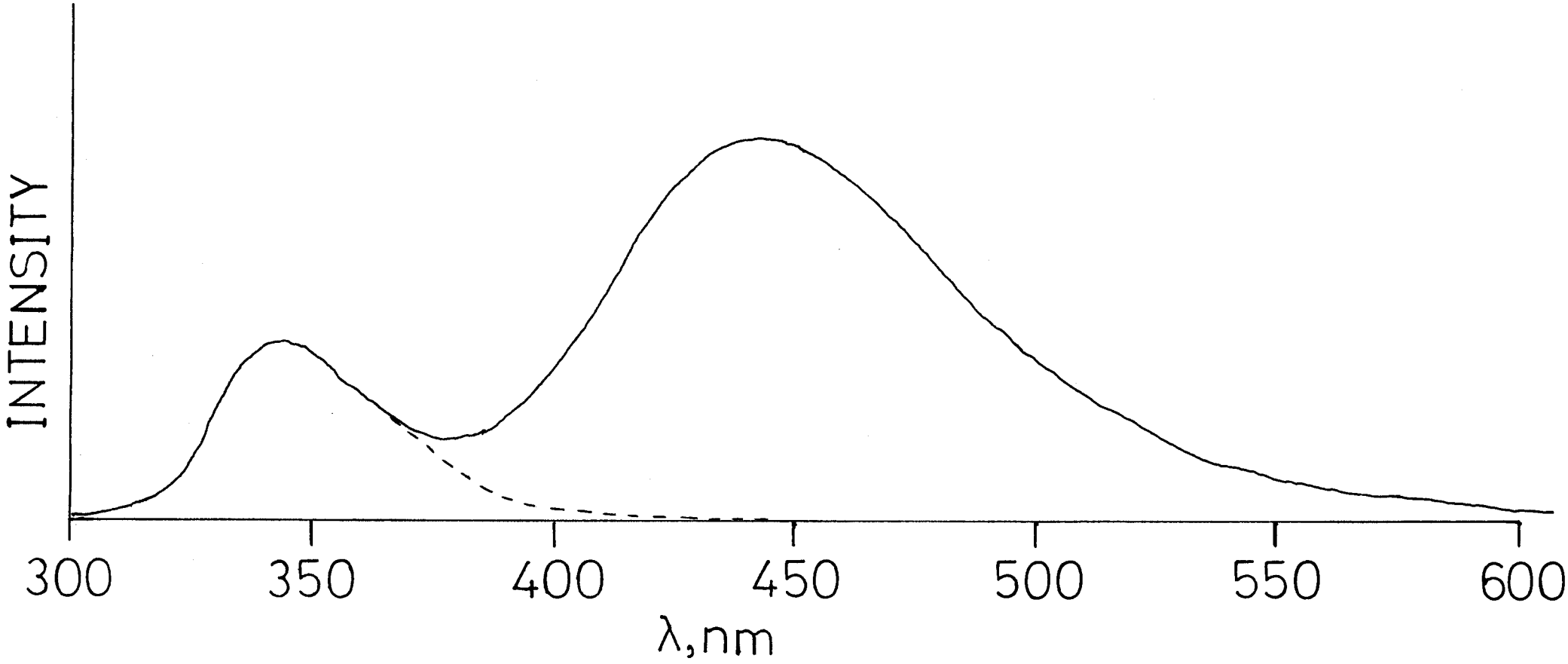

FIGURE 4.1. Fluorescence Emission Spectrum of 1,4 DCN/DMHD system. Temperature = 453 K. EXCITATION WAVELENGTH = 300 nms. Concentration of DMHD = 3.8×10^{-2}M. At this temperature both components are in the vapour phase.

found that 2,5 Dimethyl 2,4 Hexadiene quenched the 1,4 Dicyanonaphthalene (1,4 DCN) fluorescence (pressure of 1,4 DCN = 0.5 torr) and this was accompanied by the appearance of a broad, structureless fluorescence peak red-shifted from the 1,4 DCN emission (see figure 4.1), the dashed line represents the spectral shape of the unquenched monomer fluorescence. On quenching the monomer emission further with increasing concentrations of added DMHD, there was an intensification of this prominent, new spectral peak which, for reasons given later in this chapter, has been assigned to the fluorescence arising from an exciplex formed between 1,4 DCN and DMHD.

For a study of exciplex kinetics this system was far superior to the 9CNA/amine systems mainly because the fluorescence lifetime of the vibrationally relaxed 1,4 DCN monomer was measured to be 9.5 $\pm$ 0.1 nanoseconds at 457^{o}K, thus allowing the transient kinetics of fluorescence quenching to be examined over a wide range of added quencher concentration. Coupled with this was the fact that the dye laser system, could now be employed to excite the monomer, so that lifetimes as short as 300 ($\pm$ 100) ps could in principle be measured with confidence.

In this chapter the emission and excitation fluorescence spectra for the vapour phase 1,4 DCN/DMHD exciplex system will be discussed and a comparison with solution phase behaviour will be made. Analyses of the fluorescence decay curves and steady-state emission quenching for this system will also be presented. This section will be followed by a full discussion of the kinetic and thermodynamic properties for the 1,4 DCN/DMHD vapour phase exciplex. Most of the results and many of the tables and figures in this chapter have already been submitted for publication.[2]

Since the analysis of the results in this work is based on conventional exciplex kinetics, these are summarised in the following section.

4.2. EXCIPLEX KINETICS

In order to interpret the fluorescence decay data quantitatively a plausible mechanism for exciplex kinetics must be proposed. The usual scheme, which satisfactorily describes excimer and exciplex formation in non-polar solvents[3] and excimer formation in the vapour phase,[4] is written as:

$$A + h\nu \xrightarrow{I_a} A^* \qquad (4.1)$$

$$A^* \xrightarrow{k_1} A + h\,\nu_M \qquad (4.2)$$

$$A^* \xrightarrow{k_2} A \qquad (4.3)$$

$$A^* + Q \xrightarrow{k_3} (AQ)^* \qquad (4.4)$$

$$(AQ)^* \xrightarrow{k_4} A^* + Q \qquad (4.5)$$

$$(AQ)^* \xrightarrow{k_5} A + Q + h\,\nu_E \qquad (4.6)$$

$$(AQ)^* \xrightarrow{k_6} \text{PRODUCTS} \qquad (4.7)$$

In step 4.1 the monomer A is excited from its ground state to the first excited singlet state (A*) at a rate governed by the pumping function, I_a, which is time independent in the steady-state experiments and time dependent in the transient lifetime studies. k_1 is the radiative rate constant for the monomer fluorescence and k_2 is the sum of the non-radiative rate constants for the radiationless deactivation of A*. The formation of the exciplex, with a bimolecular rate constant k_3, is represented by step 4.4. A* and Q are regenerated from the exciplex in the feedback process, step 4.5, at a rate governed by the rate constant k_4. k_5 is the radiative rate constant for exciplex fluorescence and k_6 is the sum of all the non-radiative rate constants

for the various pathways by which the exciplex decays. 'PRODUCTS' might denote a triplet exciplex, ground state A and Q molecules or photo-reaction products. For brevity k_o is introduced which is the total of the excited monomer unimolecular relaxation rate constants, given by:

$$k_o = k_1 + k_2 \qquad (4.8)$$

Another composite rate constant k_p is also used which is given by:

$$k_p = k_5 + k_6 \qquad (4.9)$$

With this kinetic scheme differential equations describing the rates of formation of monomer and exciplex can be written as follows:

$$\frac{d\left[A^*\right]}{dt} = I_a(t) - (k_o + k_3\left[Q\right])\left[A^*\right] + k_4\left[(AQ)^*\right] \qquad (4.10)$$

$$\frac{d\left[(AQ)^*\right]}{dt} = k_3\left[Q\right]\left[A^*\right] - (k_4 + k_p)\left[(AQ)^*\right] \qquad (4.11)$$

For δ-pulse excitation, $I_a(t) = 0$ at $t > 0$ and thus

$$\frac{d\left[A^*\right]}{dt} = k_4\left[(AQ)^*\right] - (k_o + k_3\left[Q\right])\left[A^*\right] \qquad (4.12)$$

Eq.(4.12) is then differentiated to give

$$\frac{d^2\left[A^*\right]}{dt^2} = k_4\frac{d\left[(AQ)^*\right]}{dt} - (k_o + k_3\left[Q\right])\frac{d\left[A^*\right]}{dt} \qquad (4.13)$$

Combination of (4.11) and (4.13) gives

$$\frac{d^2\left[A^*\right]}{dt^2} = k_4k_3\left[Q\right]\left[A^*\right] - k_4(k_4 + k_p)\left[(AQ)^*\right] - (k_o + k_3\left[Q\right])\frac{d\left[A^*\right]}{dt} \qquad (4.14)$$

and substitution for $\left[(AQ)^*\right]$ using (4.12) leads to

$$\frac{d^2\left[A^*\right]}{dt^2} + (k_o + k_3\left[Q\right] + k_4 + k_p)\frac{d\left[A^*\right]}{dt} + (k_o(k_4+k_p) + k_pk_3\left[Q\right])\left[A^*\right] = 0 \qquad (4.15)$$

This is a soluble linear, homogeneous, second order differential equation in A with constant coefficients[5] for which the following solution is proposed:

$$\left[A^*\right] = c.e.^{-\lambda t}$$

This leads to the AUXILIARY EQUATION (4.16)

$$\lambda^2 - (k_o + k_3\left[Q\right] + k_4 + k_p)\lambda + k_o(k_4 + k_p) + k_pk_3\left[Q\right] = 0 \qquad (4.16)$$

From this come the two solutions

$$\lambda_{1,2} = \tfrac{1}{2}\left\{ k_o + k_3\left[Q\right] + k_4 + k_p \pm \left((k_o + k_3\left[Q\right] - k_4 - k_p)^2 + 4k_4k_3\left[Q\right]\right)^{\frac{1}{2}}\right\} \qquad (4.17)$$

Therefore the time dependence of the concentration of A* molecules is given by:

$$\left[A^*\right](t) = c_1.e^{-\lambda_1 t} + c_2e^{-\lambda_2 t} \qquad (4.18)$$

$$\text{At } t = 0 \quad \left.\begin{aligned}\left[A^*\right](t) &= \left[A^*\right]_o \\ \left[(AQ)^*\right](t) &= 0\end{aligned}\right\} \qquad (4.19)$$

$$\therefore\ c_1 + c_2 = \left[A^*\right]_o \qquad (4.20)$$

Differentiation of (4.18) yields eq.(4.21).

$$\frac{d\left[A^*\right]}{dt} = -\lambda_1c_1e^{-\lambda_1 t} - \lambda_2c_2e^{-\lambda_2 t} \qquad (4.21)$$

Combination of eqns.(4.12), (4.19) and (4.21) gives

$$\lambda_1 c_1 + \lambda_2 c_2 = (k_o + k_3[Q])[A^*]_o \qquad (4.22)$$

From 4.20 and 4.22

$$c_1 = \frac{k_o + k_3[Q] - \lambda_2}{\lambda_1 - \lambda_2}[A^*]_o \qquad (4.23)$$

$$c_2 = \frac{\lambda_1 - (k_o + k_3[Q])}{\lambda_1 - \lambda_2}[A^*]_o \qquad (4.24)$$

Equations (4.21), (4.12) and (4.18) are combined to obtain the expression describing the time dependence of the exciplex fluorescence,

$$-\lambda_1 c_1 e^{-\lambda_1 t} - \lambda_2 c_2 e^{-\lambda_2 t} = k_4[(AQ)^*] - (k_o + k_3[Q])(c_1 e^{-\lambda_1 t} + c_2 e^{-\lambda_2 t}) \qquad (4.25)$$

On rearranging the above,

$$[(AQ)^*] = \frac{(k_o + k_3[Q] - \lambda_1)(k_o + k_3[Q] - \lambda_2)}{k_4(\lambda_1 - \lambda_2)} e^{-\lambda_1 t} + \frac{(k_o + k_3[Q] - \lambda_2)(\lambda_1 - k_o - k_3[Q])}{k_4(\lambda_1 - \lambda_2)} e^{-\lambda_2 t} \qquad (4.26)$$

$$\therefore [(AQ)^*](t) = c_3(e^{-\lambda_1 t} - e^{-\lambda_2 t}) \qquad (4.27)$$

$$\text{with} \quad c_3 = \frac{(k_o + k_3[Q] - \lambda_1)(k_o + k_3[Q] - \lambda_2)}{k_4(\lambda_1 - \lambda_2)}[A^*]_o \qquad (4.28)$$

From these expressions the exciplex concentration is predicted to rise exponentially to a maximum and then decays.

Equations (4.18), (4.23) and (4.24) predict that the monomer will fluoresce with two decaying components, one of them resulting from feedback from the exciplex. However, as discussed later in this chapter,

there are circumstances in which only one of these components is experimentally observed.[18] Under steady-state conditions the equations describing the rates of formation of monomer and exciplex, (4.10) and (4.11) respectively, become

$$I_a - (k_o + k_3 [Q]) [A^*] + k_4 [(AQ)^*] = 0 \qquad (4.29)$$

$$k_3[Q][A^*] - (k_4 + k_p) [(AQ)^*] = 0 \qquad (4.30)$$

The quantum yield of monomer fluorescence ϕ_M is:

$$\phi_M = \frac{k_1 [A^*]}{I_a} \qquad (4.31)$$

In the absence of quencher, $\phi_M = \phi_M^o$ and

$$\phi^o_M = \frac{k_1}{k_1+k_2} = \frac{k_1}{k_o} \qquad (4.32)$$

Combination of equations (4.29) to (4.32) yields the Stern-Volmer relation

$$\left(\frac{\phi^o_M}{\phi_M} - 1\right) \frac{1}{[Q]} = K_{SV} = \frac{k_3 k_p}{k_o(k_4+k_p)} \qquad (4.33)$$

The overall quenching rate constant k_q is given by

$$k_q = \frac{K_{SV}}{\tau_o} = \frac{k_3 k_p}{k_4+k_p} \qquad (4.34)$$

The quantum yield for exciplex fluorescence is given by

$$\phi_E = \frac{k_5 [(AQ)^*]}{I_a} \qquad (4.35)$$

Combining equations (4.30), (4.31) and (4.35) gives

$$\frac{\phi_E}{\phi_M} = \frac{k_5}{k_1} \cdot \frac{k_3[Q]}{k_4+k_p} \qquad (4.36)$$

which is used to derive the Stevens-Ban relationship.[6]

4.3 RESULTS AND DISCUSSION

4.3.1. Steady-State Measurements

All the experiments in this chapter were performed under collisionally relaxed conditions by adding n-pentane (pressure ≥ 300 torr). In figure 4.1 is presented the vapour phase fluorescence spectrum of 0.5 torr of 1,4 DCN quenched by about 1000 torr of DMHD at a temperature of 453 K. The broad structureless band extending from 380 nm - 600 nm is not present when either 1,4 DCN or the diene is excited alone. From figure 4.2 the excitation spectrum of the mixture (DOTTED LINE) was virtually identical to the excitation spectrum of the unquenched monomer (SOLID LINE) and thus there was no evidence for the formation of a stable ground state molecular complex or any photo product whose excited states could have been responsible for this prominent new fluorescence peak.

As DMHD was added to 1,4 DCN the 1,4 DCN fluorescence was quenched (Figure 4.3) and this was accompanied by the appearance and growth of the red-shifted band (Figure 4.4), there being a definite isoemissive point. Hence on the basis of the spectroscopic evidence, it seems reasonable to assign this new emission, with λ^{MAX} = 446 nms, to the fluorescent decay of an exciplex formed by the association of ground state DMHD with photo-excited 1,4 DCN. Further evidence for the existence of this vapour phase exciplex is provided by steady-state quenching and transient measurements which are discussed later in this chapter.

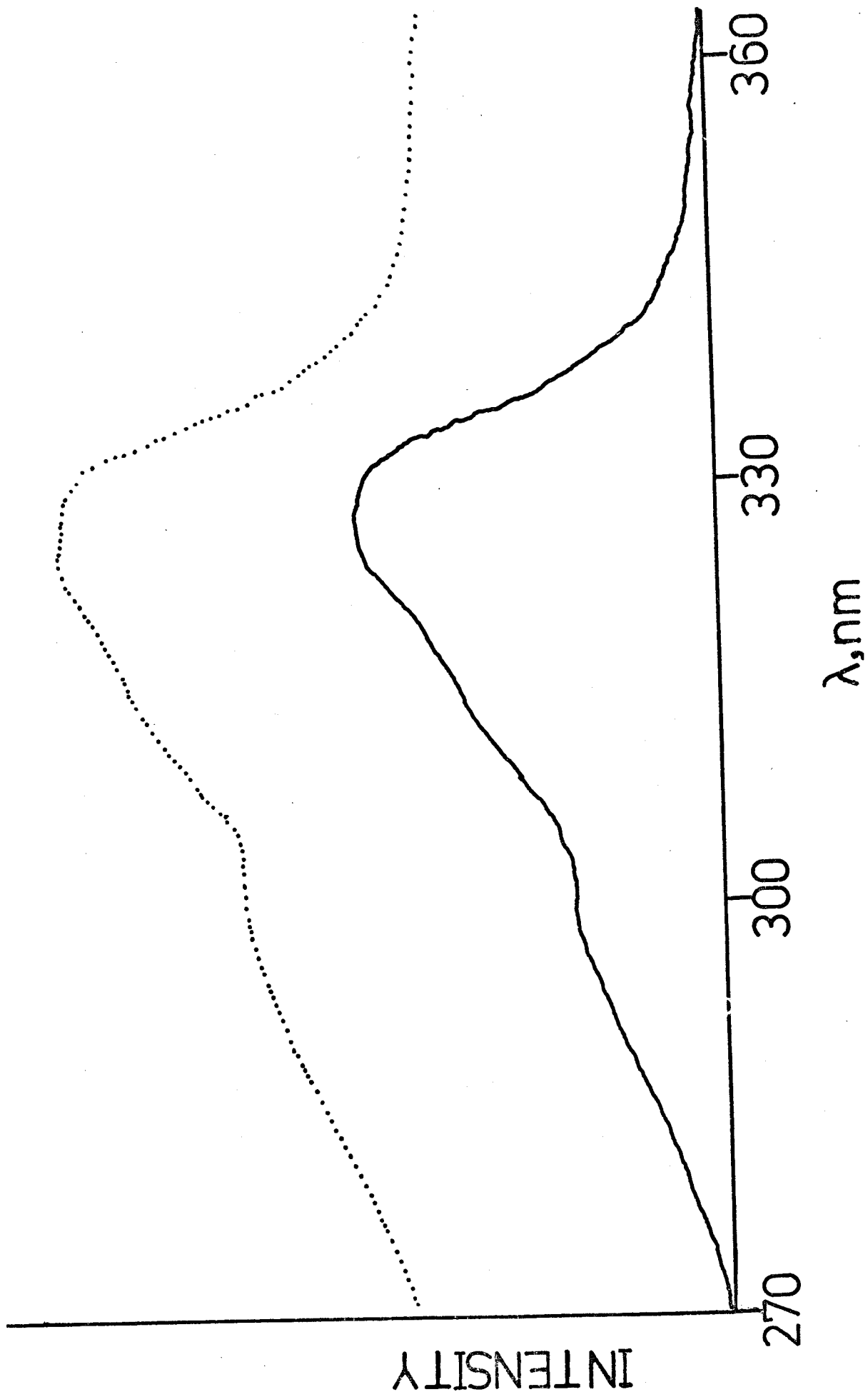

FIGURE 4.2. Fluorescence Excitation Spectra at 453 K. (a) 1,4 DCN/DMHD Exciplex System ....
(b) 1,4 DCN Monomer ——

FIGURE 4.3. Fluorescence quenching of 1,4 DCN by DMHD at 457°K. pressure 1,4 DCN (0.5 torr)

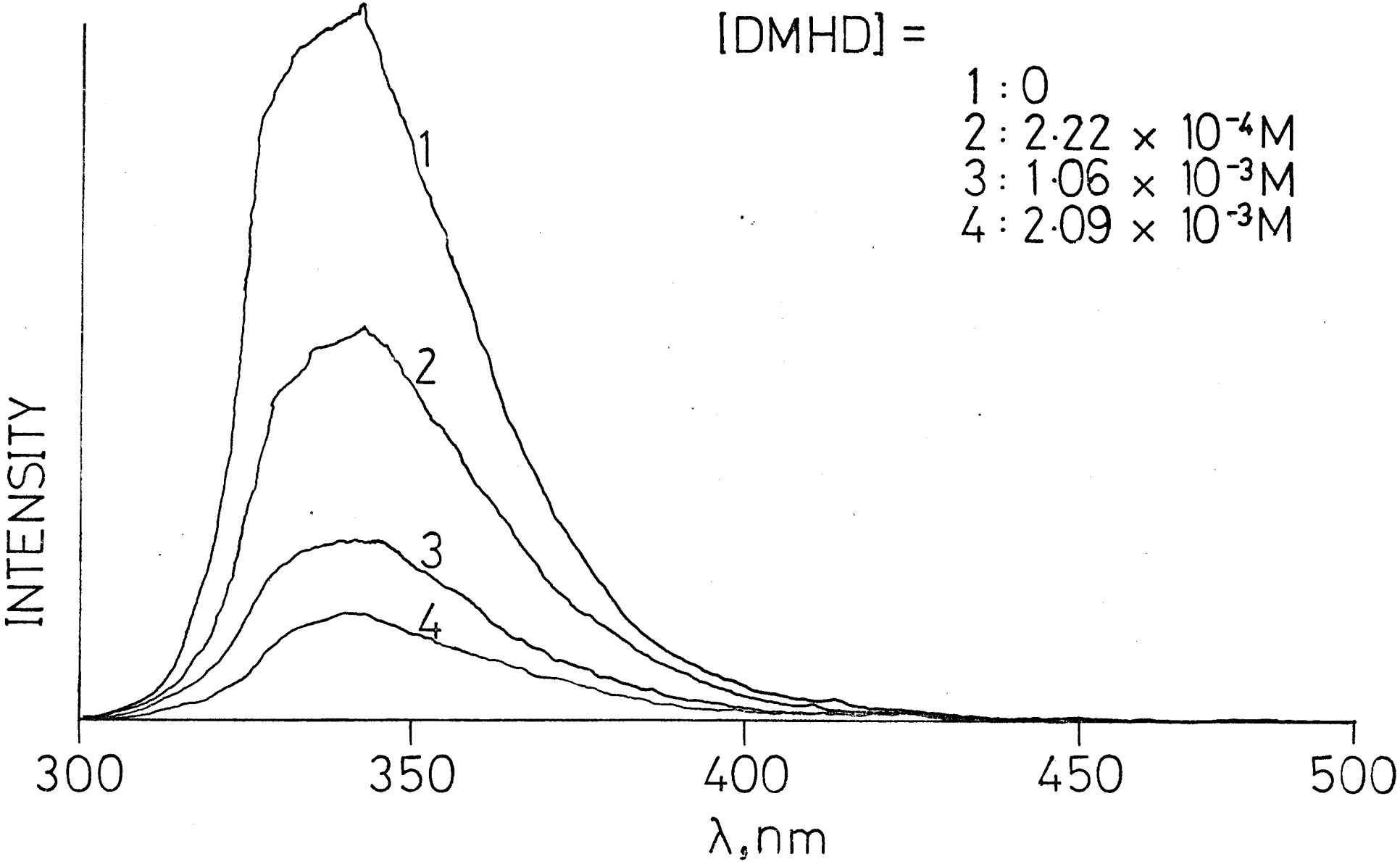

FIGURE 4.4. Fluorescence quenching of 1,4 DCN by DMHD at 457°K. Concentrations of both components are the same as in Figure 4.3. Sensitivity of spectrometer is x 12.5 that used to record the spectra in Figure 4.3.

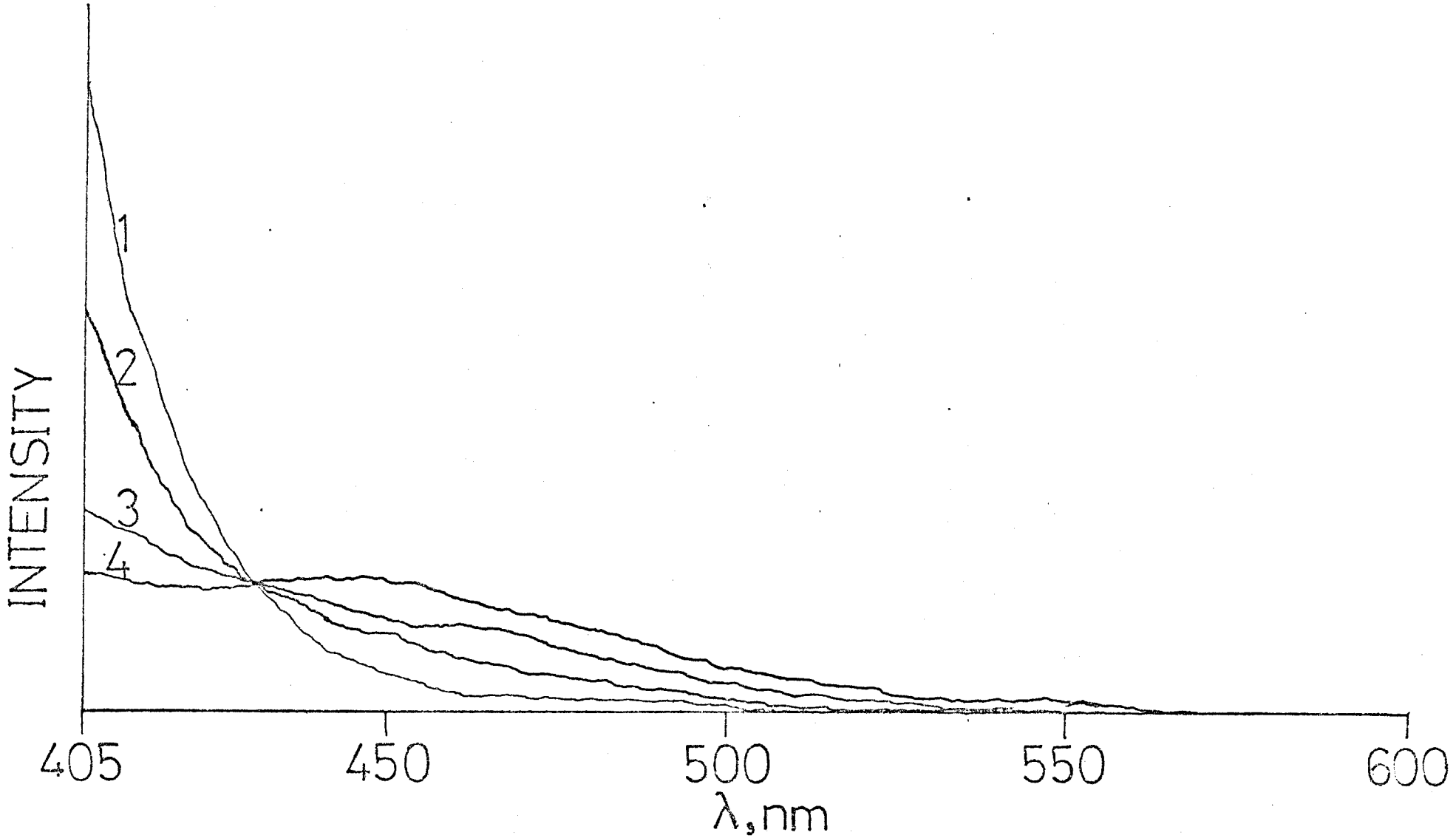

1,4 DCN and DMHD were also shown to exhibit characteristic exciplex emission when dissolved in degassed cyclohexane solvent (see Figure 4.5). Spectral data of the solution and vapour phase systems are presented in Table 4.1, from which it can be seen that there is a substantial decrease (0.145 eV) in the monomer-exciplex emission maxima energy gap in going from the solution to the vapour phases. The implication is (see Figure 1.1) that the binding energy of the exciplex is reduced in the vapour phase if there is no great difference in ground state repulsion energies (E_R) in the two phases.

In solution the wavelengths of exciplex fluorescence bands have been found to be sensitive[14,15] to the polarity of the solvent. A red-shift of $(h\nu_E)_{MAX}$ is observed with increase in solvent polarity, a manifestation of the polar structure of exciplexes. Theories of solvent effects on electronic spectra[10] applied to these solvent shifts in exciplex emission bands yield an expression[11] for the exciplex emission maximum, ν_E^{MAX}, dissolved in a solvent of static dielectric constant ε and refractive index n:

$$\nu_E^{MAX} = \nu_E^{MAX}(0) - \frac{2\mu_c^2}{hca^3}\left(\frac{\varepsilon-1}{2\varepsilon+1} - \frac{1}{2}\cdot\frac{n^2-1}{2n^2+1}\right) \qquad (4.37)$$

a is the cavity radius in the Onsager reaction field and $\nu_e^{MAX}(0)$ is the emission band maximum in a medium of zero dielectric constant. Many workers have used this expression[3,12,13,14,15] to determine the exciplex dipole moment, μ_c, by plotting ν_E^{MAX} against $f(\varepsilon,n)$, where

$$f(\varepsilon,n) = \frac{\varepsilon-1}{2\varepsilon+1} - \frac{1}{2}\cdot\frac{n^2-1}{2n^2+1} \qquad (4.38)$$

for the exciplex emission in a range of solvents of varying polarity.

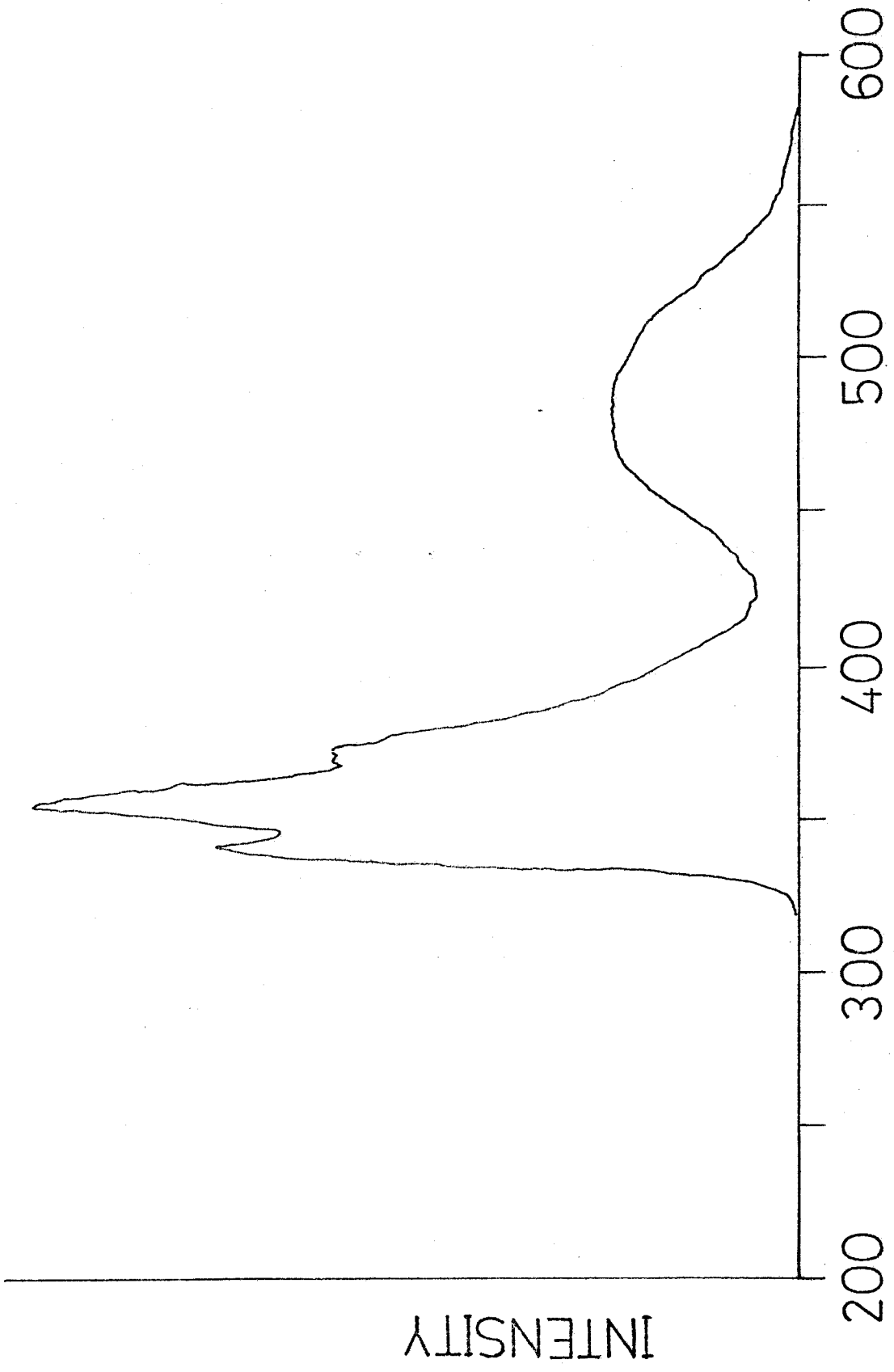

FIGURE 4.5. Fluorescence Emission spectrum of 1,4 DCN/DMHD system in Cyclohexane Solution.

TABLE 4.1

Comparison of Emission Maxima of monomer and exciplex fluorescence in the vapour and solution phases

PROPERTY	1,4 DCN/DMHD in Vapour Phase	1,4 DCN/DMHD in Cyclohexane Solution
$\lambda^{MAX}_{MONOMER}$	343 nm	348 nm
$\lambda^{MAX}_{EXCIPLEX}$	446 nm	480 nm
MONOMER-EXCIPLEX ENERGY GAP $(h\nu_M^{MAX} - h\nu_E^{MAX})$	0.835 eV	0.980 eV

The slope of a straight line fit to such a plot yields the quantity $2\mu_c^2/hca^3$ from which the dipole moment may be calculated. Since there is no dielectric medium surrounding the exciplex in the vapour phase, it would be expected that the fluorescence maximum would be blue-shifted with respect to the maximum in a non-polar solvent. As Table 4.1 demonstrates such is the case for the 1,4 DCN/DMHD exciplex, the emission maximum being blue-shifted by 34 nms in going from cyclohexane solution to the vapour phase. Thus the dipole moment of the vapour phase exciplex can be estimated from equation (4.37) where ν_E^{MAX} (0) will be the band maximum in the vapour phase. Equation (4.37) was also used to estimate the dipole moment of the vapour phase 9CNA/ DMA exciplex. The two results are given in Table 4.2. In these calculations the cavity radius was taken as 5 Å [13] and for cyclohexane, $\varepsilon = 2.023$ and $n = 1.426$.[16] The values of μ_c from Table 4.2 are almost equal and are comparable to values calculated from solution phase data.[3,12,13,14,15] The dipole moment of 14 D may be compared to the 16.8 D[30] expected for complete charge-transfer; on the basis of this comparison one would predict that there is about 80% contribution from the charge transfer configuration to the exciplex electronic structure.

However, the solvent shift technique for the calculation of exciplex dipole moments has been criticised by several workers. Groenen et al[32] used an electro-optical experiment to determine the dipole moments of several exciplex systems in solution and found that in general the values they measured were smaller than those calculated using solvent-induced fluorescence shifts. They argued that the significance of such solvent effects in a quantitative sense is limited by the uncertainty in the value

TABLE 4.2

Evaluation of dipole moments of two vapour phase exciplexes using equation (4.37)

SYSTEM	9CNA/N,N DMA		1,4 DCN/DMHD	
λ_E^{MAX}, nm	SOLUTION(C_6H_{12}) 530	VAPOUR 490	SOLUTION(C_6H_{12}) 480	VAPOUR 446
ν_E^{MAX}, cm^{-1}	1.8867×10^4	2.048×10^4	2.0803×10^4	2.2421×10^4
μ_c Debye	13.8		14.0	

of the cavity radius, a, which occurs to the third power in eq.(4.37). The factor f(ε,n), eq.(4.38), has also been criticised as being not a true measure of solvent polarity since it does not account for the reaction of the electrons of the solvent molecules to the inhomogeneous electric field set up by the dipolar solute.[17] Equation (4.37) also assumes that the electronic structure of the exciplex remains unchanged in going from the vapour to solution phases. However deviations from linearity in ν_E vs. f(ε,n) plots have been found for some solution phase systems.[3,31] These deviations were accounted for by specific solvation effects on the electronic structures of these charge-transfer complexes. Therefore the dipole moment values of Table 4.2 must be regarded as approximate; they do, however, confirm the polar character of exciplexes and have importance as comparative parameters.

The fluorescence spectrum of unquenched 1,4 DCN, $\left[Q\right] = 0$, is shown in the set of typical emission shown in figure 4.3. The emission was quenched very efficiently by the added diene and the quenching follows Stern-Volmer behaviour, the three plots are shown in figure 4.6. The linear Stern-Volmer plots are further evidence for the absence of ground state interactions since ground state complex formation would lead to non-linear Stern-Volmer plots.[18] Ground-state complexation has a complicating effect on the kinetics since the complex, AQ, competes with monomer, A, for incident photons and thus as the concentration of AQ increases, less excitation light is absorbed by A and hence there is a resultant positive deviation from linearity in the quenching plot with increase in added quencher concentration. The fraction of light, f_A, absorbed by A would be given by equation (4.38) where ε_A and ε_{AQ} are the extinction coefficients for the monomer and ground-state complex respectively,

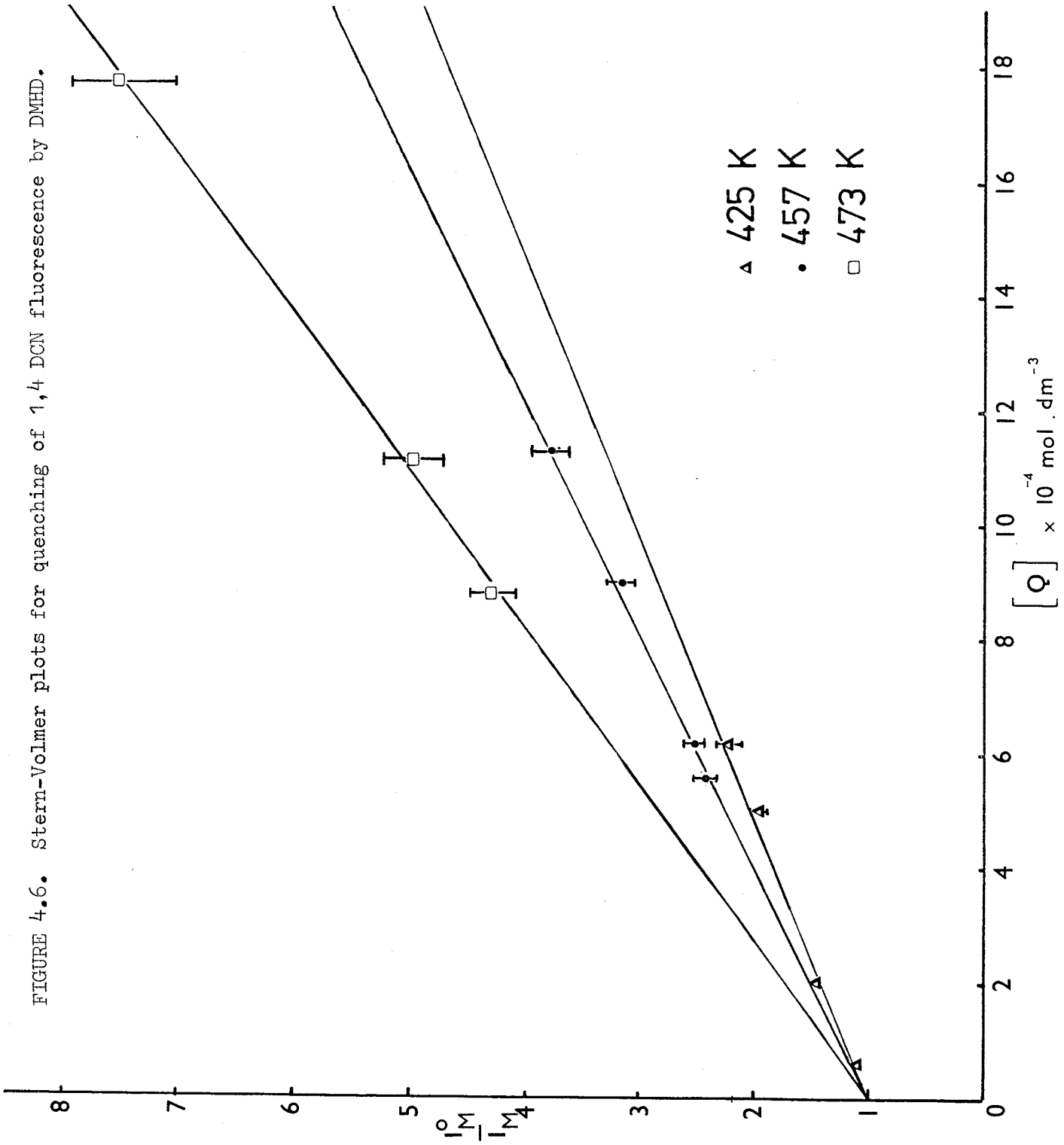

FIGURE 4.6. Stern-Volmer plots for quenching of 1,4 DCN fluorescence by DMHD.

$$f_A = \frac{\varepsilon_A [A]}{\varepsilon_{AQ} [AQ] + \varepsilon_A [A]} \qquad (4.38)$$

This complicating feature therefore does not arise in the interaction of 1,4 DCN with DMHD, since the Stern-Volmer plots are linear.

From the slopes of the plots in Figure 4.6, the Stern-Volmer constant (K_{SV}) was determined at the three temperatures, (see equation (4.33)). The second order overall quenching rate constant, k_q, was then evaluated by dividing K_{SV} by the unquenched monomer lifetime τ_o, (see equation (4.34)). Table 4.3 presents the results of these calculations at three temperatures 425°K, 457°K and 473°K.

The gas-kinetic hard-sphere collision rate, k'_{gk}, can be calculated using the well known expression,[20]

$$k'_{gk} = \sigma^2_{AB} \left(\frac{8 \pi kT}{\mu} \right)^{\frac{1}{2}} \qquad (4.39)$$

μ being the reduced mass, k Boltzmann's constant, and σ_{AB} the collision diameter). Equation (4.39) gives the rate at which molecules, temperature T K, collide in the gas phase on the assumption that the colliding partners act as hard spheres. For a collision diameter, σ_{AB}, equal to 10 Å k'_{gk} has a value equal to 7.1×10^{11} dm^3 mol^{-1} sec^{-1} for the 1,4 DCN/DMHD pair at 457°K. Thus it is evident, by comparison with the k_q values in Table 4.3, that the quenching of 1,4 DCN fluorescence by DMHD is very efficient since it occurs at a rate of the same order of magnitude as k'_{gk}.

Another important feature of the quenching process is that k_q increases with increase in temperature. If feedback was an important fate of the exciplex then the value of k_4, the rate constant for the

TABLE 4.3

The overall quenching of 1,4 DCN by DMHD

TEMPERATURE (K)	STERN-VOLMER CONSTANT $K_{SV} \times 10^3 . (dm^3 . mol^{-1})$	τ_o ns	QUENCHING RATE CONSTANT $(dm^3 mol^{-1} sec^{-1})$ $k_q \times 10^{11}$
425	2.06 ± 0.06	10.07 ± 0.02	2.05 ± 0.06
457	2.45 ± 0.07	9.50 ± 0.02	2.58 ± 0.07
473	3.62 ± 0.13	9.60 ± 0.02	3.77 ± 0.14

feedback process, which in solution phase systems usually shows a very strong temperature dependence,[19] would be the dominant factor in the variation of k_q with temperature. Equation (4.34), $k_q = k_3 k_p / k_4 + k_p$, shows therefore as k_4 increases with increasing temperature k_q would decrease. This effect has been observed for the solution phase exciplex formed between photo-excited α-cyanonaphthalene and ground state dimethylcyclopentene-1,2 in hexane solution at temperatures greater than 0°C.[19] However, in the present work the opposite effect was observed, as shown in Table 4.3. This matches the behaviour of the solution phase α-cyanonaphthalene/dimethylcyclopentene-1,2 system at temperatures below 0°C where it was shown that $k_4 \ll k_p$. For this solution phase system, k_p was observed to have a very much weaker temperature dependence than k_4, and since at temperatures $< 0^\circ C$ $k_4 \ll k_p$, then from equation (4.34) k_q now follows the temperature dependence of k_3, the rate constant for the exciplex formation step, which decreases with decreasing temperature. This trend is also observed in the present work, which suggests that k_4 is less than k_p for the decay of the vapour phase 1,4 DCN/DMHD exciplex. A similar conclusion was reached by Prochorow et al[7] in a study of vapour phase exciplex systems formed by the association of a variety of ground-state methylated benzenes with electronically excited tetracyanobenzene. However, these workers were unable to evaluate k_4 owing to the lack of sensitivity and time resolution in their single-photon counting instrument. As will be seen later in this chapter, k_4 for the 1,4 DCN/DMHD system could be evaluated and hence the importance of the individual processes in the proposed reaction scheme (equations (4.1)-(4.7)) could be judged and the resulting conclusions compared with the deductions reached from the steady-state measurements.

As shown in figure 4.3, at low concentrations of added donor, only the quenching of the 1,4 DCN fluorescence was observed. The growth of the exciplex band (see figure 4.4) was observed only when the sensitivity of the fluorimeter was raised by a factor of 12.5. Even for favourable cases, for example under the conditions used to record the emission spectrum in figure 4.1, when higher concentrations of diene (ca. 1000 torr) were present the intensity of the exciplex emission was still only a small fraction of the intensity of the unquenched 1,4 DCN fluorescence. The quantum efficiency of the exciplex emission must therefore be extremely small. This could imply that the radiative rate constant for the exciplex decay, k_5 is small in comparison to the radiative rate constant k_1, for the decay of excited state monomer. This possibility can be explored from a plot employing equation 4.36

$$\frac{\phi_E}{\phi_M} = \frac{I_E}{I_M} = \frac{k_5}{k_1} \cdot \frac{k_3}{k_4+k_p} \left[Q\right] \qquad (4.36)$$

A plot of I_E/I_M versus $\left[Q\right]$ should give a straight line, passing through the origin, with slope equal to $\frac{k_5}{k_1} \cdot \frac{k_3}{(k_4+k_p)}$. Such a plot, using data obtained at 457 K, is shown in figure 4.7 where it can be seen that all the points lie on a straight line (within experimental error) which goes through the origin. The slope equalled 22.5 dm^3 $mole^{-1}$. By substitution in equation (4.36) for k_4 and k_p whose values are given in Table 4.9, (the method of evaluation for these rate constants is given later in this chapter), the ratio k_5/k_1 was found to be 1.28×10^{-2}. Thus, as expected, the radiative rate constant for the exciplex fluorescence is about two orders of magnitude less than for monomer fluorescence.

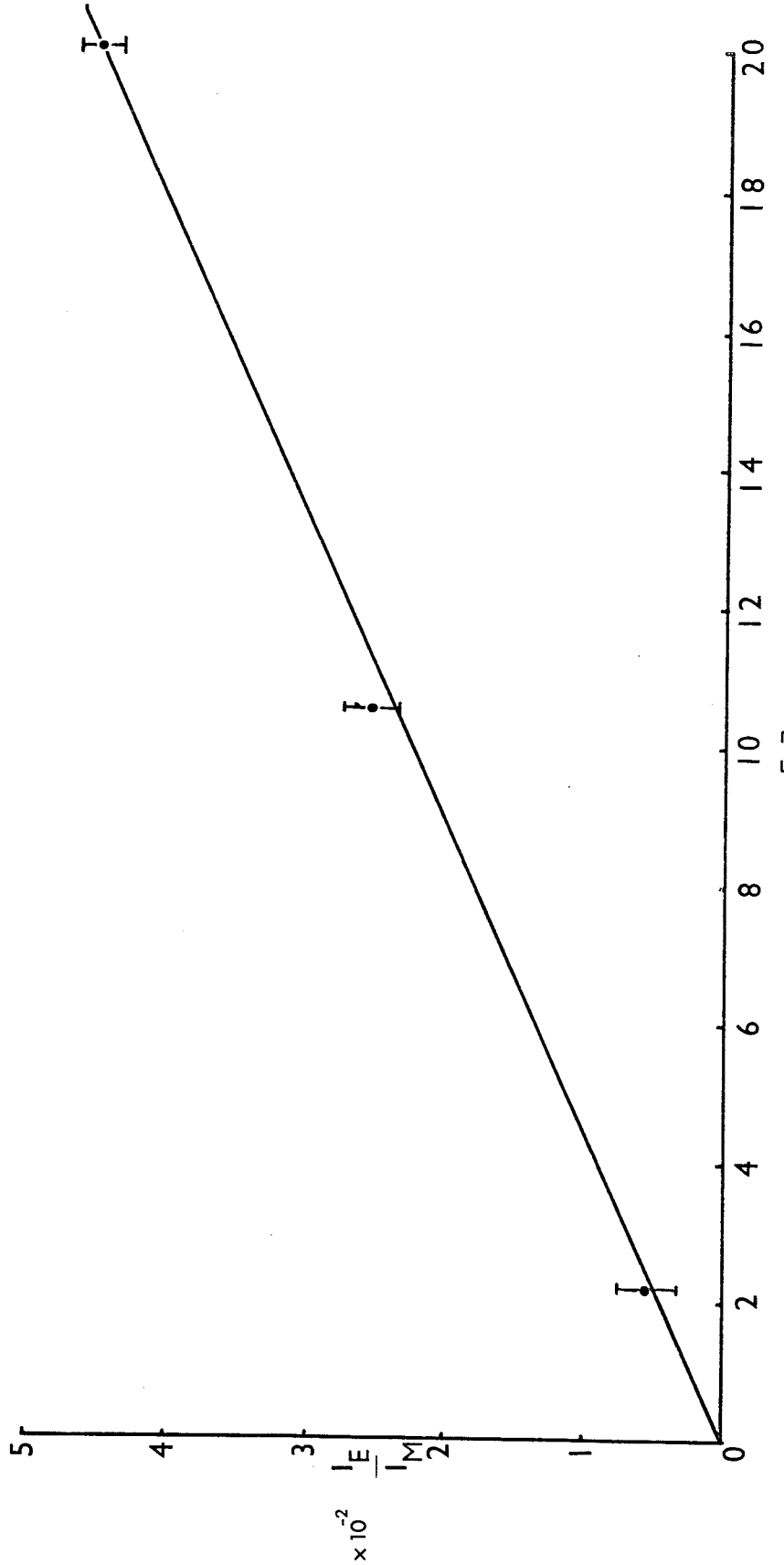

FIGURE 4.7. I_E/I_M ratio plotted as a function of DMHD concentration at 457 K.

For the 1,4 DCN/DMHD system excited at 300 nms, the exciplex/1,4 DCN emission intensity ratio decreases from 3.26 to 1.16 in going from 430°K to 517°K (pressure (DMHD) = 709 torr) as shown in figure 4.8. The dramatic decrease in the intensity of the exciplex fluorescence with increase in temperature suggests that intermolecular vibrations play an important role in the non-radiative decay of the vapour phase exciplex, a point raised by Prochorow et al.[7] Since the frequencies of these modes are very small, (probably less than 100 cms^{-1}), owing to the large masses of the two components in the oscillator thus thermal excitation of these vibrations should be considerable at the temperatures of the present experiments which are greater than 425°K.

Stevens and Ban[6] have formulated a method that can be used for determining the binding energy of an exciplex from measurements of the relative intensities of steady-state exciplex and monomer emissions as a function of temperature. Hence it can be used in the absence of decay time measurements.

The basis of this method is equation (4.36) derived in the discussion of exciplex kinetics.

$$\frac{\phi_E}{\phi_M} = \frac{I_E}{I_M} = \frac{k_5}{k_1} \cdot \frac{k_3 [Q]}{k_4 + k_p} \qquad (4.36)$$

Rearrangement of equation (4.36) leads to:

$$\ln \frac{k_1}{k_5} \cdot \frac{I_E}{I_M [Q]} = \ln \frac{k_3}{k_4 + k_p} \qquad (4.40)$$

If it can be assumed that $k_p \ll k_4$ in the temperature range under study; since k_3/k_4 is the equilibrium constant, K_A, from the thermodynamics of

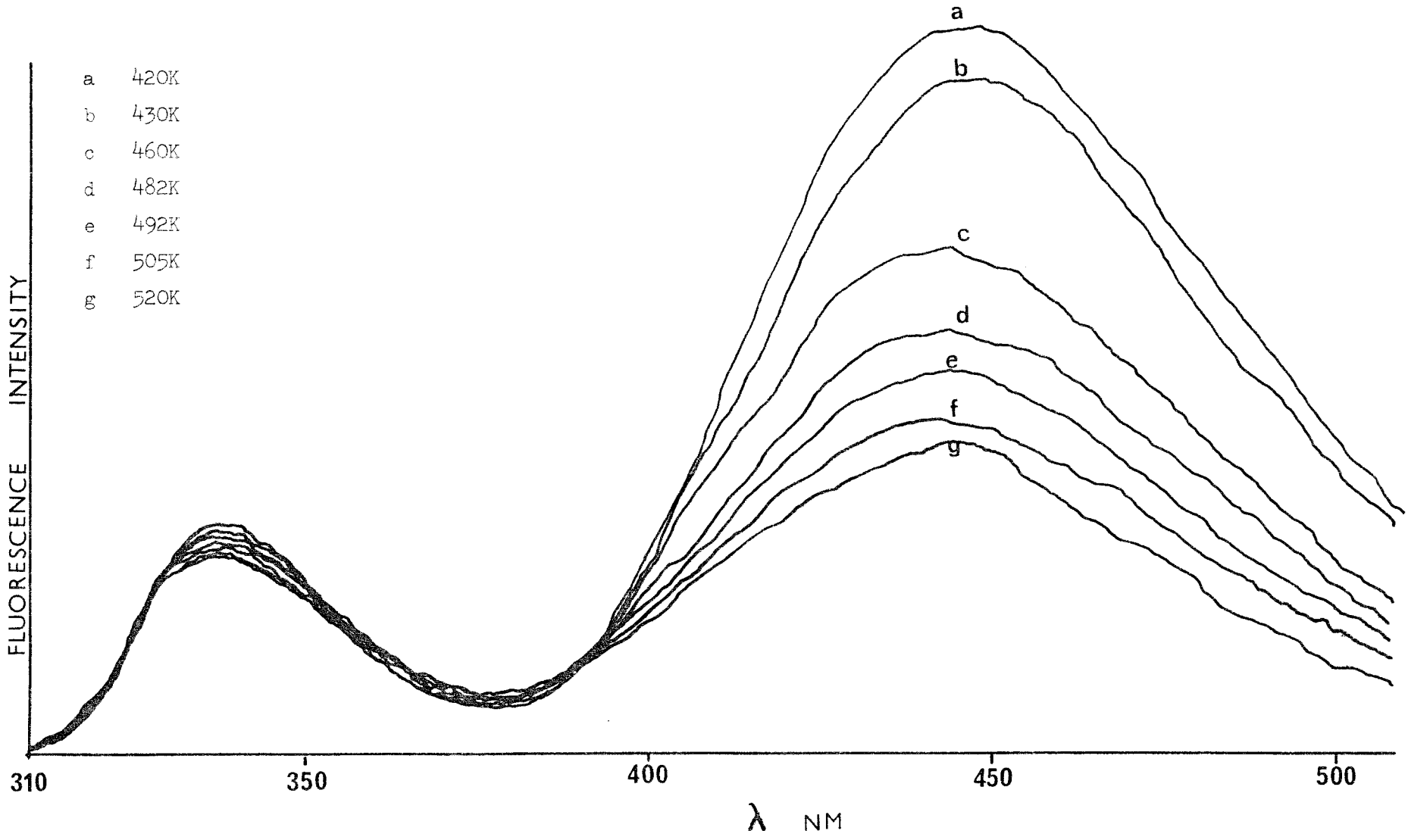

FIGURE 4.8. Temperature dependence of the fluorescence emission spectrum of the 1,4 DCN/DMHD exciplex system

chemical equilibria[22] it follows that,

$$\ln \frac{k_1}{k_5} \cdot \frac{I_E}{I_M [Q]} = \ln K_A = \frac{\Delta S^\circ}{R} - \frac{\Delta H^\circ}{RT} \qquad (4.41)$$

where ΔH° is the exciplex binding energy and ΔS° is the standard entropy change for exciplex formation. Assuming that k_1 and k_5 are temperature independent rearrangement of equation (4.41) leads to the relation,

$$\ln \frac{I_E}{I_M} = \text{CONSTANT} - \frac{\Delta H^\circ}{RT} \qquad (4.42)$$

Thus a plot of the natural logarithm of the ratio of the relative intensities as a function of inverse temperature ($^\circ K^{-1}$), termed a Stevens-Ban plot, yields a straight line with slope equal to $-\Delta H^\circ/R$ if the conditions are suitable.

Stevens and Ban[6] have stated that the criteria of the presence of an isoemissive point[8,9] in the emission spectra recorded as a function of temperature and a linear dependence of $\ln (I_E/I_M)$ on $(1/T)$ is evidence of the conditions $k_p << k_4$. In these circumstances, therefore, a binding energy can be extracted from the Stevens-Ban plot.[6] As can be seen from the spectra shown in figure 4.8 an isoemissive point was observed for the 1,4 DCN/DMHD system; the Stevens-Ban plot, shown in figure 4.9, was also linear. Therefore if the criteria are rigorous, from the positive slope of the plot a binding energy may be calculated. The value obtained is equal to -5.00 kcals.mole^{-1}. Although this value is similar to the enthalpies of formation for the exciplexes formed by other aromatic molecules with various electron donors[21] in solution, there are reservations about the method employed. The criteria employed

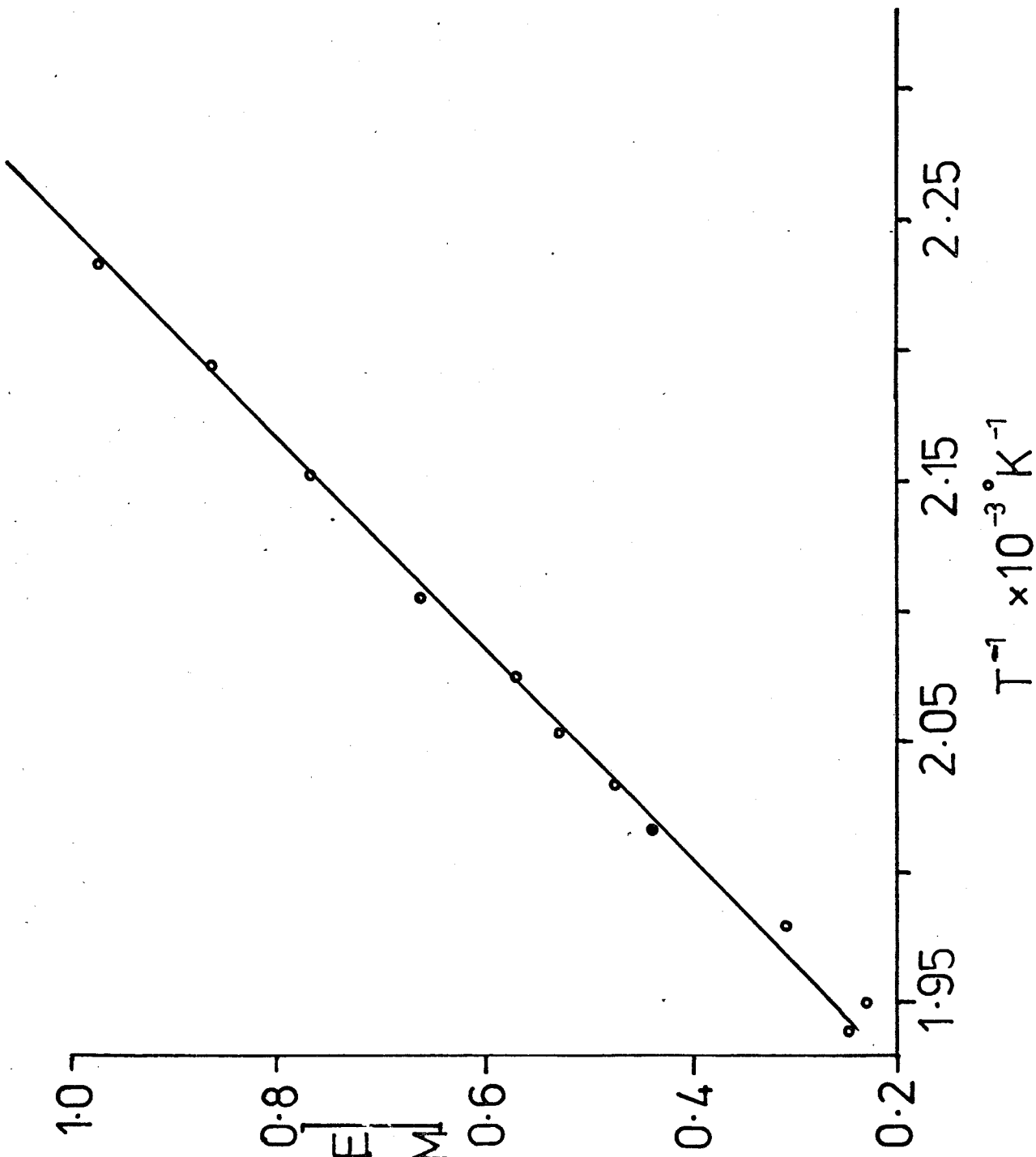

FIGURE 4.9. Stevens-Ban plot for 1,4 DCN/DMHD exciplex system. Concentration of DMHD = 2.4 x 10^{-2} mol.dm^{-3}.

to define the temperature region in which $k_p << k_4$ has been criticised by other workers, see for example reference 26, since it has been shown that the existence of isoemissive points does not necessarily depend on whether the conditions correspond to $k_p << k_4$. Isoemissive points can still be observed when $k_4 << k_p$ (see for example, references 23 and 26 and other references therein). Where the assumption $k_p << k_4$ has been incorrectly made many workers have misinterpreted the Stevens-Ban plots obtained[34,35,36] as shown in the light of more recent work.[23,26,19] (respectively) There are thus dangers in using Stevens-Ban plots to determine exciplex binding energies without independent evidence for the validity of the assumption that $k_p << k_4$. In the present work the condition that k_4 must be much greater than k_p is incompatible with the Stern-Volmer quenching results discussed previously, where it was inferred that k_p was greater than k_4. The binding energy obtained for the 1,4 DCN/DMHD exciplex is therefore suspect. Values for the individual rate constants, which can only be obtained from measurements of the fluorescence decay curves of the emitting excited state transients, are obviously needed to clarify the situation.

4.3.2 Kinetic Measurements

The unquenched monomer lifetime, τ_o, was measured under fully collisionally relaxed conditions. Deconvolution was performed with the least squares iterative convolution technique described in Section 2.3 of Chapter 2. Using this method, the fluorescence decay curve was found to be a single exponential as demonstrated by the fact that the χ^2_ν value was very close to unity for such a decay law. τ_o decreased from 10.0 ns at 425K to 9.5 ns at 457K. This corresponds to a slight increase in the unimolecular relaxation rate, k_o in equation (4.8), of 0.099 x 10^9 dm^3 mol^{-1} $sec^{-1}$to 0.105 x 10^9 dm^3 mol^{-1} sec^{-1}. Because k_1 and k_2 were not separately determined as a function of temperature, a definite statement cannot be made about the cause of this increase but because there is a slight decrease in refractive index (n) of vapour phase media with increasing temperature[16] then from the relationship given by Strickler and Berg[37] (also see Hirayama and Phillips[38] for a good discussion of the effect of n on the radiative rate constant) there should be a slight decrease in k_1, the radiative rate constant, which means that the observed increase in k_o is due to an increase in the non-radiative relaxation processes.

With addition of DMHD quencher equations (4.18), (4.23) and (4.24) predict that, on formation of the exciplex, the monomer will fluoresce with two decaying components, one of them resulting from the feedback process which regenerates excited state monomer from the complex. As expected, the monomer decay curves did exhibit double exponential behaviour since the χ^2_ν values for double exponential fits were always close to unity. However, the intensity of one of the components was weak and had very large uncertainties in both its decay times and pre-exponential factors. Hence it could not be accurately extracted from any of the decay curves. The lifetimes of

the intense component are presented in TABLE 4.4. These were measured at two temperatures as a function of DMHD concentration and the expected behaviour of decrease of lifetime with increase in quencher concentration is clearly shown. The decay times of the weak component, however, showed no discernible trend which was not surprising in view of the large errors associated with its decay parameters. Also tabulated are k_o $(= \frac{1}{\tau_o})$ and λ $(= \frac{1}{\tau})$ values.

Equations (4.27) and (4.28) predict that, in response to δ-pulse excitation, the exciplex concentration will rise exponentially to a maximum and then decay. As previously noted, the absolute intensity of the 1,4 DCN/DMHD exciplex fluorescence is very low and hence in order to observe the decay of the exciplex emission a high concentration (pressure > 300 torr) of diene had to be added. At such high quencher concentrations the exciplex was formed vary rapidly and thus the rise time of the decay curve was too fast for accurate analysis. Exciplex fluorescence decay times at two temperatures are presented as a function of quencher concentration in TABLE 4.5 . As can be seen from this table, at the high concentrations of diene used in these experiments the exciplex decay time was found to be concentration independent. To predict the behaviour of λ_1 and λ_2 as $[Q]$ becomes large, equation (4.17) is rearranged into the following form:

$$\lambda_{1,2} = \tfrac{1}{2}\left\{k_o+k_3+k_4+k_p \pm k_3[Q]\left(\frac{1+2(k_o+k_4-k_p)}{k_3[Q]} + \frac{(k_o-k_4-k_p)^2}{(k_3[Q])^2}\right)^{\frac{1}{2}}\right\}$$

The expression under the square-root is binomially expanded[5] and neglect of higher terms leads to:

$$\lambda_{1,2} = \tfrac{1}{2}\left\{k_o+k_3[Q]+k_4+k_p \pm \left(k_3[Q]+k_o+k_4-k_p+\frac{(k_o-k_4-k_p)^2}{2k_3[Q]}\right)\right\}$$

TABLE 4.4

Fluorescence decay times of photo-excited 1,4 DCN monitored at

$\lambda_{EMISSION}$ = 344 nm.

Temperature K	(DMHD) x 10^{-3} mol. dm^{-3}	τ^a ns	λ x 10^8 S^{-1}
425	0.0	10.1 ±0.02	0.993±0.002
	0.0603	9.23±0.3	1.08 ±0.01
	0.173	7.30±0.07	1.37 ±0.01
	0.301	4.52±0.04	2.21 ±0.02
	0.391	3.89±0.12	2.57 ±0.08
	0.502	3.19±0.01	3.13 ±0.01
	0.634	2.76±0.02	3.62 ±0.03
	0.755	2.65±0.30	3.77 ±0.04
457	0.0	9.50±0.02	1.05 ±0.002
	0.166	5.61±0.30	1.78 ±0.10
	0.347	3.70±0.004	2.70 ±0.003
	0.502	2.90±0.02	3.45 ±0.02
	0.711	2.10±0.002	4.76 ±0.004
	1.05	1.62±0.01	6.17 ±0.04

a. The listed errors in τ shown in the above table are the standard deviations recovered in the deconvolution procedure. These standard deviations are too low as estimates of uncertainties but they have been used as such in the present work because systematic experiments aimed at determining the actual uncertainty in the lifetime values were not carried out. This point must also be taken into account when considering the values of the exciplex decay times shown in TABLES 4.5 and 4.6.

TABLE 4.5

Fluorescence decay times of the 1,4 DCN/DMHD exciplex as a function of DMHD concentration, monitored at $\lambda_{EMISSION}$ = 446 nm.

(DMHD) x 10^{-3} moles. dm^{-3}	τ^a/ns
TEMPERATURE = 425°K	
9.2	9.51±0.02
15.0	9.30±0.02
20.0	9.32±0.02
21.6	9.15±0.02
TEMPERATURE = 473°K	
9.2	5.80±0.01
15.0	5.61±0.01
20.0	5.73±0.01
21.6	5.74±0.01

a. The exciplex fluorescence decay curves followed single exponential decay laws.

Therefore

$$\lim_{[Q]\to\infty} \lambda_1 = k_o + k_3[Q] + k_4$$

$$\lim_{[Q]\to\infty} \lambda_2 = k_p \qquad (4.43)$$

Thus λ_2 becomes equal to k_p at large values of $[Q]$, i.e. the asymptote of a λ_2 versus $[Q]$ plot would be k_p. Since the exciplex lifetime was experimentally observed to be invariant to changes in the diene concentration, it can reasonably be assumed that this asymptotic value of λ_2 has been reached, thus providing a convenient method for the evaluation of k_p, the rate constant for the deactivation of the exciplex. The exciplex decay times, at four temperatures, which were measured at $[DMHD] = 20 \times 10^{-3}$ mol. dm^{-3} are listed in TABLE 4.6 along with the calculated values of k_p. As can be seen from this table, there is approximately a two-fold increase in k_p with a rise in T of 70K.

The exciplex lifetime can also be affected by the following complicating feature in the reaction scheme:

$$(AQ)^* + Q \xrightarrow{k_7} \text{QUENCHING} \qquad (4.44)$$

Halpern[4] has shown that for the excimer system formed by 1-azabicyclo [2.2.2] octane (ABCO), quenching of the complex by ground state species was significant both in the vapour and solution phases. This effect has also been observed in studies of the kinetics of other solution phase exciplexes.[27-29] It is therefore imperative to test for this additional quenching step when performing a complete kinetic analysis.

TABLE 4.6

Exciplex decay times as a function of temperature, monitored at $\lambda_{EMISSION}$ = 446 nm

$[DMHD] = 20 \times 10^{-3}$ mol. dm^{-3}

TEMPERATURE K	τ ns	$k_p \times 10^8$ dm^3 mol^{-1} sec^{-1}
425	9.32±0.02	1.08±0.002
457	6.80±0.02	1.47±0.004
473	5.73±0.01	1.75±0.003
493	4.91±0.01	2.04±0.004

When process (4.44) complicates exciplex kinetics, equation (4.17) is altered and becomes,[24]

$$\lambda_{1,2} = \tfrac{1}{2}\left\{k_o+(k_3+k_7)\left[Q\right]+(k_4+k_p)\pm\left((k_o+(k_3-k_7)\left[Q\right]-k_4-k_p)^2+4k_4k_3\right)^{\frac{1}{2}}\right\} \tag{4.45}$$

As $\left[Q\right]$ approaches large values, the limit in equation (4.46) is reached,

$$\lim_{\left[Q\right]\longrightarrow\infty}\frac{d\lambda_2}{d\left[Q\right]} = k_7 \tag{4.46}$$

Thus when step (4.44) is important, there is an upward deviation from linearity in the λ_2 versus $\left[Q\right]$ plot which has a slope at high $\left[Q\right]$ equal to k_7. Halpern[4] used this relationship in his work from which he extracted a value of k_7 equal to 8.4×10^9 dm^3 mol^{-1} sec^{-1}. However, as has been discussed previously, in the present work the exciplex lifetime was observed to be independent of $\left[Q\right]$ at high concentrations and hence the quenching of (AQ)* by Q can be ignored.

4.3.3. Evaluation and Discussion of the Rate Constants and Thermodynamic Properties for the Formation and Decay Processes of the 1,4 DCN/DMHD vapour phase exciplex.

When it is possible to extract accurately all the decay parameters of both components in the double exponential monomer decay curves observed on addition of Q, then the rate constants k_3, k_4 and k_p are evaluated by employing the following two relations,[3,18]

$$\lambda_1 + \lambda_2 = k_o + k_3 [Q] + k_4 + k_p \qquad (4.47)$$

$$\lambda_1 \lambda_2 = k_o(k_4 + k_p) + k_p k_3 [Q] \qquad (4.48)$$

These are obtained by manipulation of eq.(4.17). k_o is known since it is the reciprocal of the unquenched monomer lifetime. From eq.(4.47) a plot of $(\lambda_1 + \lambda_2)$ versus $[Q]$ will have a slope equal to k_3. k_p may then be obtained from a $(\lambda_1 \lambda_2)$ vs $[Q]$ plot, eq.(4.48), by dividing the slope by k_3. The intercept of either plot yields k_4. Since, in this work, only one exponential term was extracted successfully from the monomer decay curves, as discussed previously, this analysis technique could not be used. Instead k_3 and k_4 (k_p has already been evaluated) were calculated using a novel approach employing a combination of the steady-state quenching results and the transient data.

If equation (4.16) is combined with the expression for the overall quenching rate constant, eq.(4.35), then on subsequent manipulation the relation given by (4.49) results,

$$\lambda^2 - k_o\lambda = k_3((\lambda - k_p)[Q] + \lambda \cdot \frac{k_p}{k_q}) \frac{-k_o k_3 k_p}{k_q} \qquad (4.49)$$

Thus a plot of $\lambda^2 - k_o\lambda$ against $((\lambda - k_p)\left[Q\right] + \lambda.\frac{k_p}{k_q})$ should yield a straight line with slope k_3. k_4 can then be calculated using a rearranged form of eq.(4.35):

$$k_4 = \frac{k_3 k_p}{k_q} - k_p \qquad (4.50)$$

Substitution in equation (4.49) of values for k_q (Table 4.3), λ (Table 4.4), k_o (Table 4.4) and k_p (Table 4.6) led to the data presented in Tables 4.7 and 4.8, which were plotted as shown in figures 4.10 and 4.11. As can clearly be seen from these plots, good straight line fits were obtained, as predicted by equation (4.49). At a temperature of 425 K, k_3 was found to be $3.07 \pm 0.1 \times 10^{11} dm^3 mole^{-1} sec^{-1}$ and increased to a value of $4.07 \pm 0.1 \times 10^{11} dm^3 mole^{-1} sec^{-1}$ at 457K. For the same temperature range k_4 was also found to increase from $0.55 \pm .09 \times 10^{11}$ sec^{-1} to $0.85 \pm .1 \times 10^8 sec^{-1}$. The values of all the rate constants obtained at 425 K and 457 K are summarised, for comparison purposes, in Table 4.9.

A check on the methods of determining these rate constants, which were evaluated by combining steady-state and transient analyses (see equations (4.49) and (4.50)), was made by substituting the values from Table 4.9 into equation (4.17) where,

$$\lambda_1 = \tfrac{1}{2}\left(k_o + k_3\left[Q\right] + k_4 + k_p + (k_o + k_3\left[Q\right] - k_4 - k_p)^2 + 4k_4k_3\left[Q\right]\right)^{\frac{1}{2}}) \qquad (4.17a)$$

and $$\lambda_2 = \tfrac{1}{2}(k_o + k_3\left[Q\right] + k_4 + k_p - ((k_o + k_3\left[Q\right] - k_4 - k_p)^2 + 4k_4k_3\left[Q\right])^{\frac{1}{2}}) \qquad (4.17b)$$

TABLE 4.7

$(\lambda^2 - k_o\lambda)$ as a function of $((\lambda - k_p)[Q] + k_p/k_q)$ at 425 K.

$[Q]$ moles.dm^{-3} x 10^{-3}	$\lambda^2 - k_o\lambda$ sec^{-2} x 10^{16}	$((\lambda - k_p)[Q] + k_p/k_q)$ moles.dm^{-3} x 10^{5}
0.0603 ± 0.003	0.094 ± 0.047	0.575 ± 0.027
0.173 ± 0.009	0.516 ± 0.023	0.779 ± 0.022
0.301 ± 0.015	2.69 ± 0.11	1.52 ± 0.04
0.391 ± 0.020	4.05 ± 0.36	1.95 ± 0.07
0.502 ± 0.025	6.69 ± 0.18	2.70 ± 0.07
0.634 ± 0.032	9.51 ± 0.33	3.54 ± 0.10
0.755 ± 0.038	10.47 ± 0.43	4.04 ± 0.13

These data are plotted in figure 4.10, from which a straight line plot resulted with a slope = 3.07 ± 0.10 dm^{3}mole^{-1}sec^{-1}.

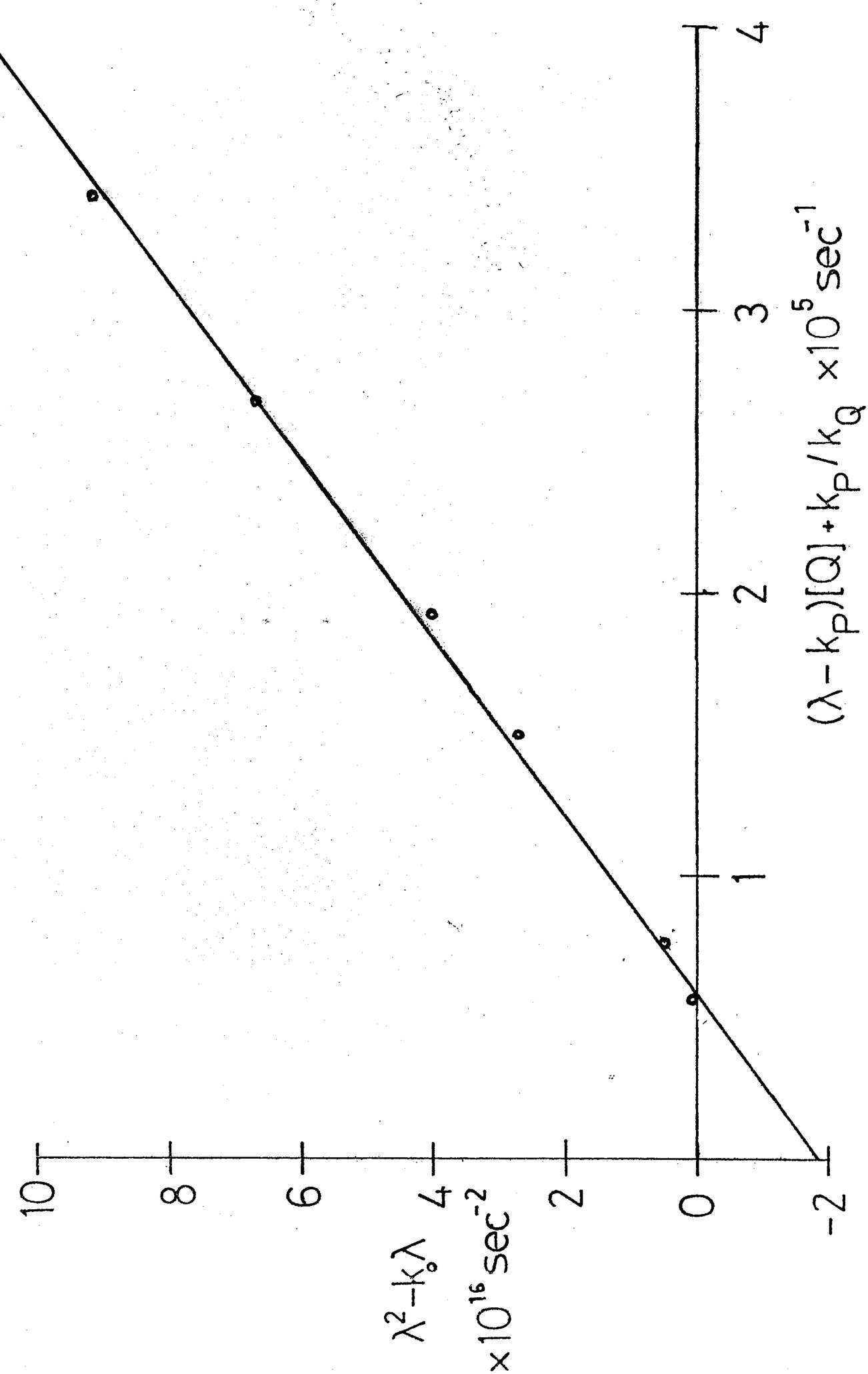

FIGURE 4.10. Plot of data presented in Table 4.7.

TABLE 4.8

$(\lambda^2 - k_o\lambda)$ as a function of $((\lambda - k_p)[Q] + k_p/k_q)$ at 457 K.

$[Q]$ moles.dm^{-3} x 10^{-3}	$(\lambda^2 - k_o\lambda)$ sec^{-2}. x 10^{16}	$((\lambda - k_p)[Q] + k_p/k_q)$ moles.dm^{-3} x 10^5
0.166 ± 0.008	1.30 ± 0.26	1.06 ± 0.06
0.347 ± 0.017	4.46 ± 0.11	1.97 ± 0.05
0.502 ± 0.025	8.28 ± 0.23	2.96 ± 0.07
0.711 ± 0.036	17.7 ± 0.49	5.05 ± 0.14
1.05 ± 0.05	31.6 ± 1.07	8.46 ± 0.26

These data are plotted in figure 4.11, from which a straight line plot resulted with a slope = 4.07 ± 0.10 dm^{3}mole^{-1}sec^{-1}.

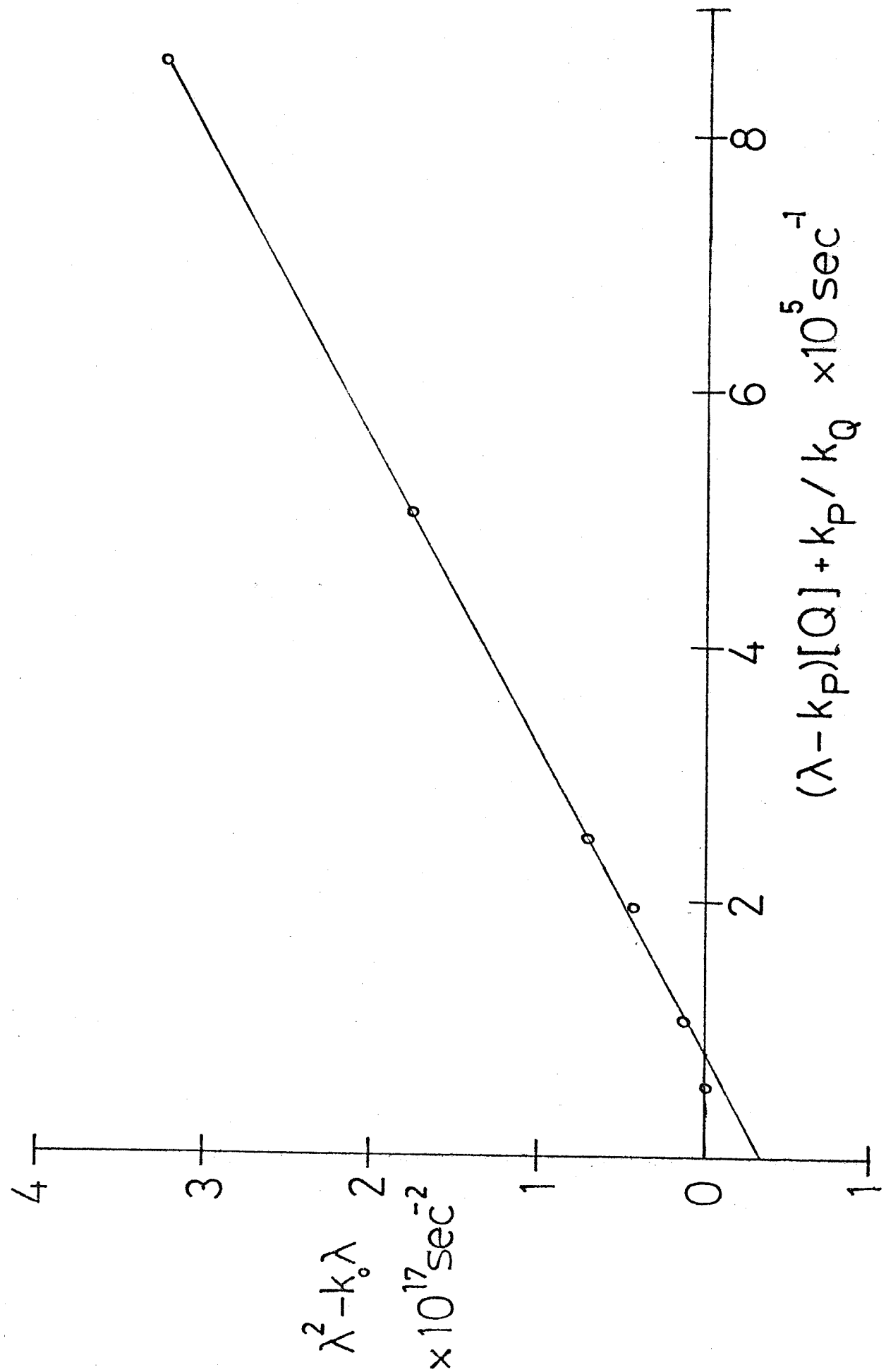

FIGURE 4.11. Plot of data presented in Table 4.8.

TABLE 4.9

Summary of rate constants derived for the formation and decay processes of the 1,4 DCN/DMHD vapour phase exciplex.

T K	k_o $sec^{-1} \times 10^8$	k_p $sec^{-1} \times 10^8$	k_3 $dm^3.mol^{-1}s^{-1} \times 10^{11}$	k_4 $sec^{-1} \times 10^8$
425	0.993 ± 0.002	1.08 ± 0.002	3.07 ± 0.10	0.55 ± 0.09
457	1.05 ± 0.002	1.47 ± 0.004	4.07 ± 0.10	0.85 ± 0.10

The concentrations of DMHD are the same as those employed in the monomer lifetime quenching experiments. The pre-exponential factors, c_1 and c_2, for the two components were also calculated using equations (4.23) and (4.24) and thus the contribution of the component with calculated time constant λ_1 was estimated from the ratio c_1/c_1+c_2. The reciprocals of the λ values are the calculated lifetimes τ_1 and τ_2 for the double exponential monomer decays predicted by exciplex kinetics (see equations (4.1) to (4.24) and these are presented in table 4.10 with the observed lifetimes. The calculated ratios, c_1/c_1+c_2, expressed as percentages, are also listed in the same table. This comparison of observed with predicted behaviour is a good test of the method used to extract the rate constants since equation (4.17) was derived using an analysis based purely on the response of the system to absorption of a δ-pulse of light, see equations (4.1) to (4.17), the relations arising from the imposition of steady-state conditions, eq. (4.35), are not involved.

Two features are immediately noticeable in Table 4.10. Firstly there is good agreement between the lifetime calculated as making the major contribution to the decay and the observed lifetime. Secondly the calculation predicts clear two-component decays, as shown by the c_1/c_1+c_2 ratios. Indeed two-component decays were observed as discussed previously, but the parameters of only one of the components could be extracted successfully from the experimental lifetime data using the standard deconvolution technique. This, however, is not surprising in view of the following considerations (1) At the concentrations of DMHD employed in this study, the calculated τ_1 and τ_2 values are very similar. In real decays non-random distortions would render their

TABLE 4.10

Comparison of observed and calculated monomer decay times

T / K	DMHD x 10^{-3} moles.dm^{-3}	Observed τ ns	Calculated τ_1, ns	Calculated τ_2, ns	Calculated $\frac{c_1}{c_1+c_2}$ percent
425	0.0603	9.2 ± 0.3	5.6 ± 0.2	9.9 ± 0.6	21
	0.173	7.3 ± 0.1	4.7 ± 0.2	9.7 ± 0.6	45
	0.301	4.5 ± 0.04	4.0 ± 0.1	9.6 ± 0.7	60
	0.391	3.9 ± 0.1	3.6 ± 0.1	9.5 ± 0.8	66
	0.502	3.2 ± 0.01	3.2 ± 0.1	9.5 ± 0.9	72
	0.634	2.8 ± 0.02	2.9 ± 0.1	9.4 ± 1.0	77
	0.755	2.7 ± 0.3	2.6 ± 0.1	9.4 ± 1.1	80
457	0.166	5.6 ± 0.3	3.5 ± 0.1	8.3 ± 0.5	32
	0.347	3.7 ± 0.01	2.9 ± 0.1	7.7 ± 0.6	53
	0.502	2.9 ± 0.02	2.5 ± 0.1	7.5 ± 0.6	64
	0.711	2.1 ± 0.01	2.0 ± 0.1	7.3 ± 0.7	73
	1.05	1.6 ± 0.01	1.6 ± 0.1	7.2 ± 0.9	81

separation extremely difficult.[39] (2) The excitation pulse profile had a F.W.H.M. of about 7 ns. This fact would render the separation referred to even more difficult. It would clearly be advantageous to excite monomer decays using pulses of much shorter duration and such experiments are planned for the near future. It must also be noted that small errors in the rate constants may cause large changes in the pre-exponential factors, eqs. (4.23 and 4.24), and hence the c_1/c_1+c_2 values listed in Table 4.10 are probably very crude estimates.[40] Values for λ_2 were also calculated by substitution of k_3, k_4 and k_p (into 4.17), at $[Q]$ used in the study of the exciplex decay times. These are compared with the measured exciplex lifetimes in Table 4.11 at 425°K and 457°K, the temperatures at which the rate constants were determined. Again the agreement is very good and the feature that at high concentrations of added diene the lifetime becomes concentration independent is mirrored in the predicted behaviour.

On the basis of all these calculations, it seems reasonable to assume that the mechanism given in equations(4.1) to (4.7) is valid and that the method used to extract k_3 and k_4 from the steady-state and transient results seems to be sound. The temperature dependence of the rate constants may be used to deduce activation properties of the exciplex formation and decay processes if it is assumed that a specific rate, k_i, is given by the Arrhenius equation:[25]

$$k_i = A_i . e^{-\Delta E_i^{\neq}/RT} \qquad (4.51)$$

where A is the frequency or pre-exponential factor and $\Delta E_i^{\neq}$ is the activation energy for the process. If the logarithm of both sides of equation (4.51) is taken then the following relation ensues,

TABLE 4.11

Comparison of calculated and observed values of exciplex lifetime

$Q \times 10^{-3}$ moles.dm^{-3}	CALCULATED $\lambda_2 \times 10^8$ sec^{-1}	CALCULATED τ_2/nanoseconds	OBSERVED τ_2/nanoseconds
TEMPERATURE = 425°K			
9.2	1.073	9.32	9.5
15.0	1.073	9.32	9.3
21.6	1.074	9.31	9.1
TEMPERATURE = 457°K			
9.2	1.4611	6.84	6.80
15.0	1.4605	6.85	6.90
21.6	1.464	6.83	6.76

$$\ln k_i = \frac{-\Delta E_i^{\neq}}{RT} + \ln A \qquad (4.52)$$

Thus if the process obeys the Arrenhius law, a plot of the logarithm of the rate constant against the reciprocal of the temperature should be a straight line with a slope equal to $-\Delta E_i^{\neq}/R$.

The Arrenhius plot for k_p, using data from Table 4.6, is shown in figure 4.12 and it can clearly be seen that all the points lie on a straight line. From the slope the activation energy, $\Delta E_p^{\neq}$, for the deactivating processes of the exciplex was calculated to be equal to 4.09 kcals.mole^{-1}. The linear Arrenhius plot is also an indication that of the two or more competing pathways by which the exciplex decays, one dominates in the vapour phase in the temperature region studied. From equation (4.9) $k_p = k_5 + k_6$ where k_6 could indicate more than one non-radiative deactivation route for the exciplex. From the plot shown in figure 4.7 it was inferred that $k_5 = 0.013\ k_1$ at 457 K. Since $k_o = 10^8$ dm^3.mole^{-1}.sec^{-1}, see Table 4.9, ($k_o = k_1 + k_2$), then k_5 must be relatively small, explaining the very low exciplex emission intensity. At the same temperature k_p was measured to be 1.47×10^8 dm^{3}mole^{-1}sec^{-1}, thus k_5 must also be a very small fraction of k_p. In vapour phase media the refractive index decreases with increased temperature, thus k_5 must also decrease.[38] Hence not only is k_6 the major contribution to k_p, it must also increase dramatically with temperature as shown by the two-fold increase in k_p with the rise in temperature of 70K (see Table 4.6). Changes in k_6 must then dominate the Arrenhius plot.

What rates k_6 is exactly describing, is more difficult to ascertain. From the fluorescence excitation spectra, see figure 4.2, there was no

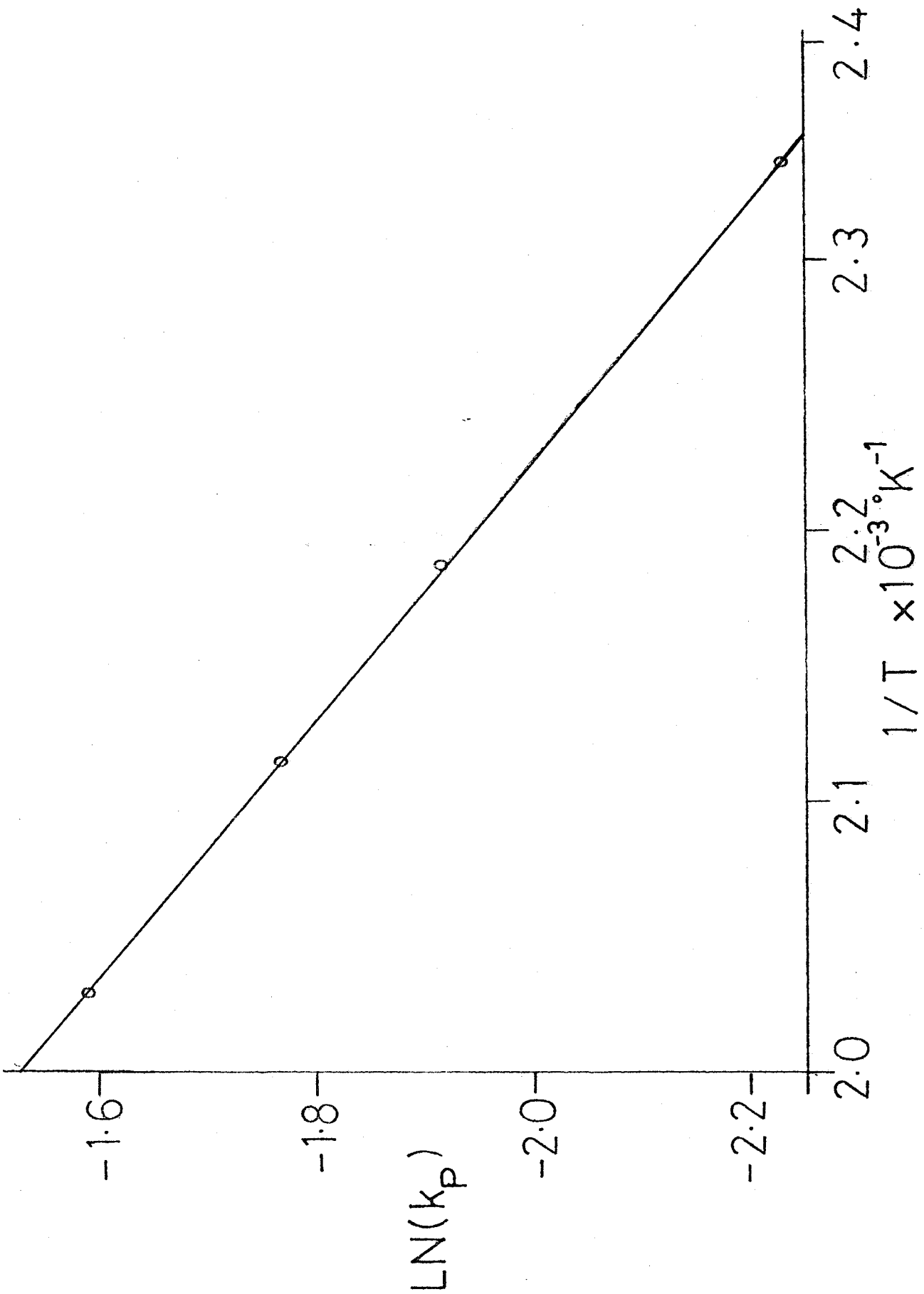

FIGURE 4.12. Arrenhius plot for the temperature dependence of k_p.

TABLE 4.12

Activation and Thermodynamic Parameters for the 1,4 DCN/DMHD vapour phase exciplex

$\Delta E_3^{\neq}$ kcal.mole^{-1}	$\Delta E_4^{\neq}$ kcal.mole^{-1}	$\Delta E_p^{\neq}$ kcal.mole^{-1}	$-\Delta H^{o}$ [a] kcal.mole^{-1}
3.1 ± 0.5	4.7 ± 2.4	4.1 ± 0.1	1.6 ± 1.1

a. The large error in ΔH^{o} is due to the propagation of the uncertainties in the rate constants (see Table 4.9) especially that of k_4.

From the values of k_3 and k_4 at 425°K and 457°K the equilibrium constants, K_i, at these temperatures was calculated. The enthalpy of exciplex formation was then calculated using the following well known equation:[25]

$$\ln K_1 - \ln K_2 = - \frac{\Delta H^o}{R} \left(\frac{1}{T_1} - \frac{1}{T_2} \right) \qquad (4.54)$$

ΔH^o (the exciplex binding energy) was thus obtained and has a value equal to -1.6 ± 1.1 kcals.mole^{-1} Although the thermodynamic properties of the 1,4 DCN/DMHD exciplex have not been determined in the solution phase, this binding energy is substantially less than values usually calculated for solution phase systems.[17] The low calculated binding energy is compatible with the data extracted from the comparison of the fluorescence emission spectra in the vapour and solution phases, where it was inferred that since there is a substantial decrease in the monomer-exciplex emission energy gap in taking the 1,4 DCN/DMHD system from cyclohexane solution to the vapour phase (see Table 4.1) then the binding energy of the vapour phase exciplex must be less than the solution phase value. This conclusion was reached from application of the equation (1.1):

$$h\nu^{0-0}_{MONOMER} - h\nu_{EXCIPLEX} = E_R + \Delta H \qquad (1.1)$$

The low binding energy in the vapour phase indicates that dipole-dipole interactions of the exciplex with the solvation shell must be important in contributing stability to solution phase systems. Equation (1.1) can also be used to calculate the repulsion energy in the ground-state

surface. From the UV absorption spectrum of 1,4 DCN in the vapour phase, the 0-0 band lies at 325.5 nms. On conversion to energy units,[25] this equalled 367.4 kJ.mole^{-1}. The exciplex emission band has an energy of 268.1 kJ. mole^{-1}. These values, together with the binding energy, were substituted into equation (1.1) and a value of E_R equal to 22.2 kcals.mole^{-1}. was obtained. This is very similar to the value obtained by Halpern[4] (21 kcals.mole^{-1}) for a study on a vapour phase excimer and since both values are greater than those found in the solution phase[3] (less than or equal to 15 kcals.mole^{-1}) close approach of the two components in vapour phase complexes is therefore indicated. This would be expected because of the absence of solvent molecules.

As discussed previously in this chapter ΔH^o can also be determined from steady-state fluorescence data by use of the Stevens-Ban method. In the present study this was shown to give a binding energy equal to -5 kcal.mole^{-1}, provided that $k_4 \gg k_p$. However, the assumption of this inequality is incompatible with the Stern-Volmer analysis from which the temperature dependence of the overall quenching rate constant, k_q, suggested that k_4 was less than k_p. The analysis of the transient measurements gives support to the conclusion reached from the Stern-Volmer results. Therefore the value of the binding energy calculated using the Stevens-Ban method must be rejected. This then prompts the question, what parameter is the slope of the Stevens-Ban plot, shown in figure 4.8, a measure of? An answer to this question is suggested by examination of equation (4.40)

$$\ln \frac{k_1}{k_5} \cdot \frac{I_E}{I_M [Q]} = \ln \left(\frac{k_3}{k_4 + k_p} \right) \qquad (4.40)$$

Assuming k_1 and k_5 are temperature independent, rearrangement of eq.(4.40) leads to

$$\ln \left(\frac{I_E}{I_M} \right) = \ln \left(\frac{k_3}{k_4+k_p} \right) + \text{CONSTANT} \qquad (4.55)$$

Substitution for k_i from the Arrenhius equation leads to:

$$\ln \left(\frac{I_E}{I_M} \right) = \ln \left\{ \frac{A_3 \cdot e^{-\Delta E_3^{\neq}/RT}}{A_4 \cdot e^{-\Delta E_4^{\neq}/RT} + A_p \cdot e^{-\Delta E_p^{\neq}/RT}} \right\} + \text{CONSTANT} \qquad (4.57)$$

Thus $\ln \left(\frac{I_E}{I_M} \right)$ plotted against $1/T$ might be an Arrenhius plot of $k_3/(k_4+k_p)$. The activation energies have already been calculated; the pre-exponential factors, A_i, can also be calculated hence an Arrenhius plot of $(k_3/k_4 + k_p)$ can be constructed over the temperature range employed in the Stevens-Ban plot. Thus, on the assumption that the rate constants for the radiative decay of monomer or exciplex are temperature independent, such a plot can be used to calculate the expected slope of the Stevens-Ban plot. The result was a " H^o" value equal to -1 kcal.mole^{-1} which has the same sign as that obtained directly from figure 4.9 of -5.0 kcals. mole^{-1}. but clearly differs numerically. Given the assumptions made in these calculations and also the fact that a complete kinetic analysis was only achieved at two temperatures, complete agreement would not be expected. However, since the binding energy as determined from the temperature dependence of the equilibrium constant (eq.4.55) was found to be -1.55 kcals.mole^{-1}, when contrasted with these other values of ΔH^o, clearly demonstrates the dangers inherent in sole reliance on Stevens-Ban plots to determine thermodynamic information.

4.4 CONCLUSIONS

(a) In theory exciplexes in the vapour phase should be a widespread phenomenon but in practise the emission may be weak.

(b) The work has further shown that it is feasible to attempt the complete kinetic analysis for the various formation and decay processes of such vapour phase exciplexes. In the 1,4 DCN/DMHD system a non-radiative deactivating process seems to dominate the exciplex decay.

(c) The result that such an exciplex has a low binding energy indicates the importance of solvent stabilisation in solution phase systems.

(d) The dangers of placing sole reliance on Stevens-Ban plots to obtain thermodynamic information have been illustrated.

REFERENCES

1. I. B. Berlman in "Handbook of Fluorescence Spectra of Aromatic Molecules", 2nd Edition, Academic Press,New York, 1971.

2. G. D. Abbott, D. V.O'Connor and D. Phillips, J.Chem.Soc., Faraday Trans.II, in press.

3. D. V. O'Connor, Ph.D. Thesis, University of Western Ontario (1977).

4. A. M. Halpern, J.Amer.Chem.Soc., 96, 4392 (1974).

5. G. Stephenson in "Mathematical Methods for Science Students", Longman, London, 1973.

6. B. Stevens and M. I. Ban, Trans.Faraday Soc., 60, 1515 (1964).

7. J. Prochorow, S. Okajima and E. C. Lim, Chem.Phys.Lett., 66, 590 (1979).

8. T.D.S. Hamilton and K. R. Naqvi, Chem.Phys.Lett., 2, 374 (1968).

9. M. D. Cohen and E. Fischer, J.Chem.Soc., 3044 (1962).

10. E. G. McRae, J.Phys.Chem., 61, 562 (1957).

11. H. Knibbe and A. Weller, Z.Phys.Chem., N.F., 56, 99 (1967).

12. N. Mataga, T. Okada and N. Yamamoto, Bull.Chem.Soc. Japan, 39, 2562 (1966).

13. H. Beens, H. Knibbe and A. Weller, J.Chem.Phys., 47, 1183 (1967).

14. H. Beens and A. Weller, in "Photophysics of Aromatic Molecules", J. B. Birks, Ed., Wiley-Interscience, London, 1970.

15. N. Mataga in "The Exciplex", M. Gordon and W. R. Ware, Eds., Academic Press, New York, 1975.

16. Handbook of Chemistry and Physics, R. C. Weast, Ed., C.R.C. Press, 1977-1978.

17. H. Knibbe, Ph.D. Thesis, Free University of Amsterdam, 1969.

18. W. R. Ware, Pure Appl.Chem., 41, 635 (1975).

19. D. V. O'Connor and W. R. Ware, J.Amer.Chem.Soc., 98, 4706 (1976).

20. K. J. Laidler in "Chemical Kinetics", McGraw-Hill, London, 1965.

21. B. Stevens, Advances in Photochem., 8, 161 (1971).

22. W. J. Moore in "Physical Chemistry", Fifth Edition, Longman, London, 1974.

23. R. J. McDonald and B. K. Selinger, Mol.Photochem., 3, 99 (1974).

24. M. H. Hui and W. R. Ware, J.Amer.Chem.Soc., 48, 4718 (1976).

25. P. W. Atkins in "Physical Chemistry", Oxford University Press, Oxford, 1979.

26. M. Cohen and B. K. Selinger, Mol.Photochem., 4, 371 (1969).

27. J. Saltiel, D. E. Townsend, B. D. Watson and P. Shannon, J.Amer.Chem.Soc., 97, 5688 (1975).

28. N. C. Yang, D. M. Shold and B. Kim, J.Amer.Chem.Soc., 98, 6587 (1976).

29. N. Nakashima, N. Mataga and C. Yamanaka, Int.J.Chem. Kinetics, 5, 833 (1973).

30. M. G. Kuzmin and L. N. Guseva, Chem.Phys.Lett., 3, 71 (1969).

31. J. Prochorow and E. Bernard, J.Luminescence, 8, 471 (1974).

32. E.J.J. Groenen and P. N. Th. Van Velzen, J.Mol.Phys., 35, 19 (1978).

33. Th. Förster and H. P. Seidel, Z.Physik.Chem., 45, 58 (1965).

34. T. Okada, H. Oohari, H. Matsumoto and N. Mataga, J.Chem.Phys., 49, 4717 (1968).

35. I. E. Obyknovennaya and A. S. Cherkasov, Opt.Spect. (USSR) (Engl. Transl.), 22, 172 (1967).

36. G. N. Taylor, Chem.Phys.Lett., 10, 355 (1971).

37. S. J. Strickler and R. A. Berg, J.Chem.Phys., 37, 814 (1962).

38. S. Hirayama and D. Phillips, Journal of Photochemistry, 12, 139 (1980).

39. D. V. O'Connor, W. R. Ware and J. C. Andre, J.Phys.Chem., 83, 1333 (1979).

40. D. V. O'Connor, Private Communication.

CHAPTER FIVE

SEMI-EMPIRICAL MOLECULAR ORBITAL CALCULATIONS

CHAPTER 5

SEMI-EMPIRICAL MOLECULAR ORBITAL CALCULATIONS

5.1. INTRODUCTION

Previously, triplet-triplet absorption spectra and triplet lifetimes of various substituted benzene molecules have been obtained using a phase-shift method[1] and laser flash photolysis.[2] Assignments of the observed electronic bands are suggested in this present work. A spectroscopically parameterized self-consistent-field CNDO/S - CI molecular orbital model is employed to investigate the electronic structures of benzene, toluene, 1,4-dimethylbenzene, 1,4-difluorobenzene, 1,3-difluorobenzene, 1,2-difluorobenzene, trifluoromethylbenzene, 1,4-ditrifluoromethylbenzene and 1,3-ditrifluoromethylbenzene in both their ground and excited electronic states.

5.2. MOLECULAR QUANTUM MECHANICS

Molecules consist of a definite number of nuclei and electrons, consequently if we want to determine the electronic properties of a molecule we are concerned with a problem of interactions between a given number of charged particles.

Quantum mechanics indicates that a molecule can only exist in discrete energy states characterized by wavefunctions which depend on the spatial and spin coordinates of all the particles in the molecule. These wavefunctions are exact solutions of the time-independent Schrödinger equation,[3]

$$\mathcal{H}\,\Psi = E\,\Psi \qquad (5.1)$$

where $\mathcal{H}$ is the Hamiltonian operator for the system and the eigenvalues, E, are the ground and excited state energies of the molecule. The wavefunctions form an orthonormal set and are defined such that the product

$\Psi^* \Psi$ represents the electronic probability density.

In this investigation the molecular properties of interest are the transition energies between the ground and excited singlet electronic states, the corresponding oscillator strengths for these transitions, the transition energies between the first excited triplet state and higher excited triplet states and the symmetrys of all the electronic states.

On absorption of a photon of light of frequency ν, a molecule initially in a state Ψ_i can be excited to a state Ψ_f, provided the transition obeys certain selection rules, where Ψ_f has an associated energy, E_f, greater than E_i given by

$$E_f - E_i = h \nu \qquad (5.2)$$

where h is Planck's constant.[4] The quantum mechanical operator yielding the state energies in the Hamiltonian introduced in eq.(5.1) and the expectation value for the energy state is then

$$E = \langle \mathcal{H} \rangle = \int \Psi \, \mathcal{H} \, \Psi \, \delta\tau \qquad (5.3)$$

Thus if Ψ_i and Ψ_f are known the energies of the initial and final states can be calculated and therefore the transition energy obtained from their difference.

The probability of a photon of light being absorbed depends on the magnitude of the transition dipole moment between the initial and final states. The dipole moment operator takes the form

$$\mu = e \sum_k \bar{r}_k \qquad (5.4)$$

where e is the electronic charge and $\bar{r}_k$ the position vector of the k th

electron, the summation extending over all the electrons in the molecule. The expectation value of the transition moment is given by

$$< \mu > = \int \Psi_i^* \mu \Psi_f \delta\tau \qquad (5.5)$$

and the square of the modulus of this integrand is proportional to the probability of the transition occurring. On application of the Born-Oppenheimer approximation the total molecular wavefunction can be factorised into a nuclear wavefunction Θ and an electronic wavefunction. The electronic wavefunction can be further factorised into a product of space (ϕ) and spin (S) functions, where μ operates only on the electronic space functions, and thus the transition moment integral becomes:

$$< \mu > = \int \Theta_i . \Theta_f \, d\tau_N \int S_i S_f d\tau_S \int \phi_i \, \mu \, \phi_f d\tau_e \qquad (5.6)$$

Within the framework of the approximations implicit in the derivation of eq.(5.6), if any one of the component integrals is zero the transition is said to be forbidden. In assigning the triplet-triplet absorption spectra in this work the symmetry species of the electronic transition moment integrand was determined, where the spin overlap integral and the overlap integral of the wavefunctions for nuclear vibrations were known to be non-zero, since to be non-zero the integrand must belong to the totally symmetric irreducible representation. The group theoretical treatment of the problem is to assign the initial and final electronic states between which the transition is thought to occur, to particular irreducible representations $\Gamma \phi_i$ and $\Gamma \phi_f$, by examining the symmetrys of the constituent molecular orbitals, and then to do the same for the Cartesian axes x, y and z (Γx , Γy , Γz). The direct products (e.g. $\Gamma \phi_i$ x Γx x $\Gamma \phi_f$) are then evaluated to find out to which irreducible representation each transition belongs. Unless one or more of

the direct products contains the totally symmetric representation then the component electronic transition moments will be zero. The electronic transition moment is resolved into three components along the Cartesian axes and for a transition to be forbidden, all three component integrals must be zero, if just one of the integrals, e.g. $\int \phi_i . \mu_x . \phi_f . d\tau_e$ is non-zero then the transition will be polarized along the x-axis of the molecule.

The transition moment is related to the observable oscillator strength, f, of an electronic absorption band by an expression derived from the Einstein coefficients,[5]

$$f = \left(\frac{8\pi^2 mc}{3he^2} \right) \nu \mu^2 \qquad (5.7)$$

In this work molecular wavefunctions are computed using the Variation Theorem which states that the energy of an electronic state described by an approximate wavefunction Ψ will be greater than or equal to the true ground-state energy of the system. If Ψ is a function of one or more variables the energy of the system may be minimized with respect to these variables. The values of these variables at the energy minimum defines the best wavefunction obtainable from this particular form of approximate wavefunction.

The most useful form of Ψ is one in which it is expressed as a linear combination of a finite set of m known functions, ϕ_j, weighted by coefficients, c_{ij}:

$$\Psi_i = \sum_j^m c_{ij} \phi_j \qquad (5.8)$$

Minimization of the total energy of the system with respect to the coefficients, c_{ij}, results in m simultaneous linear equations of the form:

$$\sum_{j}^{m} c_{ij}(H_{jk} - E_i S_{jk}) = 0, \quad k = 1,2,\ldots,m \tag{5.9}$$

where $$H_{jk} = \int \phi^*_j \mathcal{H} . \phi_k . d\tau \tag{5.10}$$

$$S_{jk} = \int \phi^*_j \phi_k . d\tau \tag{5.11}$$

These equations have solutions for the coefficients only if the determinant of the coefficients vanishes,

$$\left| H_{jk} - E_i S_{jk} \right| = 0 \tag{5.12}$$

The determinantal eq.(5.12) has m roots E_i which once determined may be substituted back into eq.(5.9) for the evaluation of the corresponding coefficients. Thus eqs.(5.12) and (5.9) provide a systematic way of computing the best wavefunction available from an approximate wavefunction of the form of eq.(5.8) - this is termed the linear variational method.

5.3. TOTAL ENERGY OF A MANY ELECTRON CLOSED SHELL MOLECULAR SYSTEM

The Hamiltonian operator for an n-electron problem takes the form

$$\mathcal{H}_e(1,2,\ldots,n) = \sum_{i}^{n} \mathcal{H}_n(j) + \sum_{i\ j}^{n} (1/r_{jk}) \tag{5.13}$$

The first summation collects terms which are functions of one electron only and is defined as:

$$\mathcal{H}_n(j) = -\tfrac{1}{2} \nabla_j^2 - \sum_{A} (Z_A/r_{jA}) \tag{5.14}$$

where z is the charge on the nucleus A and r_{jA} is the distance between the jth electron and the nucleus A. The second summation in eq.(5.13) collects two-electron terms, which arise from electron-electron interactions.

If the interelectronic energy interaction term is omitted from $\mathcal{H}_e(1,2,\ldots,n)$ in eq.(5.13) then H_e may be written as a sum of 1-electron operators

$$\mathcal{H}_e = \sum_j^n \mathcal{H}_n(j) \qquad (5.15)$$

Thus eq.(5.1) could be solved by a separation of variables, i.e. by the assumption of a solution of the form

$$\Psi_n = \prod_j^n \phi_j(j) \qquad (5.16)$$

where the ϕ_j are molecular orbitals. This is termed the orbital approximation and does not work rigorously because of the presence of the electron interaction operator, $1/r_{jk}$. However, it does suggest attempting an approximate solution in this form and compensating for it at some later stage of the calculation. This was the approach adopted by early workers and has proved successful.

In formulating a solution for the total wavefunction for the ground state of a molecular system as a product of one-electron wavefunctions, it must be recognised that with each space orbital, ϕ_j, there is associated an electron spin function, α or β . The most convenient way of associating the electron spin directly with the molecular orbital is to define 'spin orbitals' $\lambda_j(1)$ representing $\phi_j(1)\ \alpha\ (1)$. The total wavefunction is then a product of occupied spin orbitals. The Pauli principle requires that the total wavefunction must be antisymmetric with respect to the exchange of the coordinates of any two electrons; this is satisfied by representing the total wavefunction as a Slater determinant:

$$\Delta = \left(\frac{1}{n!}\right)^{\frac{1}{2}} \begin{vmatrix} \lambda_1(1) & \lambda_2(1) & \cdots & \lambda_n(1) \\ \lambda_1(2) & \lambda_2(2) & \cdots & \lambda_n(2) \\ \vdots & \vdots & \cdots & \vdots \\ \lambda_1(n) & \lambda_2(n) & \cdots & \lambda_n(n) \end{vmatrix} \qquad (5.17)$$

which is usually abbreviated as

$$\Delta = | \lambda_1(1)\ \lambda_2(2) \ldots\ldots\ldots\ldots \lambda_n(n) | \qquad (5.18)$$

Equation (5.1) is normally solved, when Ψ is a single determinant However, an improved solution of equation (5.1) can be expressed as a linear combination of Slater determinants of the form indicated by equation (5.17)

$$\Psi_n = \sum_I C_I \cdot \Delta_I \qquad (5.19)$$

eq. (5.19) is of the linear form of eq.(5.8) and thus the linear variational method can be applied to determine the coefficients C_I. This involves the computation of the corresponding integrals: H_{jk} and S_{jk} (see eqs.(5.10) and (5.11)), where ϕ_j can ϕ_k are replaced by the Slater determinants Δ_J and Δ_K.

From eq.(5.13) H_{JK} can be split into two parts - the one-electron and two-electron contributions respectively.

$$H_{JK} = I_{JK} + G_{JK} \qquad (5.20)$$

$$\text{where } I_{JK} = \int \Delta_J^* \sum_i^n H_n(i)\ \Delta_K\ d\tau(1).\ d\tau(2)....d\tau(n) \qquad (5.21)$$

$$\text{and } G_{JK} = \int \Delta_J^* \sum_{i<j} \left(\frac{1}{r_{ij}}\right) \cdot \Delta_K \cdot d\tau(1)d\tau(2)...d\tau(n) \qquad (5.22)$$

These integrals can be reduced to integrals involving the space orbitals ϕ from which these determinants are built. The mathematics of this problem is well documented;[8] the assumption of orthonormality of both the space and spin orbitals makes the problem a lot easier to solve. Once this has been done the expression for the expectation value of the energy of a closed shell system represented by a single determinant can be derived and takes the form:

$$E_N = 2 \sum_j I_j + \sum_{jk} (2J_{jk} - K_{jk}) \qquad (5.23)$$

The sums are over all occupied space orbitals, where

$$I_j = \int \phi_j^*(1) \mathcal{H}_N(1) . \phi_j(1) . d\tau(1) \qquad (5.24)$$

- the total one-electron energy.

$$J_{jk} = \int\int \phi_j^*(1)\phi_k^*(2) . \frac{1}{r_{12}} . \phi_j(1)\phi_k(2)\, d\tau(1) d\tau(2) \qquad (5.25)$$

- this is the Coulombic repulsion term and is the contribution of the classical electrostatic interaction between charge distributions to the total energy of that molecule and

$$K_{jk} = \int\int \phi_j^*(1)\, \phi_k^*(2) . \frac{1}{r_{12}} . \phi_k(1)\, \phi_j(2)\, d\tau(1)\, d\tau(2) \qquad (5.26)$$

this is termed the exchange integral, It has no classical analogue, and is the energy of interaction between electrons with parallel spins in different orbitals, ϕ_j and ϕ_k.

5.4. THE SELF-CONSISTENT-FIELD (S.C.F.) EQUATIONS AND THE L.C.A.O. APPROXIMATION

To find the best single determinantal wavefunction for a given electronic system a procedure called the 'self consistent field' method has been developed. The basis of the method is first to estimate the wavefunctions for all the electrons in the system. Then a wavefunction for a selected electron moving in the field of the nuclei and the averaged potential of all the other electrons in the molecule is computed using eq.(5.1). This wavefunction is used to construct an improved description of the averaged potential field and the computation is repeated on this basis. When the averaged field is the same for successive iterations, the resulting wavefunction is said to be self-consistent.

To derive the general equations of the method, the expression for E_N, eq.(5.23), is minimized subject to the conditions

$$S_{jk} = \int \phi_j^* \phi_k \, d\tau = \delta_{ij} \text{ with respect to the } \phi_j$$

Lagrange's method of undetermined multipliers is used to accomplish this.[9] The end result is the equation

$$F(1)\,\phi_j(1) = \varepsilon_j \phi_j(1) \qquad (5.28)$$

where the Hamiltonian operator in eq.(5.3) is replaced by the one-electron S.C.F. operator

$$F(1) = \mathcal{H}_n(1) + \sum_k (2J_k(1) - K_k(1)) \qquad (5.29)$$

where $\mathcal{H}_n(1)$ is defined by eq.(5.14) and J_k and K_k are the molecular Coulomb and the molecular exchange operators respectively. These are defined by the equations

$$\int \phi_j^*(1)\, J_k(1)\, \phi_j(1)\, d\tau(1) = \iint \phi_j^2(1)\left(\frac{1}{r_{12}}\right)\phi_k^2(1)\, d\tau(1)\, d\tau(2) \qquad (5.30)$$

$$\int \phi_j^*(1)\, K_k(1)\, \phi_j(1)\, d\tau(1) = \iint \phi_j^*(1)\, \phi_k^*(1)\left(\frac{1}{r_{12}}\right)\phi_j(2)\phi_k(2)\, d\tau(1)\, d\tau(2) \qquad (5.31)$$

In the previous discussion leading to the derivation of eq.(5.28) a system represented by a single determinant has been used. This is usually quite adequate for some atoms but unfortunately some molecular states can not be well represented by a single determinant. In these cases the LCAO-SCF method is employed. The spirit of the SCF treatment is retained but the functions ϕ_j are taken to be linear combinations of atomic orbitals,

$$\phi_j = \sum_s C_{js} \cdot \chi_s \qquad (5.32)$$

C_{js} are the weighting coefficients for the atomic orbitals χ_r. If equation (5.32) is inserted into equation (5.28), the expression multiplied on the left by χ_r, and integrated, eq.(5.33) results:

$$\sum_s C_{js}(F_{rs} - S_{rs} \cdot \varepsilon_j) = 0 \qquad (5.33)$$

where $$F_{rs} = \int \chi_r^* \cdot F \cdot \chi_s \cdot dV = I_{rs} + \sum_k \left(2(rs\,|\,kk) - (rk\,|\,ks)\right) \qquad (5.34)$$

where $$I_{rs} = \int \chi_r^*(1)\, \mathcal{H}_N \cdot \chi_S(1)\, dV(1) \qquad (5.35)$$

is the one-electron term, and the Coulomb and Exchange integrals are respectively

$$(rs\,|\,kk) = \iint \chi_r^*(1)\, \chi_s(1)\, \frac{1}{r_{12}}\, \chi_k^*(2)\, \chi_k(2)\, dV(1) dV(2) \qquad (5.36)$$

$$(rk\,|\,ks) = \iint \chi_r^*(1)\, \chi_k(1)\, \frac{1}{r_{12}}\, \chi_k^*(2)\, \chi_s(2)\, dV(1)\, dV(2) \qquad (5.37)$$

Also the overlap integral is given by:

$$S_{rs} = \int \chi^*_r \cdot \chi_s \cdot dV \qquad (5.38)$$

Equation (5.33) consists of simultaneous equations for the unknown C_{js}. As before, there exists a non-trivial solution of the set of secular equations providing the secular determinant vanishes:

$$\text{i.e.} \quad |F_{rs} - S_{rs} \cdot \varepsilon_j| = 0. \quad j = 1,2,\ldots,n \qquad (5.39)$$

Equation (5.33) is solved by iteration to self-consistency and the values of the weighting coefficients are estimated. F_{rs} is computed from eq.(5.34). The determinantal equation (5.39) has n roots ε_j which once determined are substituted back into eq.(5.33) to obtain the coefficients. The total energy is compared with previous values and the whole cycle is repeated until 'self-consistency' is achieved, i.e. the total energy obtained between successive cycles does not change by more than a pre-set small tolerance. Equations (5.32) to (5.39) are the Roothaan equations as derived assuming an orthonormal basis set. If this approximation is not made, the matrix element of the potential due to interelectronic interactions, G_{rs} (i.e. the 2-electron contribution to the S.C.F. operator F_{rs}, see eq.(5.34) takes the form

$$G_{rs} = \sum_{t,u} P_{tu} \left((rs \mid tu) - \tfrac{1}{2}(ru \mid st) \right) \qquad (5.40)$$

$(rs \mid tu)$ and $(ru \mid st)$ are two-electron matrix elements and are in the same form as eqs.(5.36) and (5.37).

$$\text{where} \quad P_{tu} = 2 \sum_{j}^{occ} C_{jt}^* C_{ju} \qquad (5.41)$$

$$\text{and} \quad F_{rs} = I_{rs} + G_{rs} \qquad (5.42)$$

I_{rs} takes the form of eq.(5.35).

G_{rs} is the matrix element of the potential due to other valence electrons and depends on the L.C.A.O. molecular orbitals via the population matrix P_{tu}. The summation $\sum_{j}^{occ}$ in eq.(5.41) is over occupied molecular orbitals only. The orbital energies ε_j are roots of the secular equation (5.39).

The total electronic energy of the valence electrons is:

$$E_{electronic} = \tfrac{1}{2} \sum_{r,s} P_{rs} (I_{rs} + F_{rs}) \qquad (5.43)$$

The total energy of the molecule (relative to separated valence electrons and isolated cores) is obtained by adding the repulsion energy between cores. This latter term can be well approximated by a point charge model so that:

$$E_{total} = E_{electronic} + \sum_{A<B} \sum Z_A Z_B / R_{AB} \qquad (5.44)$$

where Z_A is the core charge of atom A and R_{AB} is the A-B internuclear distance. Eqs. (5.39 to 5.44) were first put forward by Roothaan[9] and are often referred to as the Roothaan equations. Work has been carried out to simplify the Roothaan equations in a way that would make them less unwieldly, hence reducing the amount of computer time required, but still retaining the basic method. The approximations used in simplifying these equations are discussed in the next section.

5.5. THE CNDO APPROXIMATIONS

The evaluation and handling of a large number of electron interaction integrals (see previous section) is the most difficult and time consuming part of LCAO self-consistent molecular orbital calculations. Many of these electron interaction integrals have values near zero, especially those involving $\chi_j(1)$ $\chi_k(1)$ with $j \neq k$.[10] Thus in order to reduce the number of

two-electron integrals a useful approach is the systematic neglect of electron repulsion integrals having uniformly small values.[11] This has been effected by considering the Roothaan equations in terms of the 'complete neglect of differential overlap' approximations[12-14,16-18] which are given below and are presented in order of their importance.

Approximation 1:

The atomic orbitals χ_r are treated as if they form an orthonormal set, i.e. the overlap integrals become,

$$S_{rs} = \int \chi_r(1)\ \chi_s(1)\ dV = \delta_{rs} = \begin{cases} 0 & r \neq s \\ 1 & r = s \end{cases} \qquad (5.45)$$

The coefficients of the atomic orbitals in a molecular orbital C_{jr} then form an orthogonal matrix and the orthonormality condition for ϕ_j, the molecular orbital, becomes

$$\sum_r C_{jr} \cdot C_{kr} = S_{jk} \qquad (5.46)$$

Therefore, the diagonal matrix elements, P_{rr} correspond to the electron densities of the atomic orbitals, χ_r and

$$\sum_r P_{rr} = 2N \qquad (5.47)$$

where 2N is the total number of valence electrons. The off-diagonal matrix elements, P_{rs} are usually referred to as orbital bond orders between atomic orbitals χ_r and χ_s although they only correlate with bond energies if r and s are orbitals on bonded centres.

Approximation 2:

All two-electron integrals which depend on the overlapping of charge densities of different basis orbitals are neglected. That is, integrals of the form,

$$\int\int \chi_r(1)\ \chi_u(1)\left(\frac{1}{r_{12}}\right)\chi_s(2)\ \chi_t(2)\ dv(1)dv(2) = 0 \qquad (5.48)$$

unless r = u, and s = t. Such non-zero integrals are written as

$$\Gamma_{rs} = \int\int \chi_r(1)\ \chi_r(1)\left(\frac{1}{r_{12}}\right)\chi_s(2)\ \chi_s(2)\ dv(1)dV(2)$$

$$= \delta_{ru}\ \delta_{st}\ \int\int \chi_r(1)\ \chi_u(1)\left(\frac{1}{r_{12}}\right)\chi_s(2)\ \chi_t(2)\ dv(1)dv(2) \qquad (5.49)$$

This is the 'zero differential overlap' (ZDO) approximation and is consistent with Approximation 1.

Approximation 3:

The electron-interaction integrals, Γ_{rs} are assumed to depend only on the atoms to which the orbitals χ_r and χ_s belong and not to the actual type of orbital (s, p or d). This means that there remains only a set of atomic electronic interaction integrals Γ_{AB} measuring an average repulsion between an electron in a valence atomic orbital on A and another in a valence orbital on atom B. There are various methods used to calculate Γ_{AB}, e.g. previous workers[34] have used the Mataga interpolation method[5] where

$$\Gamma_{AB} = 1/(R_{AB} + (2/(\Gamma_{AA} + \Gamma_{BB})) \qquad (5.50)$$

where R_{AB} is the internuclear distance and Γ_{AA} is the one-centre integral.

In this work a Slater-type basis set is used to theoretically calculate the two centre integrals.

Using Approximations 1 and 2 the matrix elements F_{rs}, see eqns. (40)-(42), become

$$F_{rr} = I_{rr} + \tfrac{1}{2}P_{rr}\,\Gamma_{rr} + \sum_{u(\neq r)} P_{uu} \qquad (5.51)$$

$$F_{rs} = I_{rs} - \tfrac{1}{2}P_{rs}\,\Gamma_{rs} \quad (r \neq s) \qquad (5.52)$$

With the addition of Approximation 3 F_{rr} may be written as

$$F_{rr} = I_{rr} - \tfrac{1}{2}P_{rr}\,\Gamma_{AA} + P_{AA}\,\Gamma_{AA} + \sum_{B\neq A} P_{BB}\,\Gamma_{AB} \qquad (5.53)$$

where r belongs to atom A and P_{BB} is the total valence electron density on atom B.

$$P_{BB} = \sum_{s}^{B} P_{ss} \qquad (5.54)$$

I_{rs}, see eqs.(5.35) and (5.14), the matrix element of the one-electron Hamiltonian, can be expressed in the form

$$I_{rs} = \int \chi_r^* \left(-\tfrac{1}{2}\nabla^2 - \sum_A V_A(r) \right) \chi_s \, d\tau \qquad (5.55)$$

This includes the kinetic energy and the potential energy in the electrostatic field of the core, this being written as a sum of potentials $V_A(r)$ for various atoms A in the molecule. The core consists of the nucleus and all electrons below the valence shell. In developing the diagonal core matrix elements I_{rr} the potential energy term can be conveniently separated to give

$$I_{rr} = (r \mid -\tfrac{1}{2}\nabla^2 - V_A \mid r) - \sum_{B(\neq A)} (r \mid V_B \mid r)$$

$$= U_{rr} - \sum_{B(\neq A)} (r \mid V_B \mid r) \qquad (5.56)$$

where U_{rr} is the diagonal matrix element of χ_r with respect to the one-electron Hamiltonian containing only the core of its own atom. U_{rr} is essentially an atomic quantity measuring the energy of the atomic orbital χ_r. In this work the core integral is approximated by[34]

$$U_{rr} = -\tfrac{1}{2}(I_r + A_r) - (Z_A - \tfrac{1}{2})\ \Gamma_{AA} \qquad (5.57)$$

In molecular orbital theory the tendency for an atomic orbital, χ_r, both to acquire and to lose electrons should be accounted for and therefore the use of the average value of I_r and A_r, the ionization potential and the electron affinity for a valence electron on atom A respectively, is adopted - see Table 5.1 for values of I_r and A_r on page 140.

The remaining terms in eq.(5.56) give the interaction of an electron in χ_r with the cores of other atoms B.

The off-diagonal core matrix elements I_{rs} must also be considered. Here it is convenient to distinguish cases where χ_r and χ_s are on the same or different atoms. If both belong to the same atom, e.g. A, then I_{rs} is written analogously to eq.(5.56),

$$I_{rs} = U_{rs} - \sum_{B(\neq A)} (r \mid V_B \mid s) \qquad (5.58)$$

where again U_{rs} is the one-electron matrix element using the local core Hamiltonian. The remaining terms in eq.(5.58) represent the interactions of the distribution $\chi_r \chi_s$ with cores of other atoms. Since differential overlap is being neglected in corresponding electron-interaction integrals, it is consistent to neglect these contributions. Hence we have Approximation 4.

Approximation 4:

When χ_r and χ_s belong to atom A, $I_{rs} = 0$ if $r \neq s$. If $r = s$ the integral is taken to be the same for all valence atomic orbitals on atom A, hence,

$$(r \mid V_B \mid r) = V_{AB} \tag{5.59}$$

In consequence, $I_{rr} = U_{rr} - \sum_{B(\neq A)} V_{AB}$ (r on atom A) (5.60)

Further, the B core will be treated as a point charge at the B nucleus. Thus eq.(5.60) becomes

$$I_{rr} = U_{rr} - \sum_{B(\neq A)} Z_B \Gamma_{AB} \tag{5.61}$$

where Z_B is the core charge of B.

$$I_{rs} = 0 \ (r \neq s \text{ but both on the same atom}) \tag{5.62}$$

In order to complete the approximations we need to discuss the matrix elements I_{rs} where χ_r and χ_s are on different atoms. The elements, I_{rs}, depend on the local electron distribution between the two atoms. I_{rs} is then a measure of the electrostatic interaction between the two orbitals and is often referred to as a 'resonance integral' β_{rs}. To estimate it Approximation 5 is adopted.

Approximation 5

The above 4 approximations are those employed in specifying the CNDO method[12-14] as formulated by Pople and co-workers and have been adopted in this work. However, in the original CNDO framework the approximation used to estimate β_{rs} was based on a parameterization which describes average ground-state properties. This parameterization is inadequate for excited state properties and thus fails to provide an adequate interpretation of either ultraviolet absorption spectra or ultraviolet photoemission spectra of even simpler polyatomic molecules, e.g. benzene. To alleviate this inconsistency Del Bene and Jaffe[16-19] introduced the CNDO/S parameterization

in which they chose to distinguish the β_{rs} where r and s are σ orbitals from those where r and s are π orbitals by introducing a new empirical parameter K. This approximation is employed in the present work and results in improvement in calculated electronic transition energies. Thus the off-diagonal core matrix elements between atomic orbitals on different atoms are given by[16]

$$I_{rs} = \beta_{rs} = \tfrac{1}{2}\,(\beta^{o}_{A} + \beta^{o}_{B})(S^{\sigma}_{rs} + K\,S^{\pi}_{rs}) \qquad (5.63)$$

where S^{σ}_{rs} and S^{π}_{rs} are the σ and the π components of the overlap integral - calculated using a Slater-type basis set.[20] β^{o}_{A} is an atomic resonance integral. - This is evaluated empirically and is chosen to fit experimental data or to reproduce results obtained by complete a priori calculations.[12] In this work values of β^{o}_{A} were taken from reference 34, page 48, and are listed in Table 5.1. Variation of K over wide limits showed that a value of 0.585 gave the most consistent spectroscopic data in the present series of compounds.[16] The F_{rs} matrix elements now reduce to the form (χ_r belonging to Atom A and χ_s to atom B).

$$F_{rr} = -\tfrac{1}{2}(I_r + A_r) + ((P_{AA}-Z_A) - \tfrac{1}{2}(P_{rr}-1))\;\Gamma_{AA} + \sum_{B\neq A}(P_{BB}-Z_B)\,\Gamma_{AB} \qquad (5.64)$$

$$F_{rs} = \tfrac{1}{2}(\beta^{o}_{A} + \beta^{o}_{B})(S^{\sigma}_{rs} + K\,S^{\pi}_{rs}) - \tfrac{1}{2}P_{rs}\,\Gamma_{AB} \qquad (5.65)$$

Eq.(5.65) applies even if χ_r and χ_s are on the same atom A, when $S^{\sigma}_{rs} = 0$, $S^{\pi}_{rs} = 0$ and Γ_{AB} is replaced by Γ_{AA}.

Using the same approximations we may derive an expression for the total energy from eq.(5.44). The terms are conveniently collected into one- and two-atom types, giving

$$E_{total} = \sum_{A} E_A + \sum_{A<B}\sum E_{AB} \qquad (5.66)$$

where

$$E_A = \sum_r^A P_{rr}U_{rr} + \tfrac{1}{2}\sum_r^A \sum_s^A (P_{rr}P_{ss} - \tfrac{1}{2}P_{rs}^2)\ \Gamma_{AA} \qquad (5.67)$$

and

$$E_{AB} = \sum_r^A \sum_s^B ((2P_{rs}\beta_{rs} - \tfrac{1}{2}P_{rs}\Gamma_{AB}) + Z_A Z_B/R_{AB}$$

$$- (P_{AA}Z_B + P_{BB}Z_A - P_{AA}P_{BB})\Gamma_{AB}) \qquad (5.68)$$

This completes the specification of the CNDO method as formulated by Pople et al.[12-14] and is modified by Del Bene and Jaffe,[16] i.e. the CNDO/S method. This was the method employed in this work and the values of the CNDO parameters used are listed in Table 5.1.

Table 5.1

The CNDO parameters (eV)

Element	Γ_{AA}	$\frac{1}{2}(I_s+A_s)$	$\frac{1}{2}(I_p+A_p)$	$-\beta^o_A$
H	12.85	7.175		12.0
C	10.93	14.96	5.805	17.5
F	17.36	28.48	12.18	50.0

The transition energies calculated from the CNDO results were then refined by a configuration-interaction calculation to obtain the energies and wavefunctions of the various excited states. Configuration interaction is a method of generating spectroscopic states by allowing states which arise from different electronic configurations to interact and is discussed in the next section. A more recent CNDO model parameterization has been proposed by Lipari and Duke[22] called the CNDO/S2 method which differs from

earlier ones primarily in its use of atomic orbital exponents as variable parameters to describe the range of one-electron overlap integrals. This method has proven successful in interpreting the electronic structure of benzene,[22] some dialkylbenzenes,[22] para-cyclophenes,[23] polyacenes,[24] diphenylpolyenes,[25] azulene,[25] orthorhombic sulphur,[26] alloys of sulphur and selenium with arsenic[27,28] and nitrogen,[29] and some fluorobenzenes.[30]

One of the arguments made by Lipari and Duke[22] for the construction of a new CNDO model was that the closed shell 'spectroscopic' CNDO/S parameterization of Del Bene and Jaffe[16] failed to correctly order the benzene valence states. However this claim has been refuted in a recent publication by R. W. Bigelow[31] who has shown that the ordering of the benzene occupied states predicted by the CNDO/S method is in fact in accord with the ab initio[35,36] and the CNDO/S2 results of Lipari and Duke.[22] The present work confirms Bigelow's results and in fact the CNDO/S-CI method has found considerable success in the calculation of various spectral and physical properties of numerous organic molecules containing first row atoms.[32,37-56]

5.6. CONFIGURATION INTERACTION

In a closed-shell molecule if a basis set of 2m atomic orbitals is used in the S.C.F.-L.C.A.O. method, see equations (5.32) to (5.44), 2m molecular orbitals will be determined. When considering excited states, as derived from the wavefunctions and eigenvalues of the neutral molecule, considerable mixing may occur between the different excited electronic configurations so that the resulting states cannot be accurately represented by a single Slater determinant. The excited state wavefunctions are more accurately written as linear combinations of Slater determinants.

$$\Psi = \sum_i C_i \Delta_i \qquad (5.69)$$

where each Slater determinant Δ_i represents an electronic configuration of the molecule. Once the self-consistent problem for the ground state has been solved, the unoccupied molecular orbitals $\phi_{m+1}....\phi_{2m}$ are used to construct configurational wavefunctions for the excited states. The coefficients in eq.(5.69) are determined by the variation method, see eqs. (5.8) to (5.12), that is by solving:

$$\left| H_{ik} - E\, S_{ik} \right| = 0 \qquad (5.70)$$

and

$$\sum_i C_i (H_{ik} - E\, S_{ik}) = 0 \qquad (5.71)$$

We shall write $^1\chi_{i\to k}$ for the singlet configurational wavefunction in which one electron is excited from an occupied orbital ϕ_i to an unoccupied orbital ϕ_k. Thus $^1\chi_{i\to k}$ will be a sum of two Slater determinants. The corresponding triplet wavefunction will be $^3\chi_{i\to k}$.

The matrix elements, H_{ik} in eqns.(5.70) and (5.71), of the total Hamiltonian $\mathcal{H}$ between the $\chi_{i\to k}$ and χ_o can be reduced to integrals over one or two electrons utilizing the orthogonality property of molecular orbitals. The results are:[33]

$$(^1\chi_{i\to k} \mid \mathcal{H} \mid {}^1\chi_{i\to k}) - (\chi_o \mid \mathcal{H} \mid \chi_o) = E_k - E_i - (ii \mid kk) + 2(ik \mid ki) \qquad (5.72)$$

$$(^3\chi_{i\to k} \mid \mathcal{H} \mid {}^3\chi_{i\to k}) - (\chi_o \mid \mathcal{H} \mid \chi_o) = E_k - E_i - (ii \mid kk) \qquad (5.73)$$

$$(^1\chi_{i\to k} \mid \chi_o) = 0 \qquad (5.74)$$

$$({}^1\chi_{i\to k} \mid \mathcal{H} \mid {}^1\chi_{j\to l}) = 2(jl \mid ki) - (ji \mid kl) \qquad (5.75)$$

unless i = j and k = l

$$({}^3\chi_{i\to k} \mid \mathcal{H} \mid {}^3\chi_{j\to l}) = -(ji \mid kl) \text{ unless } i = j \text{ and } k = l \qquad (5.76)$$

The two-electron matrix elements being defined by

$$(pr \mid qs) = \int\int \phi^*_p(1)\,\phi_r(1)\left(\frac{1}{r_{12}}\right)\phi_q^*(2)\phi_s(2)\,dv(1)dv(2) \qquad (5.77)$$

All matrix elements between singlet and triplet functions are zero by integration over spin. Thus the energies of the excited singlet and triplet electronic states can be calculated. It should be noted that only the triplet states accessible by one-electron excitations from the closed shell ground state are calculated. In calculating the energy of a triplet-triplet absorption, this is given by the difference between the energy of the higher excited triplet state and energy of the first excited triplet state.

5.7. VALIDITY OF THE CNDO/S-CI METHOD

In order to test the validity of the previously described molecular orbital model in predicting the electronic structures of substituted benzenes calculations were performed on benzene itself. There have been exhaustive theoretical studies[35,16,22,31] of the electronic structure of benzene and the predictions of both the excited singlet and triplet state energies have been compared with experimental data using a variety of techniques.[57,58,60,61] These results were compared with the predictions of the model used in this work .

(a) Benzene belongs to the D_{6h} point group.

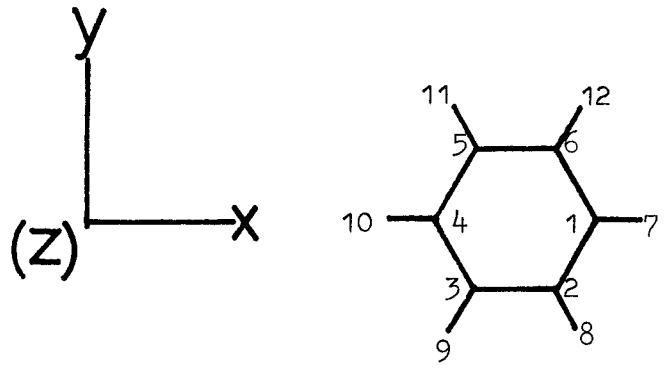

THE MOLECULAR CARTESIAN COORDINATES

ATOM	ATOMIC NUMBER	Z-COORDINATE	Y-COORDINATE	X-COORDINATE
1	6	0.0	0.0	1.397
2	6	0.0	-1.21	0.6985
3	6	0.0	-1.21	-0.6985
4	6	0.0	0.0	-1.397
5	6	0.0	1.21	-0.6985
6	6	0.0	1.21	0.6985
7	1	0.0	0.0	2.481
8	1	0.0	-2.1485	1.2405
9	1	0.0	-2.1485	-1.2405
10	1	0.0	0.0	-2.481
11	1	0.0	2.1485	-1.2405
12	1	0.0	2.1485	1.2405

(b) The ordering and energies (eV) of all occupied and lowest four unoccupied molecular orbitals.

SYMMETRY	AB INITIO[a]	CNDO/S2[b]	CNDO/S-CI[c]	THIS WORK(CNDO/S-CI)
$e_{2g}(\sigma^*)$		1.78	4.08	4.10
$b_{1u}(\sigma^*)$		0.89	3.17	3.19
$b_{2g}(\pi^*)$		.....	1.19	1.88
$e_{2u}(\pi^*)$		-0.77	-0.49	-0.49
		OCCUPIED ORBITALS		
$e_{1g}(\pi)$	-9.25	-10.04	-9.91	-9.91
$e_{2g}(\sigma)$	-13.41	-12.34	-12.42	-12.43
$a_{2u}(\pi)$	-13.74	-13.65	-14.39	-14.38
$e_{1u}(\sigma)$	-16.10	-15.21	-15.69	-15.70
$b_{2u}(\sigma)$	-16.95	-16.15	-16.53	-16.52
$b_{1u}(\sigma)$	-17.46	-17.48	-17.89	-17.92
$a_{1g}(\sigma)$	-19.48	-19.66	-23.21	-23.23
$e_{2g}(\sigma)$	-22.50	-23.66	-25.59	-25.61
$e_{1u}(\sigma)$	-27.79	-30.19	-33.44	-33.46
$a_{1g}(\sigma)$	-31.56	-35.91	-43.69	-43.69

The agreement with other work is obviously good.

a. Ref.35

b. Ref.24

c. Ref.31

(c) Comparison of ab initio and semiempirical predictions of the singlet and triplet excitation energies (eV) of benzene with experimental results.

STATE	THIS WORK	CNDO/S-CI[a]	CNDO/S2[b]	AB INITIO[c] (1+2+3)-CI (RESTRICTED)	AB INITIO[c] (1)-CI	EXPERIMENTA
$S_1(^1B_{2u})$	4.83	4.80	4.75	5.00	6.30	4.89[d]
$S_2(^1B_{1u})$	6.10	6.10	5.95	7.64	7.02	6.18[d]
$S_3(^1E_{1u})$	6.89	6.79	6.76	8.34	(8.42)[h]	6.95[d]
$S_4(^1E_{2g})$	8.00	7.98		8.33	9.09	7.3[e]
$T_1(^3B_{1u})$	3.08	3.08		3.83	3.67	3.89[d]
$T_2(^3E_{1u})$	3.96	3.96		4.98	5.15	4.85[f]
$T_3(^3B_{2u})$	4.84	4.84		7.00	6.01	5.25[f]
$T_4(^3E_{2g})$	5.56	5.56		7.28	7.86	6.55[g]

a. Ref.31.
b. Ref.24
c. Ref.35
d. Ref.60
e. Ref.62
f. Ref.63
g. Ref.64

The predictions of the CNDO/S-CI model used in this present work compare favourably with the results of other theoretical models.

5.8. PREDICTIONS OF CNDO/S-CI METHOD

The results of the CNDO/S-CI calculations for each molecule are presented in the following way:

(a) The symmetry point group, the coordinate axes, the numbering system and tabulation of the molecular Cartesian coordinates for the molecule are firstly given.

(b) The symmetrys and eigensolutions of the occupied and unoccupied molecular orbitals involved in the electronic excitations are tabulated.

(c) The eigensolutions of the singlet excited electronic states are tabulated together with the symmetrys of the excited states determined from the direct product of the symmetrys of the occupied and unoccupied molecular orbitals involved in each of the one-electron excitations. The oscillator strengths for the ground state to excited state singlet absorptions ($S_o \rightarrow S_N$) are also given.

(d) The same properties as in (c) are tabulated for the lower excited triplet electronic states except that since the transitions are spin-forbidden the oscillator strengths for the ground state singlet to excited state triplet absorptions ($S_o \rightarrow T_N$) are all zero.

(e) The predicted singlet-singlet transitions are compared with other theoretical and experimental results. The predicted triplet states which would be excited in the same energy region as the ultra-violet spectral region investigated in the experiments described in references 1,2 and 67 are then tabulated and assignments for the experimentally observed triplet-triplet absorptions are suggested.

(a) 1,4 Difluorobenzene.

1,4 Difluorobenzene belongs to the D_{2h} point group.

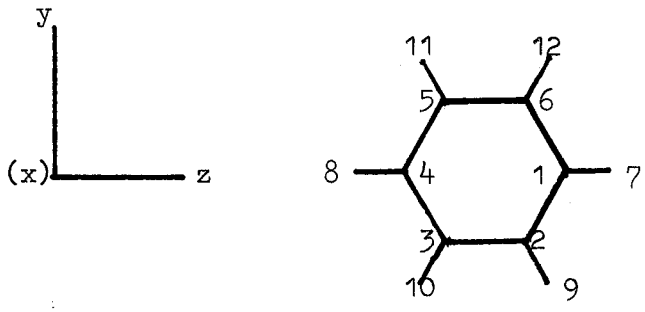

THE MOLECULAR CARTESIAN COORDINATES

ATOM	ATOMIC NUMBER	Z-COORDINATE	Y-COORDINATE	X-COORDINATE
1	6	1.397	0.0	0.0
2	6	0.6985	-1.2098	0.0
3	6	-0.6985	-1.2098	0.0
4	6	-1.397	0.0	0.0
5	6	-0.6985	1.2098	0.0
6	6	0.6985	1.2098	0.0
7	9	2.707	0.0	0.0
8	9	-2.707	0.0	0.0
9	1	1.2405	-2.1486	0.0
10	1	-1.2405	-2.1486	0.0
11	1	-1.2405	2.1486	0.0
12	1	1.2405	2.1486	0.0

(b) The ordering and energies (eV) of highest four occupied and lowest seven unoccupied molecular orbitals of 1,4 difluorobenzene.

SYMMETRY	ENERGY(eV)
UNOCCUPIED ORBITALS	
$b_{2u}(\sigma^*)$	5.12
$a_{1g}(\sigma^*)$	3.88
$b_{3g}(\sigma^*)$	3.69
$b_{1u}(\sigma^*)$	2.78
$b_{2g}(\pi^*)$	1.39
$b_{3u}(\pi^*)$	-0.93
$a_{1u}(\pi^*)$	-0.95
OCCUPIED ORBITALS	
$b_{2g}(\pi)$	-9.89
$b_{1g}(\pi)$	-10.38
$b_{3g}(\sigma)$	-12.49
$b_{3u}(\pi)$	-14.18

(c) Energies and Oscillator Strengths of singlet-singlet transitions for 1,4 difluorobenzene.

STATE NUMBER	TYPE OF TRANSITION	SYMMETRY	SINGLET EXCITATION ENERGY (eV)	OSCILLATOR STRENGTH AND POLARIZATION OF TRANSITION
1	$\pi \rightarrow \pi^*$	B_{2u}	4.64	0.009 (Y)
2	$\pi \rightarrow \pi^*$	B_{1u}	5.79	0.105 (Z)
3	$\pi \rightarrow \pi^*$	B_{2u}	6.56	0.817 (Y)
4	$\sigma \rightarrow \pi^*$	B_{1u}	6.75	1.153 (Z)

(d) Lower triplet excitation energies for 1,4 Difluorobenzene

STATE NUMBER	TYPE OF TRANSITION	SYMMETRY	TRIPLET EXCITATION ENERGY (eV)
1	$\pi \rightarrow \pi^*$	B_{1u}	2.94
2	$\pi \rightarrow \pi^*$	B_{2u}	3.75
3	$\pi \rightarrow \pi^*$	B_{1u}	3.84
4	$\pi \rightarrow \pi^*$	B_{2u}	4.73

(e) Comparison of singlet excitation energies (eV) for 1,4 Difluorobenzene. The experimental results are obtained from the electron-impact spectrum.[57]

METHOD	S_1	S_2	S_3	S_4
This work (CNDO/S-CI)	4.6	5.8	6.6	6.7
(CNDO/S2)[a]	4.5	5.6	6.5	6.6
(CNDO/S1)[b]	4.6	5.8	6.5	6.6
EXPERIMENTAL[c]	4.7	6.2	7.0	7.0

a. C. B. Duke et al. ref.30.

b. G. W. Kuehnlerz. ref.34.

c. R. P. Frueholz et al. ref.57.

Assignment of Triplet-Triplet Absorption Bands for 1,4 Difluorobenzene

The spectral region 225-250 nm.

Predicted Higher Triplet States Excited in 225-250 nm Spectral Region.

SYMMETRY	TRIPLET EXCITATION ENERGY (eV)	PREDICTED TRIPLET-TRIPLET ABSORPTION WAVELENGTH (nms) (T_1 = 2.94 eV)
B_{1g}	7.83	253.5
A_{1u}	7.90	250.0
B_{2g}	8.38	227.9

The first excited triplet state, T_1, belongs to the B_{1u} irreducible representation.

The separation of the lowest triplet and a given higher excited triplet is used as an estimate of a triplet-triplet absorption position. The inverse of this value is then multiplied by a conversion factor equal to 1.2398×10^4 to convert to an absorption wavelength.

The above higher triplet states will only be excited from the first excited triplet state if the transition moment integral is non-zero. This condition is fulfilled (see section 5.2) if at least one of the component integrands (the dipole moment operator in eq.(4) being a vector operator can be resolved along the Cartesian axes of space and the electronic transition moment can be similarly resolved) belongs to the totally symmetric irreducible representation. Since 1,4 Difluorobenzene belongs to the D_{2h} point group the dipole moment operator transforms as B_{3u}, B_{2u} and B_{1u} along the x, y and z axes respectively. Therefore the three components of the direct product $\Gamma_{\phi_i} \times \Gamma_{\mu} \times \Gamma_{\phi_f}$ (where ϕ_i

is the initial state, the first excited triplet state, and ϕ_f is the final state, the higher excited triplet state) will be:

for a x-polarised transition:

$$B_{1u} \times B_{3u} \times \Gamma_{\phi_f} = A_{1g}$$

Therefore the higher triplet state will belong to the B_{2g} irreducible representation.

for a y-polarised transition:

$$B_{1u} \times B_{2u} \times \Gamma_{\phi_f} = A_{1g}$$

Therefore the higher triplet state will belong to the B_{3g} irreducible representation.

for a z-polarised transition:

$$B_{1u} \times B_{2u} \times \Gamma_{\phi_f} = A_{1g}$$

Therefore the higher triplet state will belong to the A_{1g} irreducible representation.

From the above table the only state which would give rise to a symmetry-allowed $T_n \leftarrow T_1$ absorption will be the B_{2g} state lying at 8.38 eV and the transition will be x-polarised with a peak maximum at 227.9 nms.

OBSERVED TRIPLET-TRIPLET ABSORPTION

a. High pressure triplet-triplet absorption spectrum using the technique of laser flash photolysis.[2] (Spectrum - reference (1), page 225, figure 49). There is a broad absorption band with a maximum located at λ_{T-T} = 227 nms. This correlates with the predicted transition at 227.9 nms, hence the assignment is $B_{2g} \leftarrow B_{1u}$.

b. Phase modulated triplet-triplet absorption spectrum. There is a broad absorption band with a maximum at λ_{T-T} = 235 nms, this again correlates with the predicted transition at 227.9 nms.

1,3 Difluorobenzene

(a) 1,3 Difluorobenzene belongs to the C_{2v} point group.

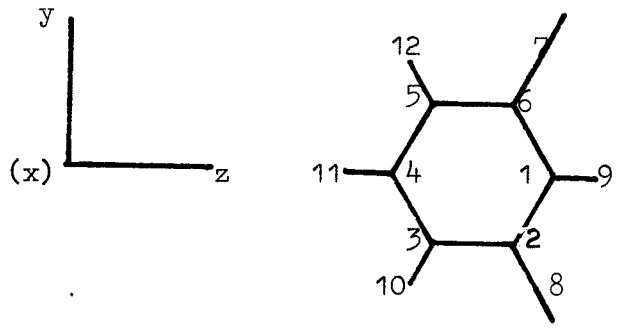

THE MOLECULAR CARTESIAN COORDINATES

ATOM	ATOMIC NUMBER	Z-COORDINATE	Y-COORDINATE	X-COORDINATE
1	6	1.397	0.0	0.0
2	6	0.6985	-1.2098	0.0
3	6	-0.6985	-1.2098	0.0
4	6	-1.397	0.0	0.0
5	6	-0.6985	1.2098	0.0
6	6	0.6985	1.2098	0.0
7	9	1.3535	2.3443	0.0
8	9	1.3535	-2.3443	0.0
9	1	2.481	0.0	0.0
10	1	-1.2405	-2.4186	0.0
11	1	-2.481	0.0	0.0
12	1	-1.2405	2.4186	0.0

(b) The ordering and energies (eV) of highest four occupied and lowest seven unoccupied molecular orbitals of 1,3 difluorobenzene.

SYMMETRY	ENERGY (eV)
UNOCCUPIED ORBITALS	
$a_1(\sigma^*)$	4.97
$b_2(\sigma^*)$	3.85
$a_1(\sigma^*)$	3.74
$a_1(\sigma^*)$	2.78
$b_1(\pi^*)$	1.39
$a_2(\pi^*)$	-0.94
$b_1(\pi^*)$	-0.94
OCCUPIED ORBITALS	
$a_2(\pi)$	-10.01
$b_1(\pi)$	-10.25
$a_1(\sigma)$	-12.90
$b_2(\sigma)$	-13.58

(c) Energies and oscillator strengths of singlet-singlet transitions for 1,3 difluorobenzene.

STATE NUMBER	TYPE OF TRANSITION	SYMMETRY	SINGLET EXCITATION ENERGY (eV)	OSCILLATOR STRENGTH AND POLARIZATION OF TRANSITION
1	$\pi \rightarrow \pi^*$	B_2	4.66	0.002 (Y)
2	$\pi \rightarrow \pi^*$	A_1	5.84	0.03 (Z)
3	$\pi \rightarrow \pi^*$	A_1	6.56	0.847 (Z)
4	$\pi \rightarrow \pi^*$	B_2	6.67	1.214 (Y)

(d) Lower triplet excitation energies for 1,3 Difluorobenzene.

STATE NUMBER	TYPE OF TRANSITION	SYMMETRY	TRIPLET EXCITATION ENERGY (eV)
1	$\pi \rightarrow \pi^*$	A_1	2.96
2	$\pi \rightarrow \pi^*$	B_2	3.81
3	$\pi \rightarrow \pi^*$	A_1	3.82
4	$\pi \rightarrow \pi^*$	B_2	4.68

(e) Comparison of singlet excitation energies (eV) for 1,3 Difluorobenzene.

METHOD	S_1	S_2	S_3	S_4
This work (CNDO/S-CI)	4.7	5.8	6.6	6.7
(CNDO/S2)[a]	4.5	5.6	6.5	6.5
(CNDO/S1)[b]	4.6	5.9	6.7	6.7
EXPERIMENTAL[c]	4.8	6.2	7.0	7.0

a. C. B. Duke et al. ref.30.

b. G. W. Kuehnlenz. ref.34.

c. R. P. Frueholz et al. ref.57.

Assignment of Triplet-Triplet Absorption Bands for 1,3 Difluorobenzene

Predicted Higher Triplet States Excited in 225-250 nm. Spectral Region.

SYMMETRY	TRIPLET EXCITATION ENERGY (eV)	PREDICTED TRIPLET-TRIPLET ABSORPTION WAVELENGTH (nms) (T_1 = 2.96 eV)
B_1	8.39	228.3

The first excited triplet state, T_1, belongs to the A_1 irreducible representation.

1,3 Difluorobenzene belongs to the C_{2v} point group and hence the dipole moment operator transforms as B_1, B_2 and A_1 along the x, y and z axes respectively. Therefore the three components of the direct product $\Gamma_{\phi_i} \times \Gamma_{\mu} \times \Gamma_{\phi_f}$ will be:

for a x-polarised transition:

$$A_1 \times B_1 \times \Gamma_{\phi_f} = A_1$$

Therefore the higher triplet state will belong to the B_1 irreducible representation.

for a y-polarised transition:

$$A_1 \times B_2 \times \Gamma_{\phi_f} = A_1$$

Therefore the higher triplet state will belong to the B_2 irreducible representation.

for a z-polarised transition:

$$A_1 \times A_1 \times \Gamma_{\phi_f} = A_1$$

Therefore the higher triplet state will belong to the A_1 irreducible representation.

The only state predicted in the spectral range scanned in the experiment (for spectrum see reference 1, page 225, figure 49) is the B_1 state which has a triplet excitation energy equal to 8.39 eV. The transition is thus predicted to be x-polarised with an absorption peak maximum at 228.3 nms.

OBSERVED TRIPLET-TRIPLET ABSORPTION.

High pressure triplet-triplet absorption spectrum using the technique of laser flash photolysis.[2] (Spectrum - reference 1, page 225, figure 49). There is a broad absorption band extending from about 225 nms to 240 nms with a maximum at λ_{T-T} = 231 nms. This correlates with the predicted transition at 228.3 nms, hence the assignment is $B_1 \leftarrow A_1$.

1,2 Difluorobenzene

(a) 1,2 Difluorobenzene belongs to the C_{2v} point group.

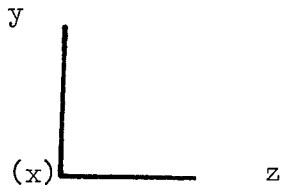

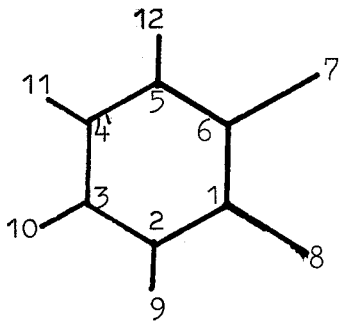

THE MOLECULAR CARTESIAN COORDINATES

ATOM	ATOMIC NUMBER	Z-COORDINATE	Y-COORDINATE	X-COORDINATE
1	6	1.2098	-0.6985	0.0
2	6	0.0	-1.397	0.0
3	6	-1.2098	-0.6985	0.0
4	6	-1.2098	0.6985	0.0
5	6	0.0	1.397	0.0
6	6	1.2098	0.6985	0.0
7	9	2.3443	1.3535	0.0
8	9	2.3443	-1.3535	0.0
9	1	0.0	-2.481	0.0
10	1	-2.1486	-1.2405	0.0
11	1	-2.1486	1.2405	0.0
12	1	0.0	2.481	0.0

(b) The ordering and energies (eV) of highest four occupied and lowest seven unoccupied molecular orbitals of 1,2 difluorobenzene.

SYMMETRY	ENERGY (eV)
UNOCCUPIED ORBITALS	
$a_1(\sigma^*)$	4.89
$b_2(\sigma^*)$	3.86
$a_1(\sigma^*)$	3.73
$b_2(\sigma^*)$	2.76
$a_2(\pi^*)$	1.39
$a_2(\pi^*)$	-0.94
$b_1(\pi^*)$	-0.95
OCCUPIED ORBITALS	
$b_2(\pi)$	-9.99
$a_2(\pi)$	-10.25
$a_1(\sigma)$	-12.75
$b_1(\sigma)$	-13.68

(c) Energies and oscillator strengths of singlet-singlet transitions for 1,2 difluorobenzene.

STATE NUMBER	TYPE OF TRANSITION	SYMMETRY	SINGLET EXCITATION ENERGY (eV)	OSCILLATOR STRENGTH AND POLARIZATION OF TRANSITION
1	$\pi \rightarrow \pi^*$	A_1	4.65	0.003(Z)
2	$\pi \rightarrow \pi^*$	B_2	5.81	0.038(Y)
3	$\pi \rightarrow \pi^*$	B_2	6.55	0.839(Y)
4	$\pi \rightarrow \pi^*$	A_1	6.67	1.208(Z)

(d) Lower triplet excitation energies for 1,2 Difluorobenzene.

STATE NUMBER	TYPE OF TRANSITION	SYMMETRY	TRIPLET EXCITATION ENERGY (eV)
1	$\pi \rightarrow \pi^*$	B_2	2.94
2	$\pi \rightarrow \pi^*$	A_1	3.79
3	$\pi \rightarrow \pi^*$	B_2	3.81
4	$\pi \rightarrow \pi^*$	A_1	4.67

(e) Comparison of singlet excitation energies (eV) for 1,2 Difluorobenzene.

METHOD	S_1	S_2	S_3	S_4
THIS WORK (CNDO/S-CI)	4.7	5.8	6.6	6.7
(CNDO/S2)[a]	4.5	5.6	6.5	6.5
(CNDO/S1)[b]	4.6	5.7	6.5	6.6
EXPERIMENTAL[c]	4.8	6.2	7.0	7.0

a. C. B. Duke et al. ref.30.
b. G. W. Kuehnlenz. ref.34.
c. R. P. Frueholz. ref.57.

Assignment of Triplet-Triplet Absorption Bands for 1,2 Difluorobenzene

Predicted Higher Triplet States Excited in 225-250 nm. Spectral Region.

SYMMETRY	TRIPLET EXCITATION ENERGY (eV)	PREDICTED TRIPLET-TRIPLET ABSORPTION WAVELENGTH (nms)
		(T_1 = 2.94 eV)
A_2	8.05	242.6
A_2	8.43	225.8

The first excited triplet state, T_1, transforms as the B_2 irreducible representation.

1,2 Difluorobenzene belongs to the C_{2v} point group and hence the dipole moment operator transforms as B_1, B_2 and A_1 along the x, y and z axes respectively. Therefore the three components of the direct product $\Gamma_{\phi_i} \times \Gamma_{\mu} \times \Gamma_{\phi_f}$ will be:

for a x-polarised transition:

$$B_2 \times B_1 \times \Gamma_{\phi_f} = A_1$$

Therefore the higher triplet state will belong to the A_2 irreducible representation.

for a y-polarised transition:

$$B_2 \times B_2 \times \Gamma_{\phi_f} = A_1$$

Therefore the higher triplet state will belong to the A_1 irreducible representation.

for a z-polarised transition:

$$B_2 \times A_1 \times \Gamma_{\phi_f} = A_1$$

Therefore the higher triplet state will belong to the B_2 irreducible representation.

The only state predicted in the spectral range scanned in the experiment (for spectrum see reference 1, page 225, figure 49) is the A_2 state which has a triplet excitation energy equal to 8.05 eV. The transition is thus predicted to be x-polarised with an absorption peak maximum at 242.6 nms.

OBSERVED TRIPLET-TRIPLET ABSORPTION.

From the high pressure triplet-triplet absorption spectrum using the technique of laser flash photolysis,[2] (Spectrum - reference 1, page 225, figure 49) there is a broad absorption band extending from 225 nms to 250 nms with a maximum at 235.6 nms. This correlates with the predicted transition at 242.6 nms, hence the assignment is $A_2 \leftarrow B_2$.

1,4 Ditrifluoromethylbenzene

(a) Ditrifluoromethylbenzene belongs to the C_{2h} point group.

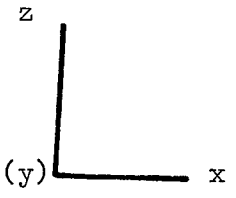

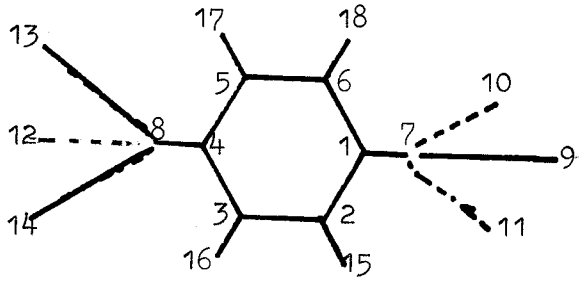

THE MOLECULAR CARTESIAN COORDINATES

ATOM	ATOMIC NUMBER	Z-COORDINATE	Y-COORDINATE	X-COORDINATE
1	6	0.0	0.0	1.397
2	6	-1.2098	0.0	0.6985
3	6	-1.2098	0.0	-0.6985
4	6	0.0	0.0	-1.397
5	6	1.2098	0.0	-0.6985
6	6	1.2098	0.0	0.6985
7	6	0.0	0.0	2.917
8	6	0.0	0.0	-2.917
9	9	0.0	1.254	3.361
10	9	1.086	-0.627	3.361
11	9	-1.086	-0.627	3.361
12	9	0.0	-1.254	-3.361
13	9	1.086	0.627	-3.361
14	9	-1.086	0.627	-3.361
15	1	-2.1486	0.0	1.2405
16	1	-2.1486	0.0	-1.2405
17	1	2.1486	0.0	-1.2405
18	1	2.1486	0.0	1.2405

(b) The ordering and energies (eV) of highest six occupied and lowest six unoccupied molecular orbitals for 1,4 ditrifluoromethylbenzene.

SYMMETRY	ENERGY (eV)
UNOCCUPIED ORBITALS	
b_g	3.5087
a_g	2.907
b_u	2.291
a_g	1.189
a_u	-1.049
b_u	-1.279
OCCUPIED ORBITALS	
b_g	-10.473
a_g	-10.49
a_g	-12.481
b_g	-12.977
b_u	-14.054
b_u	-14.81

(c) Eigensolutions and Oscillator Strengths of singlet-singlet transitions for 1,4 ditrifluoromethylbenzene.

STATE NUMBER	SYMMETRY	SINGLET EXCITATION ENERGY (eV)	OSCILLATOR STRENGTH AND POLARIZATION OF TRANSITION
1	A_u	4.76	0.003(z)
2	B_u	5.99	0.021(x)
3	B_u	6.57	0.005(x)
4	A_u	6.67	0.001(z)

(d) Lower triplet excitation energies for 1,4 Ditrifluoromethylbenzene

STATE NUMBER	TYPE OF TRANSITION	SYMMETRY	TRIPLET EXCITATION ENERGY (eV)
1	$\pi \rightarrow \pi$	B_u	3.03
2	$\pi \rightarrow \pi$	A_u	3.87
3	$\pi \rightarrow \pi$	B_u	3.90
4	$\pi \rightarrow \pi$	A_u	4.79

(e) Comparison of singlet excitation energies (eV) for 1,4 ditrifluoromethylbenzene

TECHNIQUE	S_1	S_2	S_3	S_4
THIS WORK (CNDO/S-CI)	4.8	6.0	6.6	6.7
CNDO/S2[a]	5.2	5.3	5.4	6.1
CNDO/S3[a]	4.6	5.8	6.6	6.8
EXPERIMENTAL[b]	4.7			

a. N. O. Lipari and C. B. Duke, ref.22.

b. M. G. Rockley and D. Phillips, ref.58.

Comparison with the CNDO/S2 analysis of Lipari and Duke reveals that this work provides a more accurate description of the first excited singlet state of 1,4 ditrifluoromethylbenzene. By altering the Slater orbital exponent of the substituent carbon atoms (CNDO/S3) Lipari and Duke obtain an improved description.

Assignment of Triplet-Triplet Absorption Bands for 1,4 Ditrifluoromethylbenzene

Predicted Higher Triplet States Excited in 225-250 nm Spectral Region

SYMMETRY	TRIPLET EXCITATION ENERGY (eV)	PREDICTED TRIPLET-TRIPLET ABSORPTION WAVELENGTH (nms)
		(T_1 = 3.03 eV)
B_g	8.175	240.9
A_g	8.177	240.8

The first excited triplet state transforms as the B_u irreducible representation. The dipole moment operator transforms as B_u, B_u and A_u along the x, y and z axes respectively. Therefore the three components of the direct product $\Gamma_{\phi_i} \times \Gamma_{\mu} \times \Gamma_{\phi_f}$ will be:

for a x-polarised transition:

$$B_u \times B_u \times \Gamma_{\phi_f} = A_g$$

Therefore the higher triplet state will belong to the A_g irreducible representation.

for a y-polarised transition:

$$B_u \times B_u \times \Gamma_{\phi_f} = A_g$$

Therefore the higher triplet state will belong to the A_g irreducible representation.

for a z-polarised transition:

$$B_u \times A_u \times \Gamma_{\phi_f} = A_g$$

Therefore the higher triplet state will belong to the B_g irreducible representation.

Two states are predicted to be excited in the 225-250 nm spectral range. The two states are nearly degenerate, a B_g state has a triplet excitation energy equal to 8.175 eV and thus the triplet-triplet transition is predicted to be z-polarised with an absorption maximum at 240.9 nms. An A_g state is predicted to have an energy equal to 8.177 eV and thus the triplet-triplet absorption will be either x or y-polarised with an absorption peak maximum at 240.8 nms.

OBSERVED TRIPLET-TRIPLET ABSORPTION.

The triplet-triplet absorption spectrum of 1,4 Ditrifluoromethylbenzene was obtained using an electrodeless, modulated mercury discharge lamp with phase sensitive detection.[1]

(Spectrum - reference 1, page 144, Figure 28).

Three sharp bands are observed between 233 and 243 nms. The peak maxima are located at 236.5 nms, 237.5 nms and 240.5 nms. These correlate with the predicted transitions at 240.9 nms and 240.8 nms, but since the calculation only predicts two triplet-triplet absorptions one of the peaks could be a vibrational component of one of the pure electronic transitions. The assignments are $A_g \leftarrow B_u$ and $B_g \leftarrow B_u$ for the pure electronic transitions.

1,3 Ditrifluoromethylbenzene.

(a) 1,3 Ditrifluoromethylbenzene belongs to the C_2 point group when it adopts the lowest energy conformation.

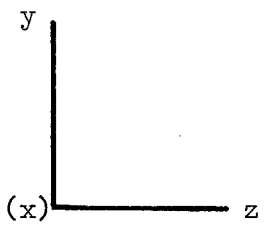

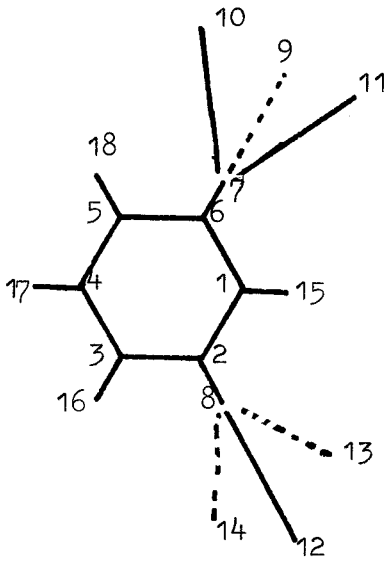

THE MOLECULAR CARTESIAN COORDINATES

ATOM	ATOMIC NUMBER	Z-COORDINATE	Y-COORDINATE	X-COORDINATE
1	6	1.397	0.0	0.0
2	6	0.6985	-1.2098	0.0
3	6	-0.6985	-1.2098	0.0
4	6	-1.397	0.0	0.0
5	6	-0.6985	1.3098	0.0
6	6	0.6985	1.2098	0.0
7	6	1.4585	2.5262	0.0
8	6	1.4585	-2.5262	0.0
9	9	1.6805	2.9107	-1.254
10	9	0.740	3.4537	0.627
11	9	2.621	2.3677	0.627
12	9	1.6805	-2.9107	1.254
13	9	2.621	-2.3677	-0.627
14	9	0.740	-3.4537	-0.627
15	1	2.481	0.0	0.0
16	1	-1.2405	-2.1486	0.0
17	1	-2.481	0.0	0.0
18	1	-1.2405	2.1486	0.0

(b) The ordering and energies (eV) of highest seven occupied and lowest six unoccupied molecular orbitals for 1,3 Ditrifluoromethylbenzene.

SYMMETRY	ENERGY (eV)
UNOCCUPIED ORBITALS	
a	3.392
b	3.054
a	2.252
b	1.195
b	-1.112
a	-1.217
OCCUPIED ORBITALS	
b	-10.477
a	-10.485
b	-12.525
a	-12.801
b	-14.751
b	-14.888
a	-15.024

(c) Energies and Oscillator Strengths of singlet-singlet transitions for 1,3 Ditrifluoromethylbenzene.

STATE NUMBER	SYMMETRY	SINGLET EXCITATION ENERGY (eV)	OSCILLATOR STRENGTH AND POLARISATION OF TRANSITION
1	B	4.77	0.001 (Y)
2	A	5.99	0.005 (Z)
3	B	6.63	0.006 (Y)
4	A	6.67	0.001 (Z)

(d) Lower triplet excitation energies for 1,3 Ditrifluoromethylbenzene.

STATE NUMBER	TYPE OF TRANSITION	SYMMETRY	TRIPLET EXCITATION ENERGY (eV)
1	$\pi \rightarrow \pi^*$	A	3.03
2	$\pi \rightarrow \pi^*$	B	3.89
3	$\pi \rightarrow \pi^*$	A	3.90
4	$\pi \rightarrow \pi^*$	B	4.75

(e) Comparison of singlet excitation energies (eV) for 1,3 Ditrifluoromethylbenzene.

TECHNIQUE	S_1	S_2	S_3	S_4
THIS WORK (CNDO/S-CI)	4.8	6.0	6.6	6.7
EXPERIMENTAL[a]	4.7			

a. M. G. Rockley and D. Phillips, ref.58.

Assignment of Triplet-Triplet Absorption Bands for 1,3 Ditrifluoromethylbenzene

Predicted Higher Triplet States Excited in 225-250 nm Spectral Region

SYMMETRY	TRIPLET EXCITATION ENERGY (eV)	PREDICTED TRIPLET-TRIPLET ABSORPTION WAVELENGTH (nms)
		(T_1 = 3.03 eV)
A	8.11	244.4
B	8.21	239.7
B	8.28	236.3

The first excited triplet state transforms as the A irreducible representation.

1,3 Ditrifluoromethylbenzene belongs to the C_2 point group and hence the dipole moment operator transforms as B, B and A along the x, y and z Cartesian axes respectively. Therefore the three components of the direct product

$$\Gamma_{\phi_i} \times \Gamma_{\mu} \times \Gamma_{\phi_f} \text{ will be:}$$

for a x-polarised transition:

$$A \times B \times \Gamma_{\phi_f} = A$$

Therefore the higher triplet state will belong to the B irreducible representation.

for a y-polarised transition:

$$A \times B \times \Gamma_{\phi_f} = A$$

Therefore the higher triplet state will belong to the B irreducible representation.

for a z-polarised transition:

$$A \times A \times \Gamma_{\phi_f} = A$$

Therefore the higher triplet state will belong to the A irreducible representation.

Three states are predicted to be excited in the 225-250 nm spectral region. An A state has a triplet excitation energy equal to 8.11 eV and thus the triplet-triplet transition is predicted to be z-polarised with an absorption maximum at 244.4 nms. A B state has a triplet excitation energy equal to 8.21 eV and thus the triplet-triplet transition is predicted to be either x- or y-polarised with an absorption maximum at 239.7 nms. A B state is predicted to have an excitation energy equal to 8.28 eV and thus the triplet-triplet transition is predicted to be either x- or y-polarised with an absorption maximum at 236.3 nms.

OBSERVED TRIPLET-TRIPLET ABSORPTION

The triplet-triplet absorption spectrum of 1,3 Ditrifluoromethylbenzene was obtained using an electrodeless, modulated, mercury discharge lamp with phase sensitive detection.[1]

(Spectrum - reference 1, page 219, figure 47).

Three very sharp bands lie between 236 and 241 nms. The peak maxima are located at 237.4 nms, 238.9 nms and 239.1 nms. These correlate with the predicted transitions at 244.4 nms, 239.7 nms and 236.3 nms. The assignments are A $\leftarrow$ A, B $\leftarrow$ A and B $\leftarrow$ A respectively.

Trifluoromethylbenzene

Trifluoromethylbenzene belongs to the C_s point group.

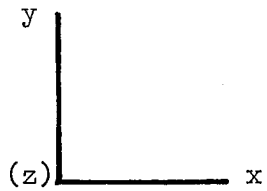

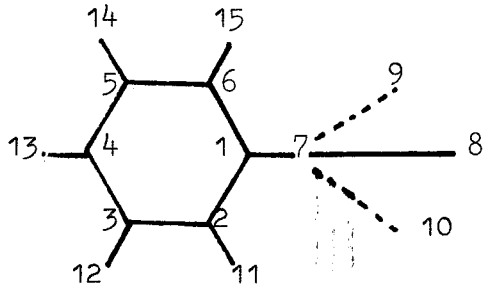

THE MOLECULAR CARTESIAN COORDINATES

ATOM	ATOMIC NUMBER	X-COORDINATE	Y-COORDINATE	Z-COORDINATE
1	6	1.897	0.0	0.0
2	6	0.6985	-1.2098	0.0
3	6	-0.6985	-1.2098	0.0
4	6	-1.397	0.0	0.0
5	6	-0.6985	1.2098	0.0
6	6	0.6985	1.2098	0.0
7	6	2.917	0.0	0.0
8	9	3.361	0.0	1.254
9	9	3.361	1.086	-0.627
10	9	3.361	-1.086	-0.627
11	1	1.2405	-2.1486	0.0
12	1	-1.2405	-2.1486	0.0
13	1	-2.491	0.0	0.0
14	1	-1.2405	2.1486	0.0
15	1	1.2405	2.1486	0.0

(b) The ordering and energies of the highest four occupied and lowest six unoccupied molecular orbitals for trifluoromethylbenzene.

SYMMETRY	ENERGY (eV)
UNOCCUPIED ORBITALS	
a"	3.79
a'	3.50
a'	2.66
a'	1.53
a"	-0.78
a'	-0.90
OCCUPIED ORBITALS	
a"	-10.20
a'	-10.21
a'	-12.41
a"	-12.71

(c) Eigensolutions and Oscillator Strengths of singlet-singlet transitions for trifluoromethylbenzene.

STATE NUMBER	SYMMETRY	SINGLET EXCITATION ENERGY (eV)	OSCILLATOR STRENGTH AND POLARIZATION OF TRANSITION
1	A"	4.80	0.001 (z)
2	A'	6.04	0.006 (x)
3	A'	6.69	0.003 (x)
4	A"	6.77	0.001 (z)

(d) Lower triplet excitation energies for Trifluoromethylbenzene

STATE NUMBER	TYPE OF TRANSITION	SYMMETRY	TRIPLET EXCITATION ENERGY (eV)
1	$\pi \rightarrow \pi^*$	A'	3.06
2	$\pi \rightarrow \pi^*$	A''	3.92
3	$\pi \rightarrow \pi^*$	A'	3.93
4	$\pi \rightarrow \pi^*$	A''	4.79

(e) Comparison of singlet excitation energies (eV) for Trifluoromethylbenzene

TECHNIQUE	S_1	S_2	S_3	S_4
THIS WORK (CNDO/S-CI)	4.8	6.0	6.7	6.8
(CNDO/S1)[a]	4.8	6.0	6.8	6.9
EXPERIMENTAL[b]	4.7			

a. G. W. Kuehnlenz. ref.34.

b. H. Sponer, J.Chem.Phys., 22, 234 (1953).

Assignment of Triplet-Triplet Absorption Bands

for Trifluoromethylbenzene

Predicted Higher Triplet States Excited in 225-250 nm Spectral Region

SYMMETRY	TRIPLET EXCITATION ENERGY (eV)	PREDICTED TRIPLET-TRIPLET ABSORPTION WAVELENGTH (nms) (T_1 = 3.06 eV)
A'	8.15	243.6
A''	8.26	238.4
A'	8.38	233.0

The first excited triplet state transforms as the A' irreducible representation.

Trifluoromethylbenzene belongs to the C_s point group and hence the dipole moment operator transforms as A', A' and A'' along the x, y and z axes respectively. Therefore the three components of the direct product $\Gamma_{\phi_i} \times \Gamma_{\mu} \times \Gamma_{\phi_f}$ will be:

for a x-polarised transition:

$$A' \times A' \times \Gamma_{\phi_f} = A'.$$

Therefore the higher triplet state will belong to the A' irreducible representation.

for a y-polarised transition:

$$A' \times A' \times \Gamma_{\phi_f} = A'.$$

Therefore the higher triplet state will belong to the A' irreducible representation.

for a z-polarised transition:

$$A' \times A'' \times \Gamma_{\phi_f} = A'.$$

Therefore the higher triplet state will belong to the A'' irreducible representation.

Three excited triplet states are predicted to be excited in the 225-250 nm spectral region. An A' state has a triplet excitation energy equal to 8.15 eV and thus the triplet-triplet transition is predicted to be either x- or y-polarised with an absorption maximum at 243.6 nms. An A'' state has a triplet excitation energy equal to 8.26 eV and thus the transition is predicted to be z-polarised with an absorption maximum at 238.4 nms. An A' state has a triplet excitation energy equal to 8.38 eV and thus the transition is predicted to be either x- or y-polarised with an absorption maximum at 233.0 nms.

OBSERVED TRIPLET-TRIPLET ABSORPTION.

The triplet-triplet absorption spectrum of Trifluoromethylbenzene was obtained using an electrodeless, modulated, mercury discharge lamp with phase sensitive detection.

(Spectrum - reference 1, page 146, figure 29).

Three very sharp bands lie between 233 and 243 nms. The peak maxima are located at 237.4 nms, 238.9 nms and 240.0 nms. These bands correlate with the predicted transitions at 233 nms, 238.4 nms and 243.6 nms. The assignments for the observed bands are A' $\leftarrow$ A', A'' $\leftarrow$ A' and A' $\leftarrow$ A' respectively.

TOLUENE

(a) Toluene belongs to the C_s point group.

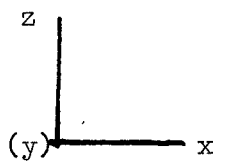

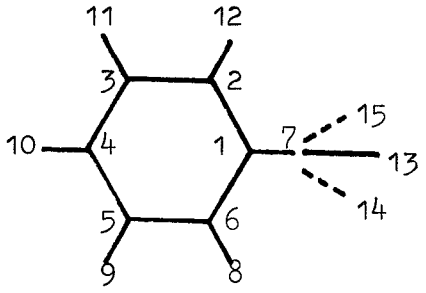

MOLECULAR CARTESIAN COORDINATES

ATOM LABEL	ATOMIC NUMBER	X-COORDINATE	Z-COORDINATE	Y-COORDINATE
1	6	1.397	0.0	0.0
2	6	0.6985	1.2098	0.0
3	6	-0.6985	1.2098	0.0
4	6	-1.397	0.0	0.0
5	6	-0.6985	-1.2098	0.0
6	6	0.6985	-1.2098	0.0
7	6	2.917	0.0	0.0
8	1	1.2405	-2.1486	0.0
9	1	-1.2405	-2.1486	0.0
10	1	-2.481	0.0	0.0
11	1	-1.2405	2.1486	0.0
12	1	1.2405	2.1486	0.0
13	1	3.281	0.0	1.028
14	1	3.281	-0.89	-0.514
15	1	3.281	0.89	-0.514

(b) The ordering and energies (eV) of highest four occupied and lowest seven unoccupied molecular orbitals of toluene.

SYMMETRY	ENERGY (eV)
UNOCCUPIED ORBITALS	
a'	4.49
a"	4.14
a'	3.93
a'	3.15
a'	1.92
a'	-0.40
a"	-0.47
OCCUPIED ORBITALS	
a'	-9.55
a"	-9.89
a'	-12.13
a"	-12.28

(c) Energies and Oscillator Strengths of singlet-singlet transitions for toluene.

STATE NUMBER	SYMMETRY	SINGLET EXCITATION ENERGY (eV)	OSCILLATOR STRENGTH AND POLARIZATION OF TRANSITION
1	A"	4.74	0.006 (z)
2	A'	5.94	0.043 (x)
3	A"	6.75	0.044 (z)
4	A'	6.78	0.444 (x)

(d) Lower triplet excitation energies for toluene.

STATE NUMBER	SYMMETRY	TRIPLET EXCITATION ENERGY (eV)
1	A'	3.03
2	A''	3.85
3	A'	3.90
4	A''	4.78

(e) Comparison of singlet excitation energies (eV) for toluene.

METHOD	S_1	S_2	S_3	S_4
THIS WORK (CNDO/S-CI)	4.74	5.94	6.75	6.78
CNDO/S1[a]	4.7	5.9	6.8	6.8
CNDO/S-CI[b]	4.73	5.93	6.58	6.59
EXPERIMENTAL[c]	4.6	5.8	6.6	6.6

a. G. W. Kuehnlenz ref.34

b. R. W. Bigelow ref.32

c. K. Kimura and S. Nagakura ref.65.

Assignment of Triplet-Triplet Absorption Bands for Toluene

Predicted Higher Triplet States Excited in 225-250 nm spectral region.

SYMMETRY	TRIPLET EXCITATION ENERGY	PREDICTED TRIPLET-TRIPLET ABSORPTION WAVELENGTH (nms) (T_1 = 3.028 eV)
A'	8.134	242.8
A''	8.264	236.8
A'	8.363	232.3

The first excited triplet state, T_1, transforms as the A' irreducible representation.

Since toluene belongs to the C_s point group the dipole moment operator transforms as A', A' and A'' along the x, y and z axes respectively.

Therefore the three components of the direct product will be:

$(\Gamma_{\phi_i} \times \Gamma_{\mu} \times \Gamma_{\phi_f})$.

for a x-polarised transition:

$$A' \times A' \times \Gamma_{\phi_f} = A'.$$

Therefore the higher triplet state will belong to the A' irreducible representation.

for a y-polarised transition:

$$A' \times A' \times \Gamma_{\phi_f} = A'.$$

Therefore the higher triplet state will belong to the A' irreducible representation.

for a z-polarised transition:

$$A' \times A'' \times \Gamma_{\phi_f} = A'$$

Therefore the higher triplet state will belong to the A" irreducible representation.

Three excited states are predicted to be excited in the 225-250 nm. spectral region. An A' state has a triplet excitation energy equal to 8.134 eV and thus the triplet-triplet transition is predicted to be either x- or y-polarised with an absorption maximum at 242.8 nms. An A" state has a triplet excitation energy equal to 8.264 eV and thus the transition is predicted to be z-polarised with an absorption maximum at 236.8 nm. An A' state has a triplet excitation energy equal to 8.363 eV and thus the transition is predicted to be either x- or y-polarised with an absorption maximum at 232.3 nms.

OBSERVED TRIPLET-TRIPLET ABSORPTION

The triplet-triplet absorption spectrum of toluene was obtained using an electrodeless, modulated, mercury discharge lamp with phase sensitive detection.

(Spectrum - reference 1, page 216, figure 44).

A broad absorption band extends from about 225 to 250 nms with a peak maximum at 240 nms. This correlates with the predicted transition at 242.8 nms and thus the assignment is A' ← A'.

1,4 DIMETHYLBENZENE (PARA-XYLENE)

(a) 1,4 Dimethylbenzene belongs to the C_{2h} point group.

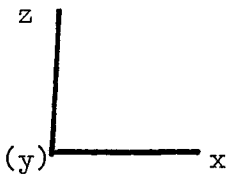

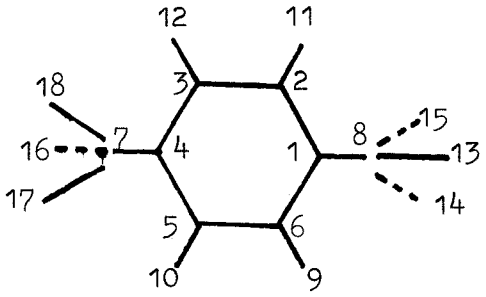

THE MOLECULAR CARTESIAN COORDINATES

ATOM LABEL	ATOMIC NUMBER	X-COORDINATE	Z-COORDINATE	Y-COORDINATE
1	6	1.397	0.0	0.0
2	6	0.6985	1.2098	0.0
3	6	-0.6985	1.2098	0.0
4	6	-1.397	0.0	0.0
5	6	-0.6985	-1.2098	0.0
6	6	0.6985	-1.2098	0.0
7	6	-2.917	0.0	0.0
8	6	2.917	0.0	0.0
9	1	1.2405	-2.1486	0.0
10	1	-1.2405	-2.1486	0.0
11	1	1.2405	2.1486	0.0
12	1	-1.2405	2.1486	0.0
13	1	3.281	0.0	1.028
14	1	3.281	-0.89	-0.514
15	1	3.281	0.89	-0.514
16	1	-3.281	-0.0	-1.028
17	1	-3.281	-0.89	-0.514
18	1	-3.281	0.89	0.514

(b) The ordering and energies (eV) of highest six occupied and lowest six unoccupied molecular orbitals for para-xylene.

SYMMETRY	ENERGY(eV)
UNOCCUPIED ORBITALS	
b_g	4.18
a_g	3.82
b_u	3.14
a_g	1.94
b_u	-0.32
a_u	-0.45
OCCUPIED ORBITALS	
a_g	-9.23
b_g	-9.87
a_g	-11.89
b_g	-12.18
b_u	-13.42
a_u	-13.93

(c) Eigensolutions and Oscillator Strengths of singlet-singlet transitions for Para-Xylene.

STATE NUMBER	SYMMETRY	SINGLET EXCITATION (ENERGY eV)	OSCILLATOR STRENGTH AND POLARIZATION OF TRANSITION
1	A_u	4.62	0.021 (z)
2	B_u	5.77	0.124 (x)
3	A_u	6.63	0.035 (z)
4	B_u	6.71	0.672 (x)

(d) Lower triplet excitation energies for Para-xylene

STATE NUMBER	SYMMETRY	TRIPLET EXCITATION ENERGY (eV)
1	B_u	2.97
2	A_u	3.68
3	B_u	3.85
4	A_u	4.79

(e) Comparison of singlet excitation energies (eV) for para-xylene

TECHNIQUE	S_1	S_2	S_3	S_4
THIS WORK (CNDO/S-CI)	4.62	5.77	6.63	6.71
CNDO/S2[a]	4.62	5.72	6.52	6.56
EXPERIMENTAL[b]	4.59	5.59	6.41	6.41

a. N. O. Lipari and C. B. Duke, ref.22.

b. J. Petruska, ref.66.

Assignment of Triplet-Triplet Absorption Bands for Para-Xylene

Predicted Higher Triplet States Excited in 225-250 nm Spectral Region

SYMMETRY	TRIPLET EXCITATION ENERGY (eV)	PREDICTED TRIPLET-TRIPLET ABSORPTION WAVELENGTH (nms)
		(T_1 = 2.97 eV)
A_u	8.155	238.9
A_g	8.198	237.0

The first excited triplet state transforms as the B_u irreducible representation.

Para-xylene belongs to the C_{2h} point group and hence the dipole moment operator transforms as B_u, B_u and A_u along the x, y and z axes respectively. Therefore the three components of the direct product $\Gamma_{\phi_i} \times \Gamma_{\mu} \times \Gamma_{\phi_f}$ will be:

for a x-polarised transition:

$$B_u \times B_u \times \Gamma_{\phi_f} = A_g$$

Therefore the higher triplet state will belong to the A_g irreducible representation.

for a y-polarised transition:

$$B_u \times B_u \times \Gamma_{\phi_f} = A_g$$

Therefore the higher triplet state will belong to the A_g irreducible representation.

for a z-polarised transition:

$$B_u \times A_u \times \Gamma_{\phi_f} = A_g$$

Therefore the higher triplet state will belong to the B_g irreducible representation.

From the above table the only state which would give rise to a symmetry-allowed $T_N \leftarrow T_1$ absorption will be the A_g state lying at 8.198 eV and the transition will be either x-polarised or y-polarised with an absorption maximum at 237 nms.

OBSERVED TRIPLET-TRIPLET ABSORPTION

The triplet-triplet absorption spectrum of para-xylene was obtained using an electrodeless, modulated mercury discharge lamp with phase sensitive detection.[1]

(Spectrum - reference 1, page 218, figure 46).

One absorption band lies between 228 nms and 240 nms with a peak maximum located at 232 nms. This correlates with the predicted transition at 237 nms and hence the assignment is $A_g \leftarrow B_u$.

REFERENCES

1. M. E. Sime, Ph.D. Thesis. University of Southampton 1978.

2. R. Bonneau, J. Faure, J. Joussot-Dubien, L. Lindqvist, C. Barthelemy, Compt.Rend.Acad.Sci., 2673, 412 (1968).

3. L. Pauling, J.Amer.Chem.Soc., 53, 1367 (1931).

4. M. Planck, Ann.d.Physik (4th Folge), 4, 553 (1901).

5. A. Einstein, Phys.Z., 18, 121 (1917).

6. C. Eckart, Phys.Revs., 36, 878 (1930).

7. W. Pauli, Zeit.F.Physik, 31, 765 (1925).

8. R. G. Parr, 'The Quantum Theory of Molecular Electronic Structure', W. A. Benjamin Inc., New York (1964).

9. C.C.J. Roothen, Revs.Mod.Phys., 23, 161 (1951).

10. J. A. Pople and D. A. Beveridge, 'Approximate Molecular Orbital Theory' McGraw-Hill, New York (1970).

11. R. G. Parr, J.Chem.Phys., 20, 239 (1952).

12. J. A. Pople, D. P. Santry and G. A. Segal, J.Chem.Phys., 43, S129 (1965).

13. J. A. Pople and G. A. Segal, J.Chem.Phys., 43, S136 (1965).

14. J. A. Pople and G. A. Segal, J.Chem.Phys., 44, 3289 (1966).

15. K. Nishimoto and N. Mataga, Z.Physik.Chem. (Frankfurt), 12, 335 (1957); 13, 140 (1957).

16. J. Del Bene and H. H. Jaffe, J.Chem.Phys., 48, 1807 (1968).

17. J. Del Bene and H. H. Jaffe, J.Chem.Phys., 48, 4050 (1968).

18. J. Del Bene and H. H. Jaffe, J.Chem.Phys., 49, 1221 (1968).

19. J. Del Bene and H. H. Jaffe, J.Chem.Phys., 50, 1126 (1969).

20. J. C. Slater, Phys.Revs., 36, 57 (1930).

21. R. Parisier and R. G. Parr, J.Chem.Phys., 21, 767 (1953).

22. N. O. Lipari and C. B. Duke, J.Chem.Phys., 63, 1748 (1975).

23. C. B. Duke, N. O. Lipari, W. R. Salaneck and L. B. Scheir, J.Chem.Phys., 63, 1758 (1975).

24. N. O. Lipari and C. B. Duke, J.Chem.Phys., 63, 1768 (1975).

25. K. L. Yip, N. O. Lipari, C. B. Duke, B. S. Hudson and J. Diamond, J.Chem.Phys., 64, 4020 (1976).

26. W. R. Salaneck, N. O. Lipari, A. Paton, R. Zallen and K. S. Liang, Phys.Rev., B12, 1493 (1975).

27. W. R. Salaneck, K. S.Liang, A. Paton and N. O. Lipari, Phys.Rev., B12, 725 (1975).

28. C. B. Duke, W. R. Salaneck, A. Paton, K. S. Liang, N. O. Lipari and R. Zallen, in Structure and Excitations of Amorphous Solids, Edited by G. Lucovsky and F. L. Galeener (AIP, New York, 1976), p.23.

29. W. R. Salaneck, J. W.-p. Lin, A. Paton, C. B. Duke and G. P. Caesar, Phys.Rev., B13, 4517 (1976).

30. C. B. Duke, K. L. Yip, G. P. Caesar, A. W. Potts and D. G. Streets, J.Chem.Phys., 66, 256 (1977).

31. R. W. Bigelow, J.Chem.Phys., 66, 4241 (1977).

32. R. W. Bigelow, J.Chem.Phys., 70, 2315 (1979).

33. J. A. Pople, Proc.Phys.Soc.(London), A63, 81 (1955).

34. G. W. Kuehnlenz, Ph.D. Thesis, University of Cincinnati (1972).

35. P. J. Hay, I. Shavitt, J.Chem.Phys., 60, 2865 (1974).

36. W. C. Price, A. W. Potts and T. A. Williams, Chem.Phys.Letters, 37, 17 (1976).

37. R. W. Bigelow, J.Chem.Phys., 68, 5086 (1978).

38. H. Dickerson, S. Ferlber and F. S. Richardson, Theoret.Chim.Acta (Berlin) 42, 333 (1976).

39. J. H. Obbink and A.M.F. Hezemans, Theoret.Chim.Acta (Berlin), 43, 75 (1976).

40. A. P. Volosov and V. A. Zubkov, Theoret.Chim.Acta(Berlin), 44, 375 (1977).

41. H. Weiler Fielchenfeld, R. E. Linder, G. Barth, E. Bunnerberg and C. Djerassi, Theoret.Chim.Acta (Berlin), 46, 79 (1977).

42. J. Spranget-Larsen, R. Glieter, R. Haidu and E. W. Thulstrup, Mol.Phys., 34, 1049 (1977).

43. D. Dougherty, J. J. Broomfield, G. R. Newkome, J. F. Arnett and S. P. McGlynn, J.Phys.Chem., 80,2212 (1976).

44. C. J. Seliskar, J.Phys.Chem., 81, 660, 1331 (1977).

45. E. M. Evleth, O. Chalvet and P. Bamlere, J.Phys.Chem., 81, 1913 (1977).

46. T. D. Bowman and D. A. Lightner, J.Amer.Chem.Soc., 98, 3145 (1976).

47. T. S. Rosenfield and E. Charney, J.Amer.Chem.Soc., 99, 3209 (1977).

48. A. Kaito and M. Hatano, J.Amer.Chem.Soc., 100, 2034 (1978).

49. C. Yu, S. Peng, I. Akiyara, J. Lin and P. R. Lebreton, J.Amer.Chem. Soc., 100, 2303 (1978).

50. C. J. Seliskar and R. E. Hoffnan, Chem.Phys.Lett., 43, 481 (1976).

51. Z. Latajka and H. Ratajczak, Chem.Phys.Lett., 49, 407 (1977).

52. J. H. Obbink and A.M.F. Herzemans, Chem.Phys.Lett., 50, 133 (1977).

53. R. W. Bigelow and R. W. Anderson, Chem.Phys.Lett., 58, 114 (1978).

54. G. Olbrich, O. E. Polansky and M. Zander, Ber.Bunsenges.Phys.Chem., 81, 692 (1977).

55. W. Runge, W. Kosbahn and J. Kroner, Ber.Bunsenges.Phys.Chem., 81, 826, 841 (1977).

56. H. Meyer, K-W. Schultz and A. Schweig, Chem.Phys.Lett.,31, 187 (1975).

57. R. P. Frueholz, W. M. Flicker, O. A. Mosher and A. Kuppermann, J.Chem.Phys., 70, 3057 (1979).

58. M. G. Rockley and D. Phillips, J.Phys.Chem., 78, 7 (1974).

59. H. Sponer, J.Chem.Phys., 22, 234 (1953).

60. J. P. Doering, J.Chem.Phys., 67, 4065 (1977).

61. E. N. Lassettre, A. Skerbale, M. Dillon and K. Ross, J.Chem.Phys., 48, 5066 (1968).

62. R. Bonneau, J. Joussot-Dubien and R. Bensasson, Chem.Phys.Lett., 3, 353 (1969).

63. J. Callomon, J. Dunn and I. Mills, Philos.Trans.R.Soc. London Ser.A, 259, 499 (1966).

64. R. Astier and Y. H. Meyer, Chem.Phys.Lett., 6, 352 (1970).

65. K. Kimura and S. Nagakura, Mol.Phys., 9, 117 (1965).

66. J. Petruska, J.Chem.Phys., 34, 1120 (1961).

67. R.D.S. Stevens, R. Bonneau, J. Joussot-Dubien, J.Chem.Phys., 57, 5340 (1972).

CHAPTER SIX

THE DETECTION LIMITS OF SULPHUR DIOXIDE USING THE MATRIX ISOLATION SAMPLING TECHNIQUE

CHAPTER 6

THE DETECTION LIMITS OF SULPHUR DIOXIDE USING THE MATRIX ISOLATION SAMPLING TECHNIQUE

6.1. INTRODUCTION

The positive qualitative identification and subsequent quantitative studies of pollutants in stack emission has become a major industrial problem in recent years. The major primary pollutant in the stack gas of oil-burning power stations is sulphur dioxide and there is an urgent need for a method of detection which is capable of high sensitivity and rapid execution. An atypical sampling technique involving cryogenic equipment leading to such advantages has been suggested where some of the commonly employed spectroscopic techniques would be used to analyse the condensed sample. This would be synonomous with the experiment in which vapour-deposited molecules are embedded in a weakly interacting matrix where the salient features of such matrices are as follows:[1] the inert matrix separates guest molecules from each other and thus reduces chemical and physical interaction between them - thus radicals and other chemically reactive species can be stored and studied. The spectra of the matrix-isolated species contain fewer lines, which are also sharper, than spectra in the gas phase. This point will be discussed in greater detail in relation to infrared spectra. Finally, a large number of molecules are contained in a small volume.

In the industrial application, stack gas emission will be condensed onto a cold window and the sample analysed, at ground level, using a conventional spectroscopic technique. The purpose of this work was to determine the detection limits of three fundamental properties of matrix-isolated sulphur dioxide namely:

(i) the infrared absorption of the fundamental vibrations

(ii) the ultraviolet absorption to the first two singlet excited electronic states

(iii) the phosphorescence from the first excited triplet state.

where the three spectrometers used were:

(i) Grubb-Parsons Spectromajor double-beam infrared spectrometer

(ii) Pye-Unicam SP 1800 Ultra-violet spectrometer

(iii) Farrand Mark 1 spectrofluorimeter

6.2 EXPERIMENTAL

1. Apparatus

The cryogenic system employed was an Air Products and Chemicals Inc. Displex closed-cycle refrigeration system (model CSA 202), employing helium as the working medium (see page 114-115, J. R. Sodeau, Ph.D. thesis, University of Southampton, for further details)[2]. The shroud vacuum (ca. 10^{-6} torr) was achieved by means of a two-stage pumping system mounted on the expander module trolley and consisted of a N.G.N. Ltd. rotary vacuum pump (Model PD/2) and an Edwards air-cooled oil diffusion pump (Model E02) with a nitrogen trap.

Samples were prepared on a mercury-free greaseless vacuum line and expanded into a bulb of known volume (1 litre).

The resultant matrix mixture was deposited on a cooled Li F window at 10^{o}K using the pulsed deposition method where the pulsing volume equalled 9.8 cms.

2. Materials

Sulphur dioxide. (B.D.H. Chemicals) was twice distilled from trap to trap with retention of only the middle boiling third of the sample.

Matrix gases. Argon (Research Grade X, B.O.C.)

Oxygen (Research Grade X, B.O.C.).

Both were used without further purification.

6.3. RESULTS

Infrared Absorption

Thre three fundamental vibrations of sulphur dioxide correspond to the following irreducible representations[3]

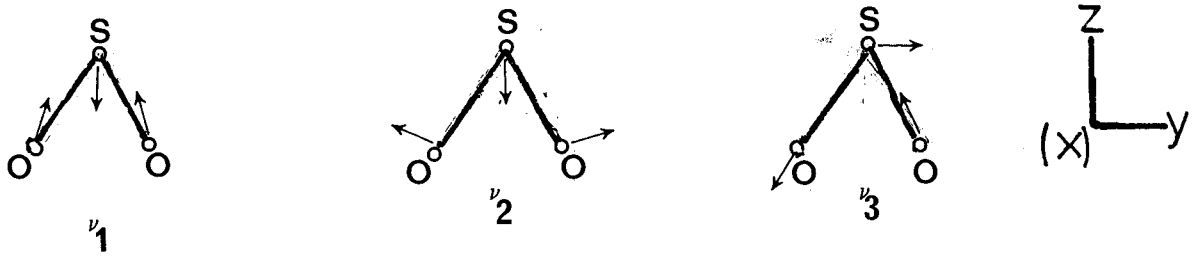

The observed frequencies of these fundamentals in the infrared spectrum of a matrix mixture of sulphur dioxide:argon (matrix ratio $1:10^4$) condensed at $10^{\circ}K$ are given below in Table 1.

TABLE 6.1

Observed frequencies (cm^{-1}) in the infrared spectrum of SO_2: Argon (MR = $1:10^4$)

CORRECTED BAND POSITION (cms^{-1})	ASSIGNMENT
1350.7 (vs)	ν_3 (b_2) ^{32}S $^{16}O_2$
1333.3 (w)	ν_3 (b_2) ^{34}S $^{16}O_2$
1150.3 (s)	ν_1 (a_1) ^{32}S $^{16}O_2$
1153.8 (w)	ν_1 (a_1) ^{34}S $^{16}O_2$
522.6 (m)	ν_2 (a_1) ^{32}S $^{16}O_2$
527.9 (w)	ν_2 (a_1) ^{34}S $^{16}O_2$

The most intense absorption band has been assigned to the ν_3 fundamental mode and in order that the lower limit of detection could be estimated the absorbance of this band was plotted as a function of the number of pulsing volumes of the sulphur dioxide:argon gas mixture sprayed onto the cold window. (See Table 2).

TABLE 6.2

Number of pulsing volumes sprayed onto the window	Absorbance
5	0.046
10	0.068
20	0.134
50	0.272
100	0.432
200	0.620

The lower limit of detection occurs when the concentration of SO_2 gives an absorption signal which just becomes distinct from the background noise and from the spectra obtained this point occurred when the absorbance of the signal, $\log \frac{I_o}{I_T}$ was equal to 0.01.

From the plot of the results shown in table 6.2, I_o is the incident intensity of radiation on the sample. I_T is the transmitted intensity. This lower limit is equal to the detection of the first pulsing volume of the $1:10^4$ sulphur dioxide:argon matrix mixture on the cold window.

1. Partial pressure of sulphur dioxide in 1 pulsing volume of $1:10^4$ mixture (Total pressure in bulb = 100 torr).

Using BOYLE'S LAW: $P_1V_1 = P_2V_2$

$V_1 = 1000.0$ cms^3 (volume of sample bulb)

$P_1 = \frac{100}{10^4 \times 760}$ atmospheres (pressure of SO_2 in sample bulb)

V_2 = 1009.8 cms^3 (volume of sample bulb plus pulsing volume)

P_2 = Pressure of SO_2 in one pulsing volume

= $\underline{13 \times 10^{-6}}$ atmospheres

2. Concentration of sulphur dioxide (moles) in one pulsing volume

Pulsing volume = 9.8 cms^3

Pressure of Sulphur Dioxide = 13×10^{-6} atmospheres

Temperature of gaseous SO_2 = 298°K

R = 82.0575 cc atm. $°K^{-1}$ $mole^{-1}$ [6]

Then on applying the equation of state of an ideal gas:

$$PV = n RT$$

$$\underline{n = 5.2 \times 10^{-9} \text{ moles}}$$

Ultraviolet Absorption

The most intense absorption system in the ultraviolet region lies between 200 and 230 nms for SO_2 isolated in an argon matrix. For such a system, Jones and Coon[3] have assigned the vibrational bands in which the most intense band, positioned at 215 nms (46470 cms^{-1}) was assigned to the J_1 label. This band was plotted as a function of the number of pulsing volumes of sulphur dioxide:argon gas mixture sprayed onto the window (temperature ca. 10°K), see Table 6.3 .

TABLE 6.3

Matrix Ratio of SO_2:Argon is 1:500

Number of pulsing volumes sprayed onto the window	Absorbance
5	0.07
10	0.13
35	0.38
70	0.60

From table 6.3, the lower detection limit is equal to the detection of the first pulsing volume of the 1:500 SO_2:argon matrix, i.e. where the absorbance is equal to 0.01.

1. Partial Pressure of sulphur dioxide in one pulsing volume of 1:500 mixture. (Total pressure in bulb = 100 torr)

Using BOYLE'S LAW: $P_1V_1 = P_2V_2$

$V_1 = 1000.0\ cms^3$ (volume of sample bulb)

$P_1 = \frac{100}{500 \times 760}$ atmospheres (pressure of SO_2 in sample bulb)

$V_2 = 1009.8\ cms^3$ (volume of sample bulb plus pulsing volume)

P_2 = Pressure of SO_2 in one pulsing volume

$= \underline{2.6 \times 10^{-4}\ \text{atmospheres}}$.

2. Concentration of sulphur dioxide (moles) in one pulsing volume

Pulsing Volume $= 9.8\ cms^3$

Pressure of Sulphur Dioxide $= 2.6 \times 10^{-4}$ atmospheres

Temperature of gaseous $SO_2 = 298^oK$

$R = 82.0575$ cc.atm. $^oK^{-1}$ $mole^{-1}$ [6]

Then on applying the equation of state of an ideal gas:

$\therefore \quad \underline{n = 1.04 \times 10^{-7}\ \text{moles}}$

Phosphorescence

In a low temperature matrix, at 10^oK, sulphur dioxide does not fluoresce,[5] however excitation into the first two allowed absorption bands leads to strong phosphorescence in the 390-480 nm. region. The intensity of phosphorescence seems greater for excitation into the first allowed absorption band.

For the spectra taken,

$$\lambda_{EXCITATION} = 305 \text{ nms}$$
$$\lambda_{MAXIMUM}(\text{emission}) = 431 \text{ nms.}$$

The intensity of the maximum was plotted as a function of the number of pulsing volumes of SO_2:Argon mixture (matrix ratio 1:80) sprayed onto the cold window.

TABLE 6.4

Number of pulsing volumes sprayed on	Intensity of I_{max} (cms of chart paper)
5	0.07
10	0.13
15	0.18
25	0.29

From table 6.4, the lower detection limit is equal to the detection of the first pulsing volume of the 1:80 SO_2:argon mixture, i.e. where the peak height is equal to 0.5 cms on the chart paper.

1. Partial pressure of sulphur dioxide in one pulsing volume of 1:80 mixture (total pressure in bulb = 100 torr).

USING BOYLE'S LAW: $P_1V_1 = P_2V_2$

V_1 = 1000 cms^3 (volume of sample bulb)

$P_1 = \frac{100}{80 \times 760}$ atmospheres (pressure of SO_2 in sample bulb)

V_2 = 1009.8 cms^3

$\therefore$ P_2 = partial pressure of SO_2 in one pulsing volume

Volume = $\underline{1.63 \times 10^{-3} \text{ atmospheres}}$

2. Concentration of sulphur dioxide (moles) in one pulsing volume

Pulsing volume = $9.8\ cms^3$

Pressure of sulphur dioxide = 1.63×10^{-3} atmospheres

Temperature of gaseous SO_2 = 298^oK

R = 82.0575 cc atm. $^oK^{-1}$ $mole^{-1}$ [6]

Then on applying the equation of state for an ideal gas

$$PV = n\,RT$$

$$\therefore \quad n = 6.5 \times 10^{-4} \text{ moles}$$

6.4 CONCLUSIONS

From the results infrared absorption appears to be the most sensitive technique for the detection of the condensed sulphur dioxide. In fact, the detection limit will in reality be lower than the calculated value since about 90% of the pulsing volume actually condenses on the cold window,[6] the excess is lost to the vacuum pumps.

Advantages of employing a sampling technique involving cryogenic equipment

Although it is a well established technique, the analysis of gaseous samples utilizing infrared spectrometry is not completely satisfactory. This is because gas-phase spectra have characteristically broad spectral distributions since not only do transitions corresponding to the pure vibrational mode, ν_o, occur but also absorptions corresponding to $\nu_o \pm \nu_r$, where ν_r represents a rotational frequency. Thus, since there are many different rotational states in a finite sample, there will be a whole series of lines corresponding to different ν_r values. This results in extensive overlap of spectral lines for mixtures of gaseous samples. At high temperatures 'hot' bands complicate the spectra further. Relatively concentrated samples are therefore required for positive qualitative identification and for quantitative studies.

However, at cryogenic temperatures half-height bandwidths of 3-5 cms^{-1} are observed, since only the pure vibration occurs. This also results in enhanced absorption coefficients thus lowering the detection limit for the characterisation of a sample. Thus, since the frequencies of normal vibrations are very sensitive to overall molecular structure, the use of both a cryogenic sampling technique and an infrared spectrometric technique could be a powerful tool in the detection of pollutants in stack gas emission.

REFERENCES

1. B. Meyer, Science, 168, 783-789 (1970).

2. J. R. Sodeau, Ph.D. Thesis, University of Southampton, 1976.

3. G. Herzberg, in "Molecular Spectra and Molecular Structure" Vol.2, D. Van Nostrand, London (1968).

4. V. T. Jones and J. B. Coon, J.Mol.Spec., 47, 45 (1973).

5. L. F. Phillips, J. J. Smith, B. Meyer, J.Mol.Spec., 29, 230 (1968).

6. A. J. Rest, Private Communication.